A COMPARISON OF RADAR-DERIVED PRECIPITATION AND RAIN GAGE PRECIPITATION IN NORTHEASTERN COLORADO

Peter Clark Clement

Thomas B. McKee

Colorado State University

DEPARTMENT OF ATMOSPHERIC SCIENCE

PAPER NO. 579

A COMPARISON OF RADAR-DERIVED PRECIPITATION AND RAIN GAGE PRECIPITATION IN NORTHEASTERN COLORADO

Peter Clark Clement

Thomas B. McKee

Department of Atmospheric Science
Colorado State University
Fort Collins, CO 80523

May 1995

Atmospheric Science Paper No. 579

ABSTRACT

A COMPARISON OF RADAR-DERIVED PRECIPITATION AND RAIN GAGE PRECIPITATION IN NORTHEASTERN COLORADO

Accurate precipitation measurement is desired over large areal extents in fine temporal and spatial resolution for a myriad of scientific disciplines and practical applications. Hydrological sciences and federal and local government agencies would benefit from improved precipitation measurements. The question is can radars satisfy this desire for better precipitation measurements. The WSR-88D radar network will provide nearly complete radar coverage of the contiguous United States and has the ability to operationally measure large areal extents in fine temporal and spatial resolutions. Precipitation products derived from the WSR-88D networks are becoming readily more accessible and steadily gaining in popularity and use, often without any reference to accuracy.

This study is a comparison of precipitation from the CSU-CHILL multiparameter research radar, National Weather Service's WSR-88D located outside Denver, CO (KFTG), and networks of tipping bucket gages. Comparisons are made to reveal spatial coverage of precipitation, time distribution of precipitation, and quantify amounts of precipitation derived from the two radars and gage networks from three convective precipitation events in northeastern Colorado.

This study finds the multiparameter variable, specific differential phase derived precipitation (R(KDP)) compared well with gage precipitation for rainfall accumulations greater than 1 cm. On 20 June 1994 for 12 gages with four-hour accumulated precipitation greater than 1 cm, the

R(KDP) to gage precipitation ratio was 0.89. On 21 June 1994 for 3 gages with one-hour accumulated precipitation greater than 1 cm, the R(KDP) to gage ratio was 1.37. For precipitation accumulations less than 1 cm, R(KDP) greatly overestimated gage precipitation which is consistent with previous findings. On 20 June at one gage site (FOR) with a known 30-minute period of mixed phase precipitation, R(KDP) showed an eight percent overestimate of gage precipitation. This result demonstrates R(KDP)'s ability to accurately measure rainfall in mixed phase precipitation.

The time distribution of precipitation rates for the radar and gage are in reasonable agreement. In most cases, the radar-derived precipitation captures the temporal pattern of the gage's precipitation event well. However, the amplitude of the precipitation amounts differed appreciably.

Of the three reflectivity cut offs used to minimize excessive rain rates, the 53 dBZ reflectivity cut off performed the best in comparison to the gage's peak precipitation. This result agrees with Denver WSR-88D's use of 53 dBZ as their reflectivity cut off for summer convective precipitation in northeastern Colorado.

The precipitation derived by the actual WSR-88D precipitation algorithm provided by the WSR-88D Operational Support Facility, R(OSF), consistently overestimated the gage precipitation for two days of convective storms in Colorado. On 21 June 1994 for 64 gages with one-hour accumulated precipitation, the R(OSF) to gage precipitation ratio was 2.13. On 10 August 1994 for 127 gages with two-hour accumulated precipitation, the R(OSF) to gage ratio was 1.80. Over both days, the R(OSF) provided a somewhat smaller overestimate of gage

precipitation than this study's elementary use of same level II data and Z-R relationship. This result indicates the details of data processing are extremely important.

ACKNOWLEDGMENTS

The authors would like to thank Dr. Steven Rutledge from CSU's Atmospheric Science Department and Dr. Pierre Julian from CSU's Civil Engineering Department for their review comments that improved this paper. They would also like to thank the Colorado Climate Center's staff; Odie Bliss, Nolan Doesken, John Kleist, and Matt Savoie, for all their help, support and assistance. Thank also to Larry Carey for guiding me through multiparameter radar analysis and interpretation.

This research was supported by the Colorado Agricultural Experimental Station. The CSU-CHILL Radar Facility (sponsored by National Science Foundation under Cooperative Agreement ATM 8919080) was extremely helpful in their collaboration in radar data collection, specifically Patrick Kennedy and Dave Brunkow. The CSU-CHILL data was accessed through a 20-hour small project support request through the CSU-CHILL Radar Facility. For collaboration with precipitation gage data collection, our thanks to Kevin Stewart in association with Denver Urban Drainage and Flood Control District, Northern Colorado Water Conservancy District specifically Mark Crookston, and Jim Wishborn's Mountain States Weather Services. Scott Kelly at the WSR-88D Operational Support Facility, Norman, Oklahoma, provided the WSR-88D precipitation data.

Captain Peter Clement personally thanks the U. S. Air Force for sending him to CSU for the quality graduate education he received. Also, he would like to extend very special thank you to his wife, Katrina, and son, William, for their unending love, support and understanding.

TABLE OF CONTENTS

CHAPTER I

INTRODUCTION

Accurate precipitation measurement is desired over large areal extents in fine temporal and spatial resolution for a myriad of scientific disciplines and practical applications. In hydrological sciences, Smith et al. (1994) states that "soil- water content", of which precipitation is a critical component, "is the single most important land surface variable in atmospheric prediction models." Smith et al. (1994) presents a method which integrates observed precipitation data into a hydrological model whose output, soil-water content fields, are used to initialize a mesoscale model. Federal and local government agencies would also benefit from these higher resolution precipitation data. These federal agencies are responsible for public notification and disaster relief in the event of flooding, and efficient water management in the event of drought.

The question is how to satisfy this desire for accurate precipitation measurements over large areal extents with reasonable time resolution. In-situ measurement of precipitation with rain gages typically suffers from rainfall's extreme variability in space which is further complicated by the gages low spatial resolution. The obvious advantage of remote sensing by weather radar is its ability to make high spatial resolution observations over large areal extents.

The result of the Next Generation Weather Radar (NEXRAD) program is a network of the advanced Weather Surveillance Radar -- 1988 Doppler (WSR-88D) systems that

will provide nearly complete radar coverage of the contiguous United States. Figure 1.1 shows the radar locations of the WSR-88D network. The WSR-88D has the ability to operationally measure precipitation out to a range of 230 km with a 2x2 km resolution (Crum and Alberty, 1993). Precipitation products derived from the WSR-88D networks are becoming readily more accessible and steadily gaining in popularity and use, often without any reference to accuracy.

This study is a comparison of precipitation from the CSU-CHILL multiparameter research radar, National Weather Service's (NWS) WSR-88D located outside Denver, CO (KFTG), and networks of tipping bucket gages. Comparisons are made to reveal spatial coverage of precipitation, time distribution of precipitation, and quantify amounts of precipitation derived from the two radars and gage networks from three convective precipitation events in northeastern Colorado.

Figure 1.1 Locations of WSR-88D radars across the contiguous United States when installation is completed in 1996. (taken from Crum and Alberty, 1993).

CHAPTER II

THEORY

2.1 PRECIPITATION MEASUREMENT

There are two methods to measure precipitation -- point measurement using in-situ instruments and remote sensing systems.

2.1.1 In-Situ Measurement

In-situ instruments are categorized as recording and non-recording precipitation gages. Since recording gages can determine rain rates, this study uses a collection of tipping bucket recording rain gage networks. The tipping bucket rain gage uses a funneled collector which directs the precipitation into one of two small buckets between a rocking arm. These buckets store a discrete amount of precipitation, either 1 mm or 0.01 in. When a bucket is filled, the bucket tips to empty and positions the second bucket under the funnel to be filled, so that the process can be repeated. The time of each tip is recorded, so precipitation totals and rain rates can be computed. Tips can also be easily converted to electronic signals which can be telemetered for automated remote gage sites as was the case with the gage networks used.

There are two potential problems with rain gage point measurements, representativeness of the gage's site and accuracy of point measurement. Since the gage networks used in this study are operationally used for hydrological, meteorological, and

agricultural applications, the gage sites' measurements are considered representative of the local area's precipitation. The accuracy of the point measurement can not however be taken for granted. Tipping bucket rain gages suffer from a variety of errors. Since this study concentrates on summer convective precipitation events, these errors have been limited to those associated with heavy convective precipitation. These errors adapted from Brock (1990) and Wang and Felton (1983), include funnel misdirection, splashing, faulty reed switch or bounce, funnel orifice clogging, and exposure.

Funnel misdirection occurs when a sudden onset of precipitation partially fills the collector and a vortex action is created within the funnel. This vortex action directs the collected water either partially or totally away from the collecting tipping bucket. Splashing from the collector or the tipping bucket also removes a portion of water from measurement. Therefore, funnel misdirection and splashing contributes to underestimate the precipitation. These errors tend to increase with increasing intensity -- greater underestimate with greater intensity of precipitation.

Faulty reed switch or bounce errors occur when, as the bucket tips to empty, it "bounces" immediately back to the fill position, possibly still partially filled. This error is identified by two tips in quick succession. This error tends to overestimate the precipitation.

Most tipping buckets have small funnel orifices. These small openings make great homes for spiders and insects making routine maintenance a requirement. Large graupel and hail (that don't bounce out) also can impede the instrument's ability to measure rain by partially clogging the funnel orifice. The resulting clogging increases the potential for

splash from the collector. In addition, the duration of precipitation event may be extended due to melting. In all three case study days, during some the period of study, hail and or large graupel was reported.

Exposure is the largest potential error of all others. None of the gages used in this study were shielded from wind effects. Gages exposed to the wind, suffer from turbulent flow about the gage which reduce the amount of rainfall caught. Neff (1977) found rain gages exposed to wind caught 5-15 percent less rain than pit gages. Experimental measurements show reductions of 20 percent for winds in range of 5-10 m s^{-1} and over 80 percent for winds above 10 m s^{-1} (Brock 1990). In all three case study days, strong, gusty surface winds in the range 12-20 m s^{-1} and gusts of 18-26 m s^{-1} were reported in conjunction with the heaviest precipitation events.

Overall, tipping bucket gages without faulty reed switches or histories of bounce errors, generally underestimate heavy precipitation events. Some tipping bucket rain gage instrument systems such as NWS's Automated Surface Observing System (ASOS) tipping bucket, apply an algorithm to correct this known underestimate in heavy precipitation. None of the networks used in this study apply any corrective algorithms to the tipping bucket measurements. Therefore, the gage measurements used in this study, may be an underestimate of the precipitation that actually occurred. This underestimate however can only account for at most, an approximate 20 percent error to the radar-derived precipitation.

2.2 REMOTE SENSING -- WEATHER RADAR

Of the remote sensing systems with the capability to measure precipitation, this study will only include ground based weather radars. Dedicated weather radars have been using the reflectivity factor as an estimate to rain rates since the late 1940's (Wexler, 1948; Marshall and Palmer, 1948). For a complete historical aspect of weather radars and their application to atmospheric sciences, see Atlas (1990).

The obvious advantage of radars are their ability to measure large areal extents in reasonable time scales. Before radar derived precipitation can be operationally used, one must consider the theory of how radars derive precipitation and then consider the potential sources of errors.

2.2.1 Weather Radar Theory -- Definitions and Equations

Doviak and Zrni'c (1993) and Battan (1973) give extensive overviews of weather radar theory and derivation of radar equation and applicability to rainfall measurements.

2.2.1.1 Reflectivity, Z

Radars emit pulses of electro-magnetic (EM) energy in the microwave spectrum. This EM energy, when it encounters a hydrometeor target, will be absorbed and/or scattered by the hydrometeor depending on the wavelength of the incident radiation and hydrometeor's phase and size. If the hydrometeors are smaller than the incident radiation's wavelength, then the hydrometeor scatters the incident radiation in accordance to Rayleigh scattering laws. For 10-11 cm wavelength (S-Band) weather radars, the Rayleigh approximation is valid for hydrometeor diameters less than 7 mm. By assuming the Rayleigh approximation, the direction and pattern of scattering by the hydrometeor can be

determined. The scattering of interest is the amount scattered back in the direction of the radar or backscatter. By assuming the Rayleigh approximation, the backscattering cross section for a liquid hydrometeor, σ, is defined as:

$$\sigma = \frac{\pi^5}{\lambda^4}|K_w|^2 D^6 \tag{2.1}$$

where λ is the wavelength of the radar, $|K_w|$ is the complex index of refraction for water, and D is the diameter of an equivalent volume spherical raindrop.

Each pulse of energy from the radar illuminates a volume of space as defined by the radar antenna beam width, range from the radar and the pulse length of the radar. The resulting radar sampling volume as in a beam of light from a flashlight, expands in range. Therefore, the radar's transmitted energy is spread over a larger area with greater range. Since the radar is sampling from a volume of space, the backscatter measured is the result of a collection of targets or hydrometeors within that space. By using equation 2.1, reflectivity in dBZ is defined as:

$$Z = 10\log_{10}\left[\frac{\lambda^4}{\pi^5|K_w|^2}\int_0^{D_m} D^6 N(D)dD\right] \tag{2.2}$$

where D_m is the maximum drop size diameter and N(D) is the drop size distribution. Hence, reflectivity is related to the sixth power of the hydrometeor's diameter.

The definition of rain rate is the product of the drop's mass, drop size distribution, and fall speed, integrated over the range of drop diameters. Rain rate, R, expressed in depth of water per unit time is:

$$R = \frac{\pi}{6}\int_o^{D_m} D^3 N(D)v(D)dD \tag{2.3}$$

One form of the drop size distribution, N(D), is the inverse exponential, first given by Marshall and Palmer (1948) as:

$$N(D) = N_o e^{-\Lambda D} \tag{2.4}$$

Splihaus (1948) has defined an equation for fall speed as a function of diameter, $v_t(D)$, as:

$$v_t(\mathrm{D}) = 14 D^{0.5} \tag{2.5}$$

Assuming a drop size distribution as in equation 2.4 and fall speed as in equation 2.5 and combining with equations 2.2 and 2.3, we can express a Z-R relationship in the familiar form:

$$Z = A R^B \tag{2.6}$$

Battan (1973) lists a variety of Z-R relationships with their references, location derived for, and type of precipitation intensity best suited for. It is important to note that equations 2.4 and 2.5 are not unique for a given storm. In fact, the drop size distribution has been known to change throughout a convective cell's life cycle. Richards and Crozier (1983), compared disdrometer observations with radar reflectivity to show that drop size distributions vary from storm to storm and within each storm's life cycle. Joss et al. (1970) emphasize the categorizing of the type of precipitation, so a more accurate drop size distribution can be chosen, resulting in a better Z-R for a given storm. Essentially, there is not one single Z-R relationship that works best for all meteorological and precipitation conditions. The WSR-88D precipitation algorithm tries to work around this dilemma in two ways. The first way is through the use of 400 meteorological adaptable parameters (Crum and Alberty, 1993) like the A and B of equation 2.6, which can be changed to fine tune the precipitation algorithm to suit the local area's precipitation

climatology. The second way is through a near real time comparison between local gages' precipitation to radar precipitation in order to determine a multiplicative bias. Essentially, this multiplicative bias is a calibration between rain gages' precipitation and the radar-derived precipitation. This multiplicative bias is applied to the entire derived precipitation field. Brandes (1975) reviews techniques on how to apply gage to radar bias to adjust Z-R relationship.

This study uses a Z-R relationship first derived by Woodley and Herndon (1970) for Florida thunderstorms and is the default Z-R relationship used by WSR-88Ds. This relationship is given as:

$$Z = 300R^{1.4} \tag{2.7}$$

where Z is in $mm^6\ m^{-3}$. Inverting and solving equation 2.7 for rain rate, R(NX), (where NX refers to WSR-88D or NEXRAD (NX)) gives:

$$R(NX) = \left(\frac{10^{Z/10}}{300} \right)^{1/1.4} \tag{2.8}$$

where Z is reflectivity in dBZ and R is in mm $hour^{-1}$. Figure 2.1 shows a graph of this R(NX) relationship. As shown by the graph, the rain rate increases logarithmically to arithmetic increases in reflectivity (in dBZ).

2.2.1.2 Specific Differential Phase, K_{DP}

Selinga and Bringi (1978) first proposed the use of differential phase measurement to determine rain rate. Unlike reflectivity which is a measure of the back scatter, differential phase is a measure of the forward scatter. Differential phase, ϕ_{DP}, is defined as the difference between propagation phase constants for horizontal and vertical polarized

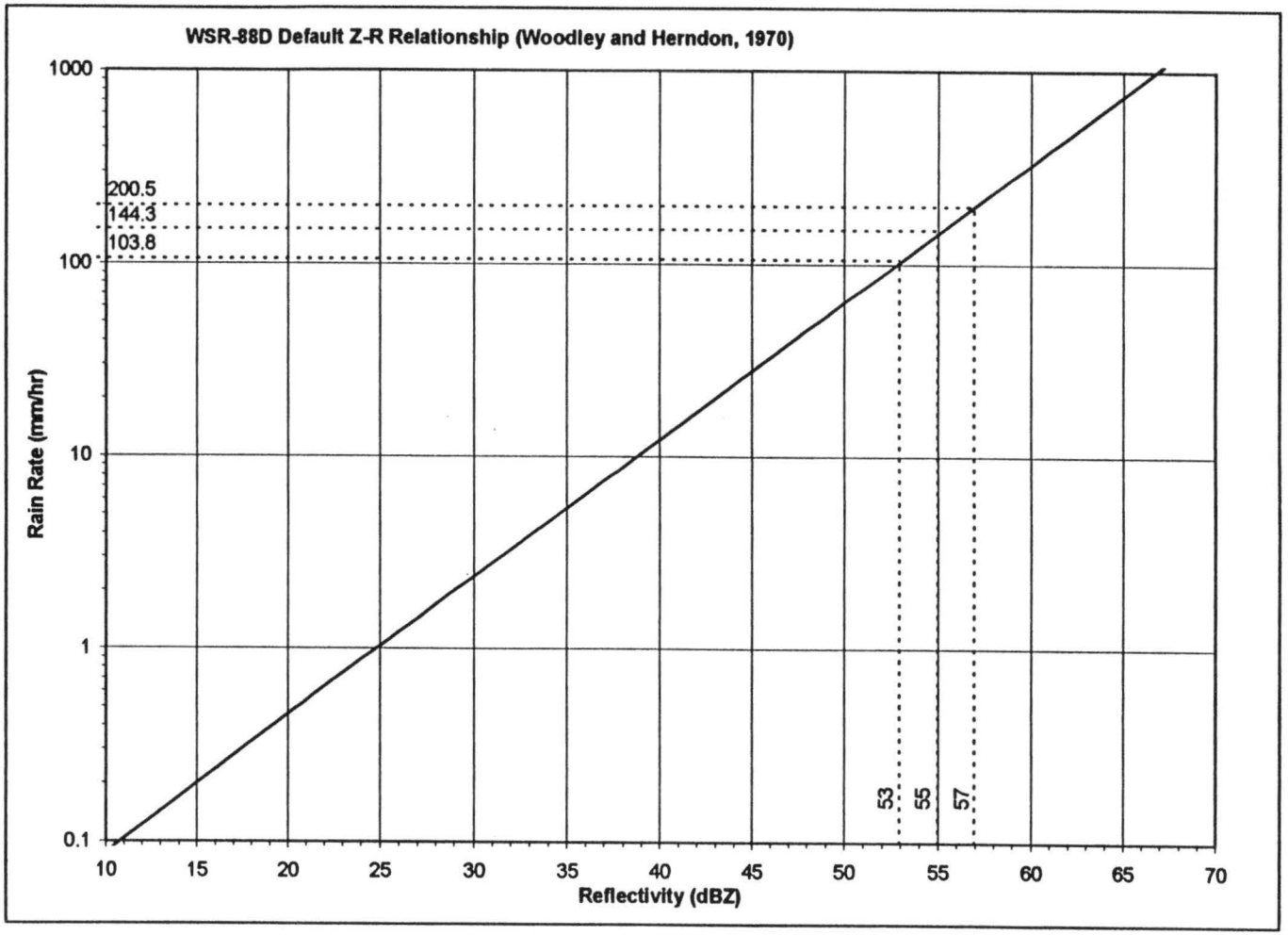

Figure 2.1 Default Z-R relationship for WSR-88D, R(NX), (Woodley and Herndon, 1970) with three reflectivity values 53, 55, and 57 dBZ, and associated rain rates identified.

waves. Specific differential phase, K_{DP}, is the range derivative of differential phase and is defined as:

$$K_{DP} = \frac{180}{\pi}\lambda \ \mathrm{Re}\int\left[f_H(D) - f_V(D)\right]N(D)dD \tag{2.9}$$

where f_H and f_V are the forward scattering amplitudes for horizontally and vertically polarized waves, respectively. K_{DP}'s units are degrees phase shift km^{-1}. K_{DP} provides information on liquid water content and the mass weighted mean axis ratio (Jameson 1985). This relationship between K_{DP}, liquid water content, w, and the mass weighted mean axis ratio, $\overline{R_m}$, can be expressed as:

$$K_{DP} \propto w\left(1 - \overline{R_m}\right) \tag{2.10}$$

K_{DP} has the unique capability to discriminate between statistically isotropic (hail) and anisotropic hydrometeors (large rain drops). Since hail is typically spherical in shape or gives the radar the appearance of a sphere due to tumbling motions (Knight and Knight, 1970), the difference of the forward scattering amplitudes for horizontally and vertically polarized waves is approximately zero. Rain drops become more oblate (horizontal axis being greater than the vertical) with increases in diameter due to aerodynamic forces (Pruppacher and Beard, 1970; Pruppacher and Pitter, 1971; Green 1975). Hence, the forward scatter along the horizontal axis lags the forward scatter along the vertical axis resulting in positive K_{DP} values. Therefore, K_{DP} detects total water content along the path and is not biased by the presence of pure ice. In addition, specific differential phase is less sensitive to variations in drop size distributions (Humphries, 1974) and is not dependent

on the radar's system calibration (Sachidananda and Zrni'c, 1987). The K_{DP}-rain rate $R(K_{DP})$ equation used was taken from Chandrasekar et al. (1990) and is given by:

$$R(K_{DP}) = 40.5(K_{DP})^{0.85} \tag{2.11}$$

Figure 2.2 shows a plot of the K_{DP} to rain rate relationship and shows how K_{DP} is nearly linearly related to rain rate. The graph shows how small values of K_{DP} result in appreciable amounts of rain. Light rain conditions, i.e., small drop diameters, produce little to no phase lag as the drops are nearly spherical. Additionally small drops have mass weighted mean axis ratios that are close to unity. These two factors, small nearly spherical drops and small amounts of water content along path, result in low values of K_{DP}. Hence, K_{DP} does not perform well in regions of light precipitation. Sachidananda and Zrni'c (1987) recommend the use of $R(K_{DP})$ for rain rates greater than 50 mm hr^{-1}, while Chandraseker et al. (1990) recommends $R(K_{DP})$ for rain rates 70 mm hr^{-1} and greater.

2.2.1.3 Correlation Coefficient (ρ_{HV})

Another multiparameter variable used was correlation coefficient, ρ_{HV}. The ρ_{HV} values were used to threshold the CSU-CHILL multiparameter data. Balakrishnan and Zrni'c (1990) give an excellent overview of ρ_{HV} and are the first to recommend the quality control application of correlation coefficients. ρ_{HV} is a measure of the correlations between horizontally and vertically polarized scattering coefficients within the radar sampling volume. These correlations are mainly affected by variability in ratios of vertical to horizontal sizes of individual hydrometeors. Factors that influence this variability are fluctuations in shape and size distributions of the hydrometeors, mixed phase precipitation,

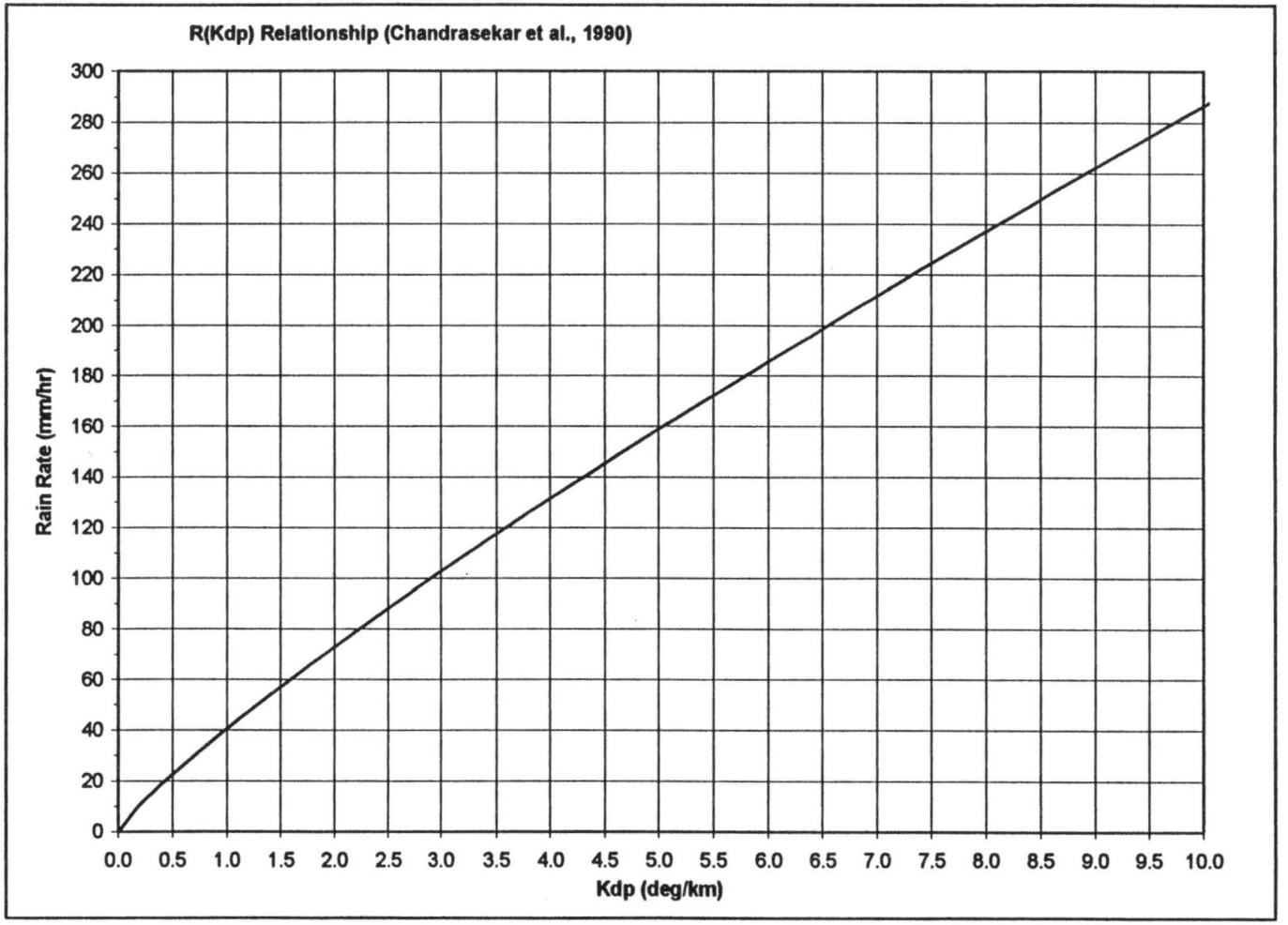

Figure 2.2 K_{DP} to rain rate relationship, R(KDP), (Chandrasekar et al., 1990)

and variance in the hydrometeor's orientation and canting angles. Low values of ρ_{HV} indicate greater variance of the hydrometeor's horizontal and vertical sizes and can be used to identify regions of low signal-to-noise ratios and/or regions of possible side lobe contamination.

2.2.2. Potential Errors in Radar Derived Precipitation

Wilson and Brandes (1979), Zawadzki (1982 and 1984) and Doviak and Zrni'c (1993) have assembled extensive overviews of the potential sources of errors in radar measurements. Some of the significant errors in radar-derived rain rates include variability of drop size distributions within the storm (as discussed in section 2.2.1.1), the advection of precipitation away from the point of radar measurement, evaporation during descent, and changes in convective cells' structure between measurements. Finally, the data processing method and height of the analysis above the ground must be chosen to minimize potential errors.

A radar measures an averaged volume of space at some height above the ground based on the radar's elevation angle and range. The surface area directly below this radar sampling volume may not receive the derived precipitation the radar variables observe due to the potential advective effects of the low level wind fields. Evaporation can also reduce the amount of precipitation the radar observes before the precipitation reaches the ground or is measured by the gage. To minimize these errors, only the lowest elevation scans are used to compute rain rates.

The radar derives a rain rate for each scan of the radar. The time period defined by the midpoints of the previous and current scan's time and the current and next scan's time,

was used to compute the rainfall. An assumption is made that the scan's measurement is representative for the time period between scans. Since the microphysical structure of a convective cell varies in just a few minutes time, the radar is incapable of observing the continuous non-linear changes in a convective cell's life cycle.

How the radar data is manipulated is very important in the determination of rain rate calculations. Gross grid resolutions can introduce smoothing or averaging of the radar data, while too fine a resolution may introduce noise into the analysis. Consideration must be given to range from the radar (beam spreading), and the scale of phenomenon one plans on measuring when one chooses a grid resolution.

Lastly, one must consider the height above the ground to choose for the analysis. As mentioned earlier, it is desired to obtain measurements as close to the ground as possible. Another consideration is the location of the freezing level and the resulting "bright band". The bright band is a region of rapidly increasing reflectivity as frozen hydrometeors melt. Therefore, radar observations to be used for rain rate calculations should be below the freezing level and associated bright band.

Likewise, precipitation that contains frozen or mixed phase hydrometeors have high values in reflectivity, since reflectivity from the radar sampling volume is dominated by the large hydrometeors. High reflectivity, greater than 55 dBZ, greatly exaggerate the rain rates. One method to prohibit exaggerated rain rates is to apply a reflectivity cut off. Reflectivity cut offs effectively cap the radar-derived rain rates to the value associated with this maximum allowed reflectivity. Figure 2.1 identifies three reflectivity values (53, 55, and 57 dBZ) and their respective R(NX) rain rates (103.8, 144.3, 200.5 mm $hour^{-1}$)

used as reflectivity cut off values. The KFTG authorized reflectivity cut off for summer season convection is 53 dBZ.

CHAPTER III

DATA

3.1 GAGE NETWORKS

This study had access to three separate gage networks. Figure 3.1 shows the area of study with terrain features and includes the locations of gages from the three networks used. The region depicted in figure 3.1 will be referred to hereafter as the Front Range. Figure 3.2 shows the same data with the areas for each of the three case study days identified. The three gage networks this study had access to are: National Oceanic and Atmospheric Administration's (NOAA) Forecast System Laboratory's (FSL) Mesonet, the Denver Urban Drainage and Flood Control District (UDFCD), and the Northern Colorado Water Conservancy District (NCWCD). Each network was designed for unique operational applications. A brief description of each network follows.

3.1.1 NOAA FSL Mesonet

The mesonet was designed to observe mesoscale meteorological phenomenon in northeastern Colorado. The mesonet is identified on figures 3.1 and 3.2 as the labeled large squares. The mesonet uses tipping bucket rain gages with 0.01 in. resolution. This network reports five-minute precipitation accumulations.

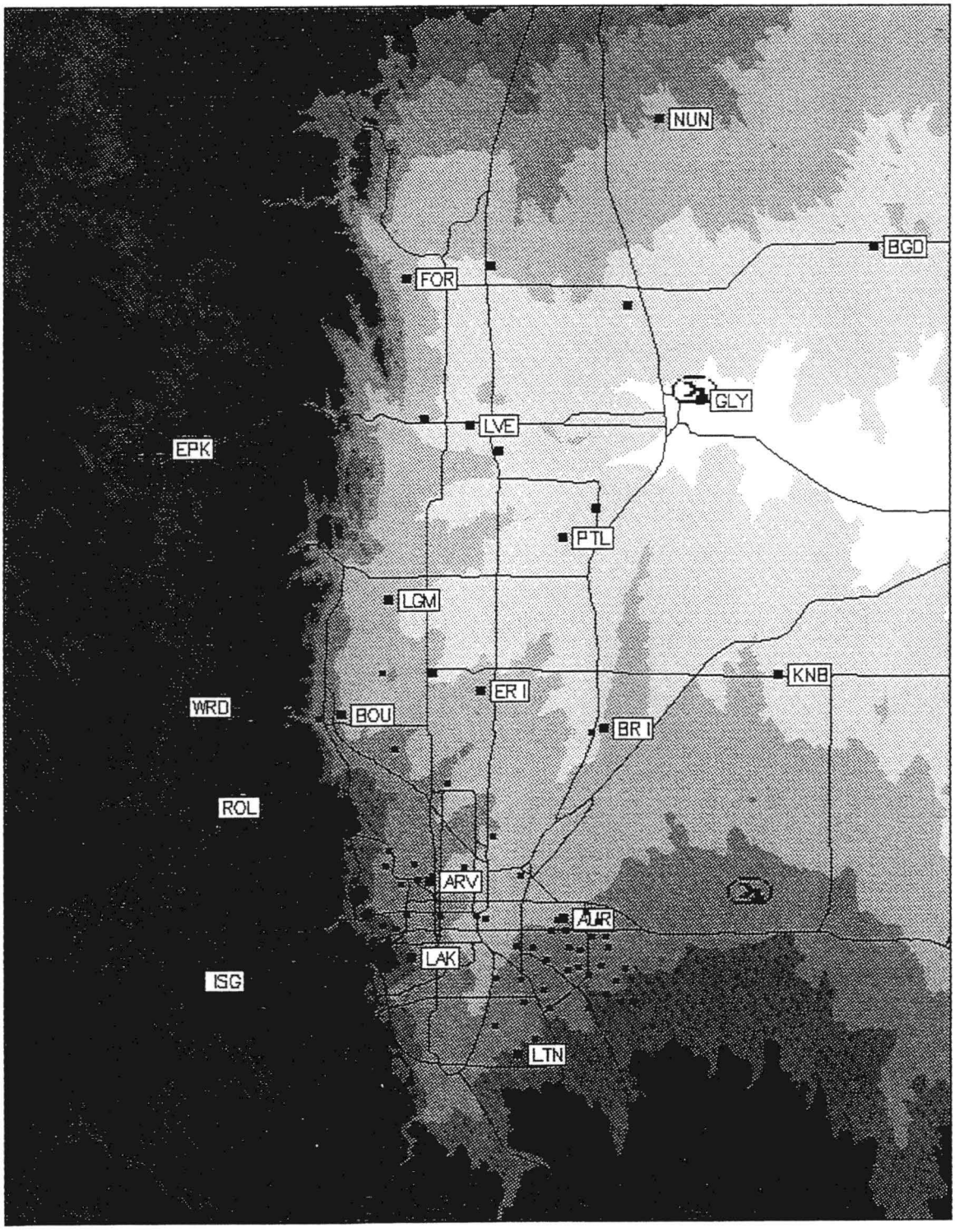

Figure 3.1 Area of study with local terrain, roads, and location of rain gages. The NOAA FSL Mesonet sites and radar locations are labeled.

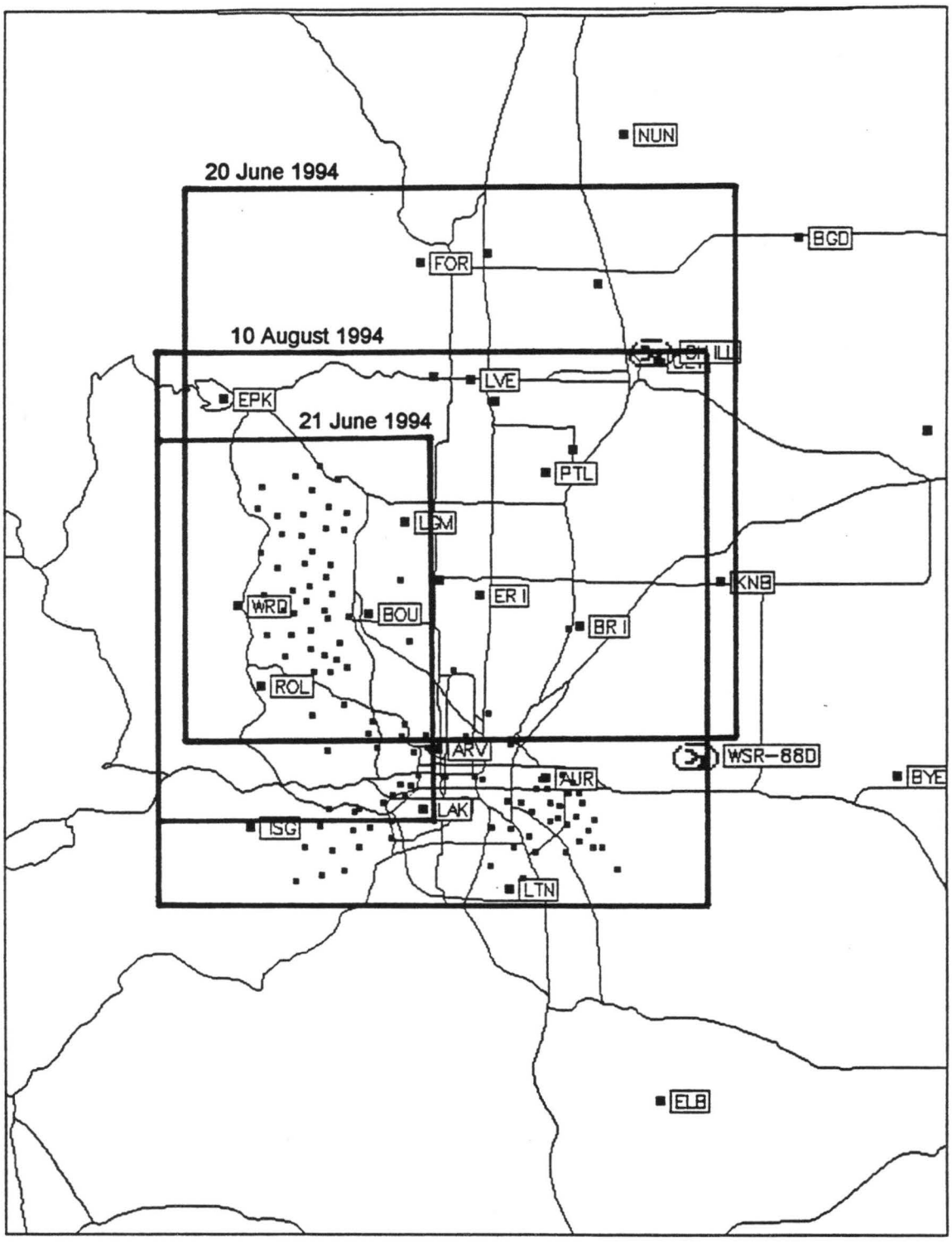

Figure 3.2 Area of study for each case study day. Rain gage and radar locations are shown.

3.1.2 UDFCD

The UDFCD operates a network of 113 precipitation gages, 61 stream stage sensors, and 28 weather stations across Boulder, Jefferson, Adams, and Arapahoe counties and the city of Denver. These gages and sensors are used for in the district's flash flood prediction program. The UDFCD rain gage network is identified as the small squares in figures 3.1 and 3.2. The precipitation gages are 12 in. tipping bucket gages with a 1 mm resolution. Each time a tip is recorded, the time and tip number is telemetered back to a UDFCD computer. Except for the Boulder county sites, the network's instruments undergo routine maintenance and are calibrated by UDFCD annually. The Boulder county network has a less stringent maintenance schedule, and have a greater probability of errors at single sites. Since this network reports each tip of the rain gage, the data was passed through a quality control program. This quality control program checked for tip number continuity, excessive rain rates, and tipping bucket bounce signatures. The tipping bucket bounce signature was identified as being two successive tips reported in under 15 seconds. The 15 second criteria was dependent on the delay associated with the communications circuitry board which handles data telemetry. The second tip of a bounce and invalid tip continuities (invalid tip number resets and decrementing tip numbers) were not used. The time period between two tips was used to compute a rain rate. This rain rate was compared to a threshold value of ~200 mm $hour^{-1}$ (8 in. $hour^{-1}$). If the rain rate was in excess of the threshold, the later tip was not used and a new time period and respective rain rate were computed using the next tip. This process was repeated until rain rates

below this threshold were computed. The resulting tips were used for time period precipitation accumulations.

3.1.3 NCWCD

The NCWCD network is designed to instrument the Platte river valley for agricultural applications. The NCWCD network is identified as the large squares without labels on figures 3.1 and 3.2. The district maintains a network of tipping bucket rain gages with 0.01 in. resolution which report 15-minute precipitation accumulations. The network is well maintained and each site routinely undergoes a scheduled maintenance inspection. Each winter, the rain gages are brought in from the field and calibrated. In addition, observations are routinely monitored for suspicious reports.

3.2 RADARS

Table 3.1 compares the CSU-CHILL (CHILL) and the WSR-88D radar's operational characteristics adapted from Kennedy and Rutledge (1995) for the CHILL and Crum and Alberty (1993) and Doviak and Zrni'c (1993) for the WSR-88D.

Table 3.1. Radar Operational Characteristics

	WSR-88D	CHILL
Wavelength (cm)	10	10.9
Antenna Diameter (m)	8.5	8.5
Beamwidth (degrees)	.95	.96
Pulse Length (m)	235.5	150
Peak Power (kW)	750	650
PRF (Hz)	320	1000
Polarization	horizontal	horizontal and vertical
Latitude (degrees)	39.787	40.446
Longitude (degrees)	104.534	104.637
Elevation (m)	1701	1432

3.2.1 CHILL

The CHILL is a 10.9 cm (S-Band) dual-polarized, multiparameter, National Science Foundation funded research radar. The radar is located about 8 km to the northeast of Greeley, CO at an elevation of 1432 meters (See figures 3.1 and 3.2). CHILL radar data were collected on two of the three case study days -- 20 June and 21 June, as part of a 20-hour research project with the CHILL facility. The scan strategies varied throughout the data collection periods. Hence, the radar data processed was a collection of horizontal and vertical cross-section scans whose times were irregular. This irregularity did not affect the analysis. In fact, the scan strategy provided a higher frequency of scans covering the significant convective cells. For the 20 June case, an assumption is made that there were no precipitating cells outside the scan limits within the region of study. The CHILL radar variables used were reflectivity (used to threshold the K_{DP} data), differential phase (from which K_{DP} was computed) and correlation coefficients to provide quality control. The CHILL data was provided in Universal File (UF) format. (Barnes, 1980)

3.2.2 KFTG

The WSR-88D for Denver, CO (KFTG) is located about 40 km to the east-northeast of Denver at an elevation of 1701 meters (see figures 3.1 and 3.2). The KFTG data was provided by National Center of Atmospheric Research's (NCAR) Research Data Program (RDP) through the CSU-CHILL facility and was provided in Level II format (Crum et al., 1993). Reflectivity was the only field used. The time interval between each scan was six minutes. The KFTG data was obtained for selective time periods for two of the case study days -- 21 June and 10 August. The KFTG had not yet been commissioned during

the period of this study. Therefore, time periods of recorded KFTG data were irregular and intermittent. The time periods for this study were primarily selected due to this constraint.

A second set of KFTG data comes from an exchange of gage site data with the WSR-88D Operational Support Facility (OSF) in Norman, Oklahoma. The OSF provided the precipitation totals from the WSR-88D precipitation algorithms for the two case study day's time periods that KFTG was recording -- 21 June and 10 August. The OSF provided time period storm totals for all the gage sites and 2x2 km gridded data over of regions of study for the two case study days. For each gage site and grid point, the OSF provided a 5x5 matrix of precipitation totals over the gage site or grid point. Only the matrice's center (closest to gage) precipitation value was used in this study. The precipitation from OSF will hereby be referred to as R(OSF).

3.3 CASE STUDY DAYS

This study uses three days with convection occurring along the Front Range of northeastern Colorado during the summer of 1994. Table 3.2 reviews each day's region and period of study. Each day had meteorological conditions favorable for heavy precipitation to occur. Weaver and Doesken (1991) have shown that moist, low-level flow from the east (upslope flow) favors convective development. A cold front passing through northeastern Colorado with surface high pressure settling in behind the front, serves as the source for the easterly upslope. When the flow aloft is weak enough to prohibit significant storm movement, the results are favorable for localized heavy rain and flash flooding (Maddox et al., 1978).

Table 3.2. Case Study Day's Periods and Regions of Study

Day	20 June	21 June	21 June	10 August
Radar Data	CHILL	CHILL	KFTG	KFTG
Time Begin (L)	14:00	14:30	14:30	21:00
Time End (L)	18:00	15:30	15:30	23:00
Grid Δ X (km)	0.5	0.5	0.5	0.5
Grid Δ Y (km)	0.5	0.5	0.5	0.5
Z level (km)	0.5	0.5	0.5	0.5
Grid Origin Location	CHILL	CHILL	CHILL	KFTG
Grid Origin Height (m)	1432	1701	1701	1701
Grid Dimensions (km)	100 x 100	50 x 70	50 x 70	100 x 100
X Minimum (km)	-85	-90	-90	-100
X Maximum (km)	+15	-40	-40	0
Y Minimum (km)	-70	-85	-85	-25
Y Maximum (km)	+30	-15	-15	+75

3.3.1 20 June 1994

The 1200 Universal Time Coordinate (UTC) (06:00 Mountain Daylight Time (MDT)) June 1994 surface analysis (figure 3.3) showed a low pressure system in eastern North Dakota with a weak frontal boundary extending across central Wyoming. The 1200 UTC (06:00 MDT) June 1994 Denver sounding (figure 3.4) showed light winds at all levels aloft. The sounding data shows the height of the freezing level to be 4.5 km and the precipitable water was 2.74 cm (1.08 in.), which was 192 percent of normal. The surface dewpoints were approximately 13 degrees Celsius (mid 50's Fahrenheit). The weak frontal boundary was observed on the CHILL as an east to west oriented convergence line moving to the south from the Wyoming-Colorado border through northeastern Colorado. The first convective cells to form on the convergence line where located just northwest of Fort Collins, CO. At CSU's Atmospheric Science building, the precipitation was observed

MONDAY, JUNE 20, 1994

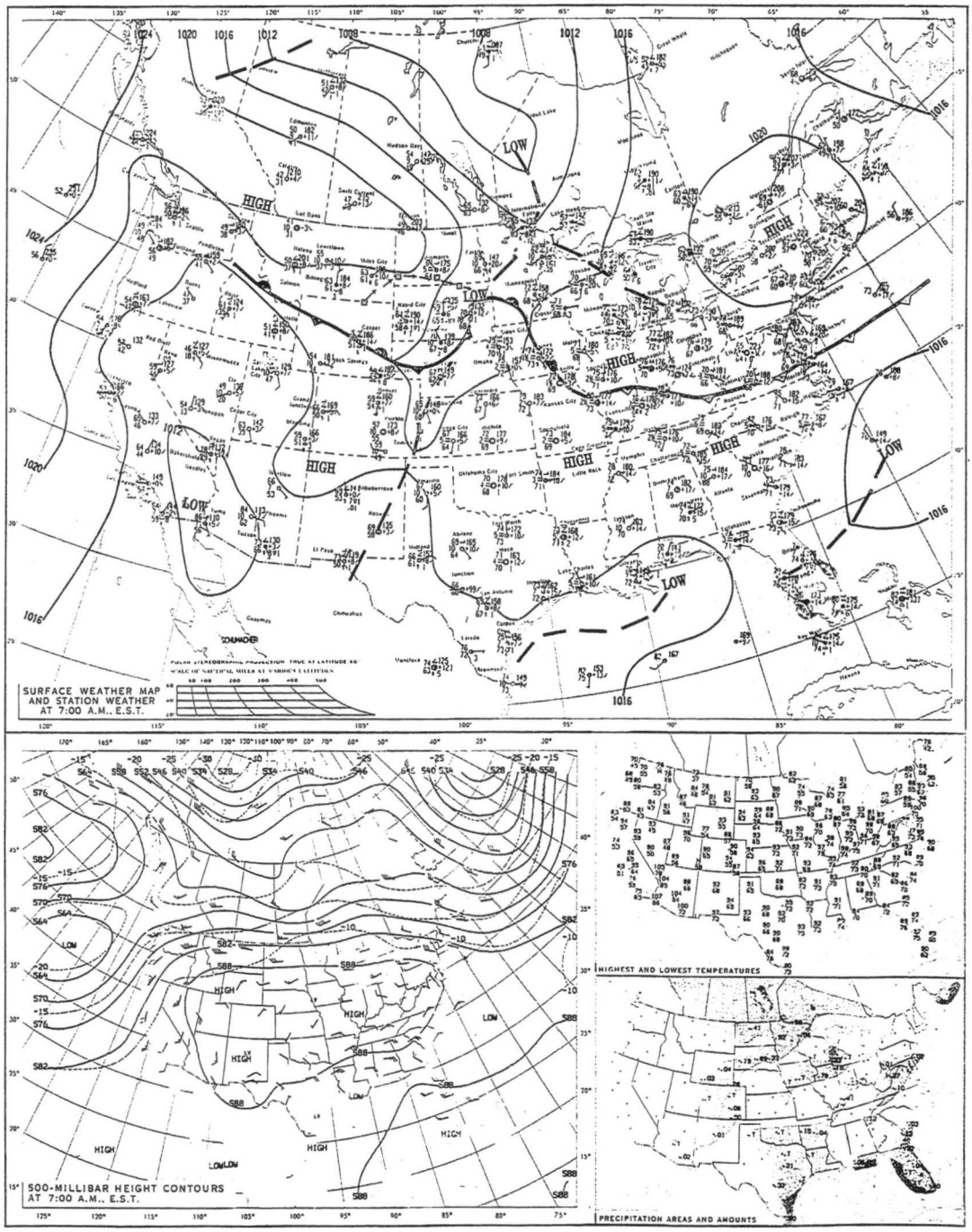

Figure 3.3 Daily weather map for 20 June 1994. Containing 20/1200 UTC June 1994 surface weather map and 500 mb height contours. (NOAA)

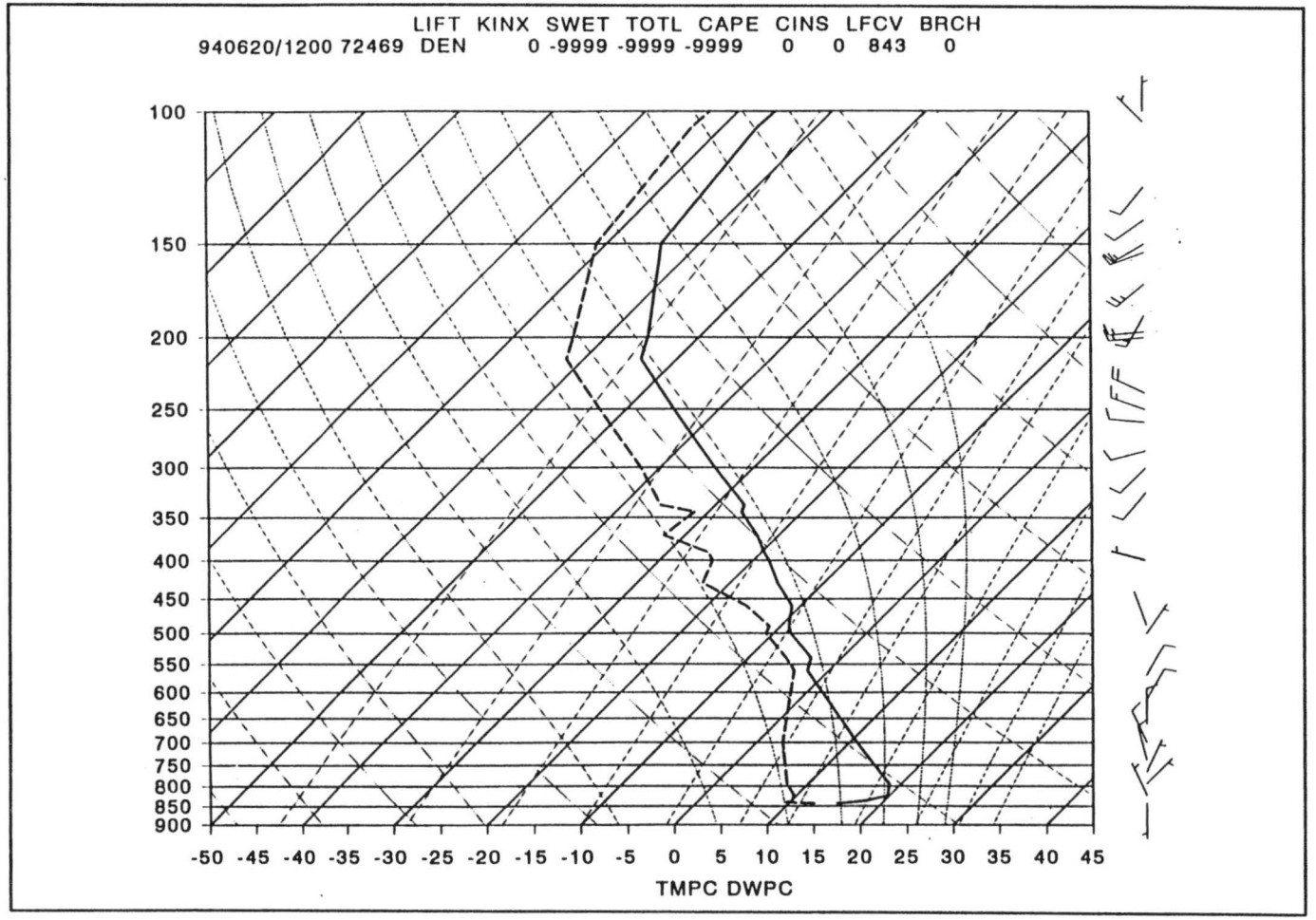

Figure 3.4 20 June 1994 Denver, CO 1200 UTC sounding.

to begin just after 14:00 MDT with marble sized (~1 cm) hail lasting until 14:30 MDT and the rain ending at 15:15 MDT. The Fort Collins mesonet site (FOR) recorded 3.06 in. (7.77 cm) of rain. This cell created an outflow boundary which interacted with the existing convergence line to create new cells along the convergence line that continued to move to the south. Additional precipitation maxima where observed in Loveland, CO (LOVE), southwest of Greeley, CO (GLY) and north of Boulder, CO (BOU).

3.3.2 21 June 1994

On the 21st of June, the 12:00 UTC synoptic analysis (figure 3.5) showed the front had passed through the state and high pressure had built into the Northern Plains centered in western North Dakota. The resulting flow created a weak, moist upslope flow along the Front Range. The 12:00 UTC June 1994 Denver sounding data (figure 3.6) showed abundant low level moisture from the surface to 750 mb and the flow aloft remained weak. The height of the freezing level to be 4.5 km and the precipitable water was 2.34 cm (0.92 in.), which was 162 percent of normal. Surface dewpoints remained high about 13 degrees Celsius. However, this day did not have an initiator of convection, like the convergence line on 20 June. The only appreciable precipitation occurred in the Boulder county foothills, fortunately in the Boulder County's portion of the UDFCD network. The maximum precipitation occurred at UDFCD station 2010 just southeast of Ward, CO (WRD) with 1.98 cm (0.78 in.). The primary reason for choosing this day as a case study day was because both radars were operating and recording data. The height of the grid origin was defined to be the elevation of KFTG. Hence, the height of the CHILL data analyses for this day were actually 0.769 km.

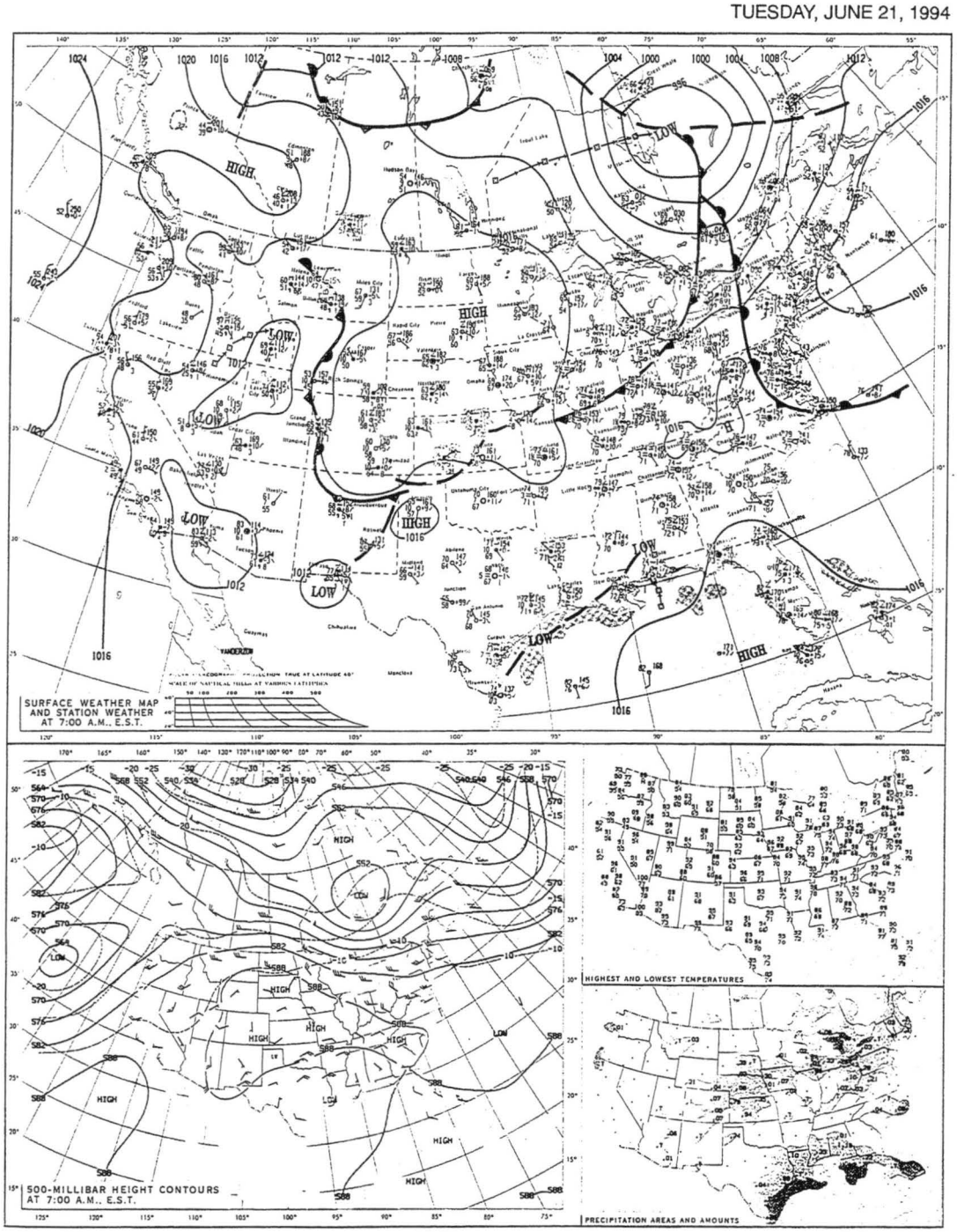

Figure 3.5 Daily weather map for 21 June 1994. Containing 21/1200 UTC June 1994 surface weather map and 500 mb height contours. (NOAA)

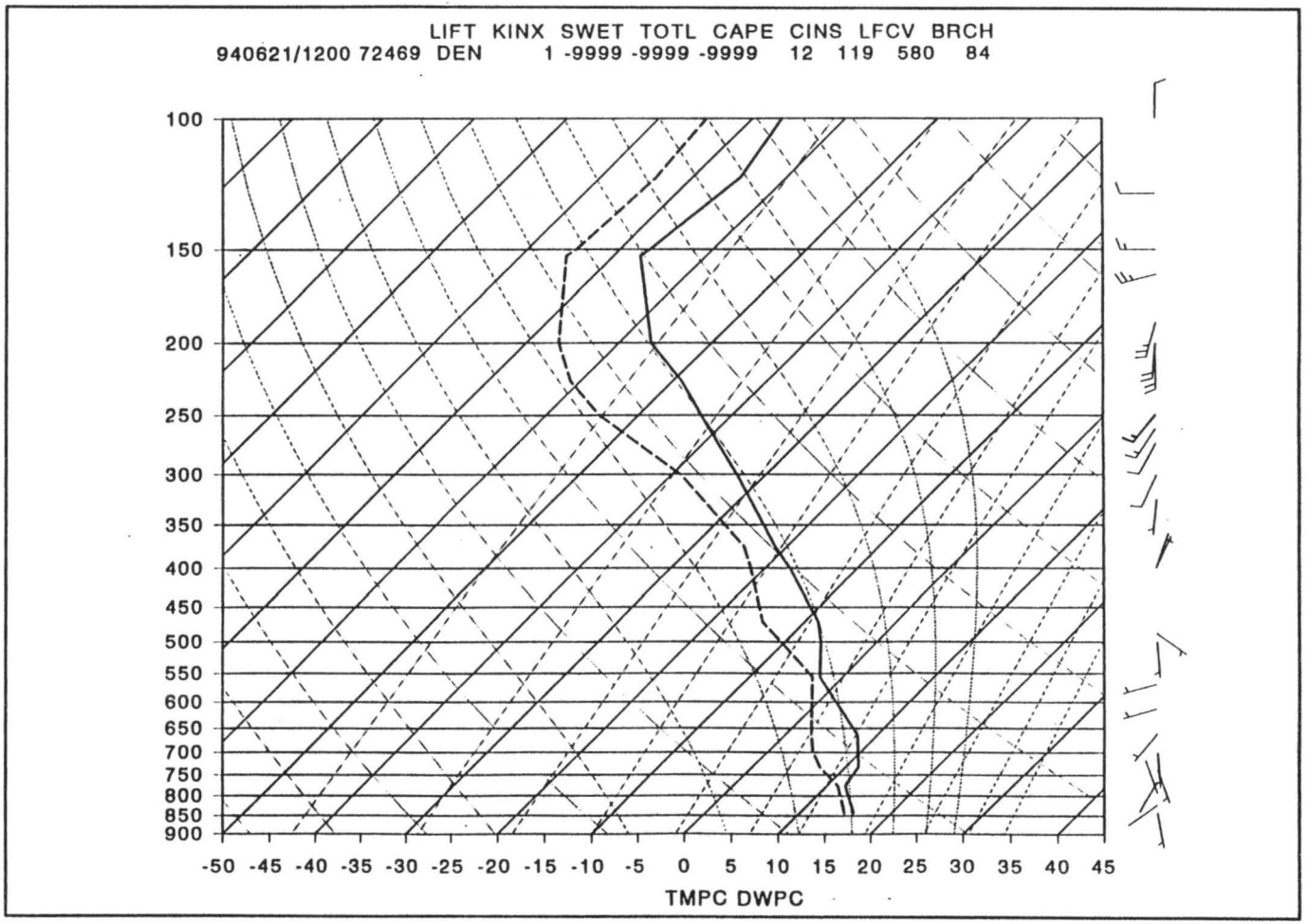

Figure 3.6 21 June 1994 Denver, CO 1200 UTC sounding.

3.3.3 10 August 1994

In the late afternoon on 10 August, a weak cold front moving toward the West had settled up against the Front Range foothills providing weak moist upslope flow. Figures 3.7 and 3.8, shows the 10 and 11 August 12:00 UTC synoptic charts across the period of study. Denver's 00:00 UTC (figure 3.9) 11 August 1994 sounding showed the Westerly flow aloft at 10 knots (5 m s^{-1}) and precipitable water was approximately 2.54 cm (1 in.) being 150 percent above normal. A weak pressure ridge aloft and associated subsidence, prohibited any convection throughout the afternoon on the 10th of August. However, by 19:00 MDT (11 August 01:00 UTC) the suppressing ridge had moved off to the east. In addition the FSL mesonet showed a 15 knot (8 m s^{-1}) surge in the upslope easterlies near the Colorado-Wyoming border. This combination of conditions created an unstable environment and by 21:00 MDT convection was initiated all along the Front Range. The first cell to form was in Virginia Dale, CO (northwest of Fort Collins) near the Colorado-Wyoming border, with 5.18 in. (13.16 cm) of storm total precipitation reported. The observer in Virginia Dale also reported 0.5 in. (1.2 cm) diameter hail. Additional significant storm totals for this evening included ~3.0 in. (7.6 cm) in Laporte (Northwest of Fort Collins), 2.5 in. (6.4 cm) in Fort Collins and 3.0 in. west of Loveland, and a couple reports of ~2.0 in. (5.0 cm) events in Denver and to the southwest of Denver. By 21:00 MDT convection had erupted throughout the entire region of study. Lots of cloud-to-cloud lightning was reported along with heavy rain and flooding. KFTG was recording this evening, but had break in recorded data between 23:00 and 00:00 MDT, limiting our period of study from 21:00 to 23:00 MDT.

WEDNESDAY, AUGUST 10, 1994

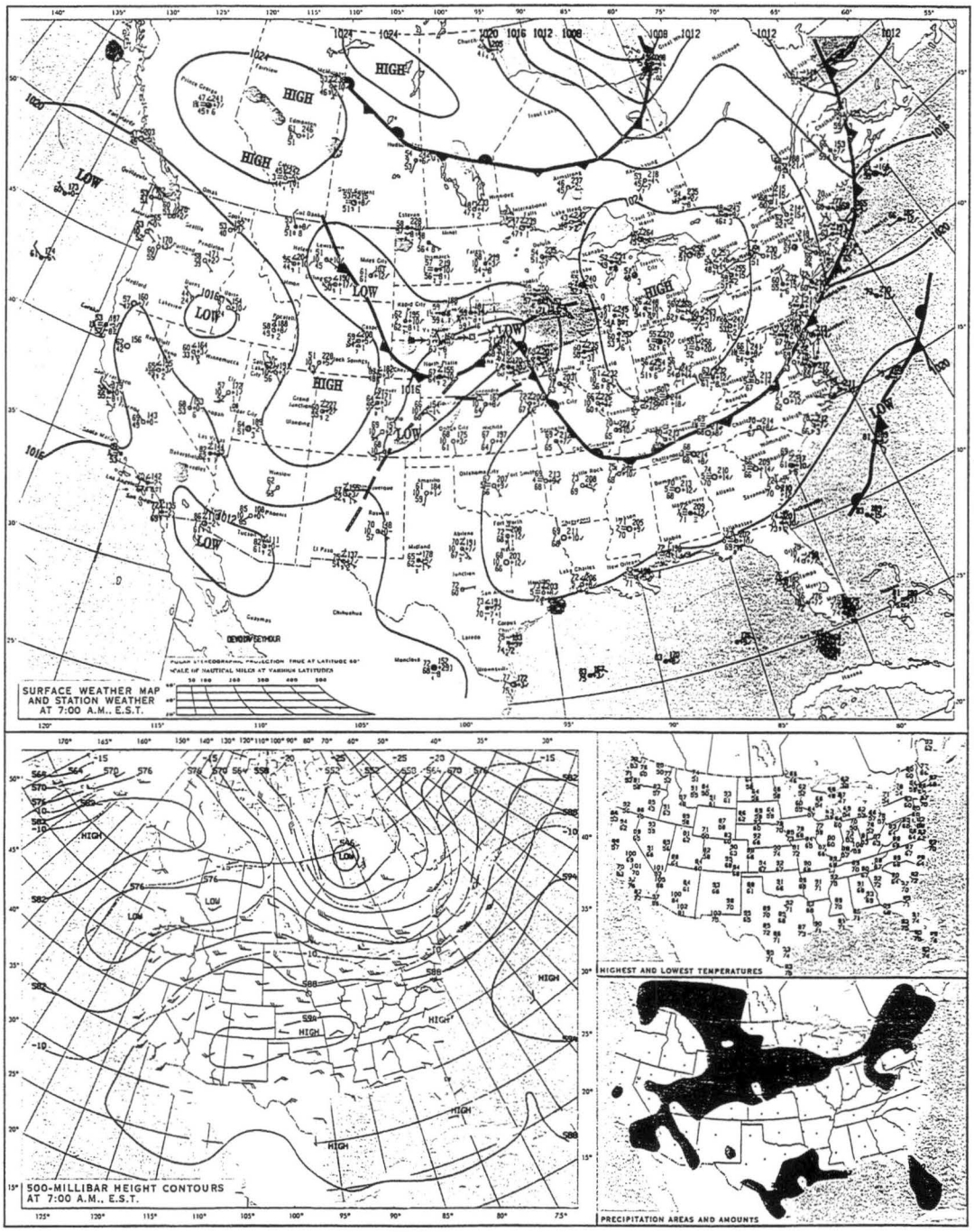

Figure 3.7 Daily weather map for 10 August 1994. Containing 10/1200 UTC August 1994 surface weather map and 500 mb height contours. (NOAA)

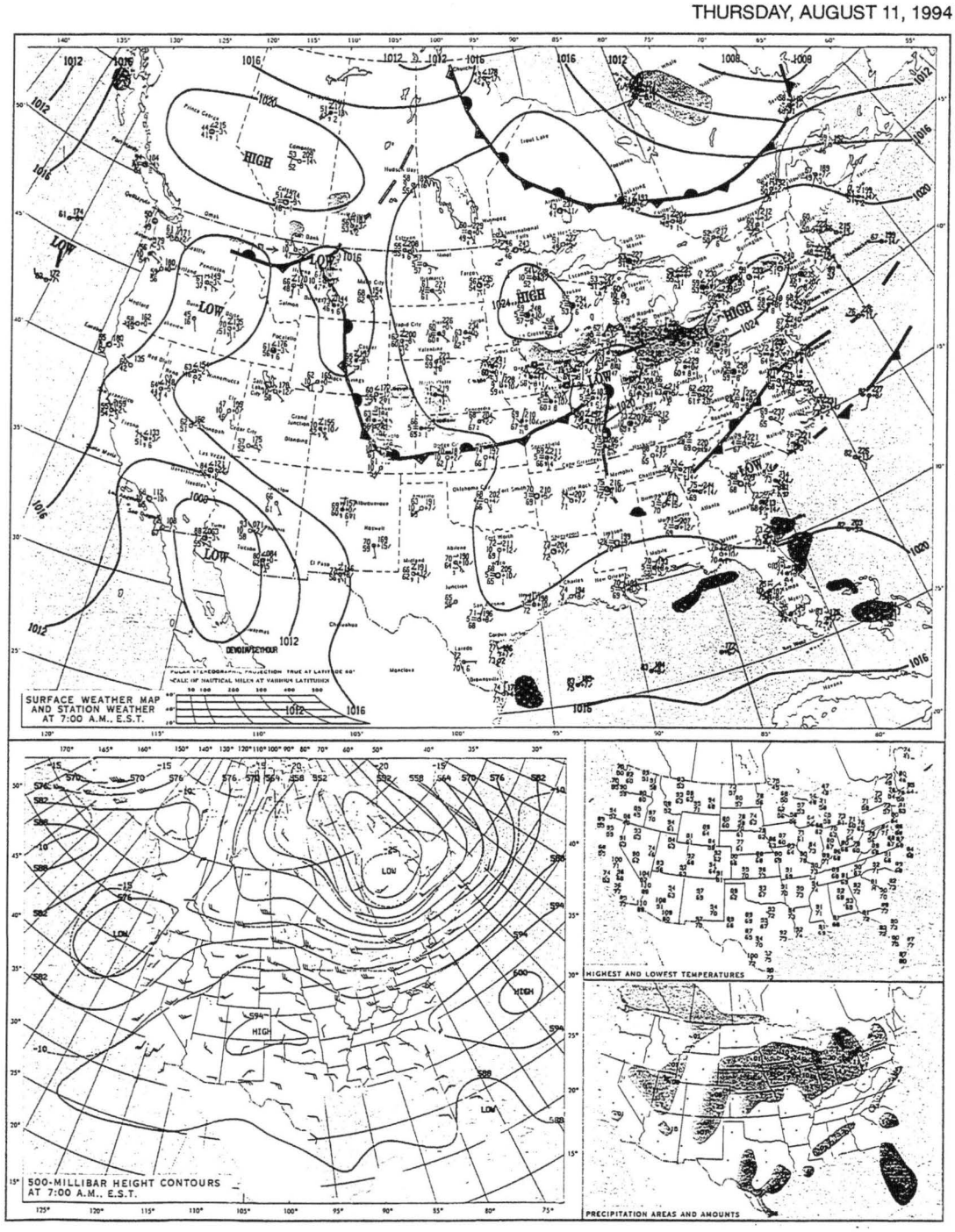

Figure 3.8 Daily weather map for 11 August 1994. Containing 11/1200 UTC August 1994 surface weather map and 500 mb height contours. (NOAA)

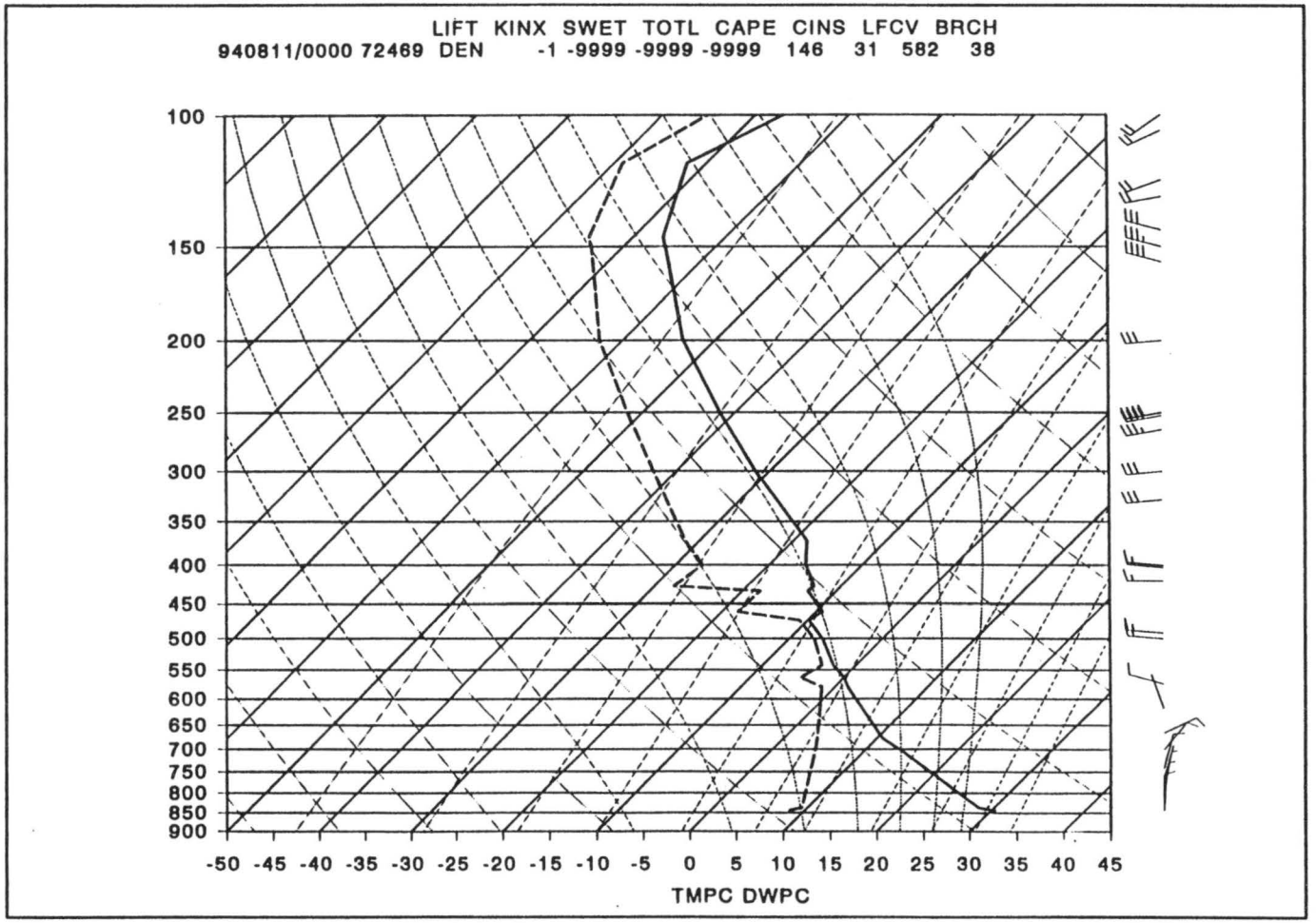

Figure 3.9 11 August 1994 Denver, CO 0000 UTC sounding.

CHAPTER IV

METHODS

4.1 RADAR DATA PROCESSING

4.1.1 WSR-88D Level II to UF Format Conversion

The WSR-88D Level II data was converted to standard UF format data using the Texas A&M program NEX2UF.

4.1.2 Ground Clutter and Bad Data Removal

NCAR's Radar Data Support System (RDSS) (Oye and Carbone, 1981) was used to threshold the radar data, and remove foothill ground clutter and suspect or bad data. Reflectivity values of less than 0.01 dBZ were removed from KFTG data and the CHILL data. For the CHILL radar data, any data with correlation coefficients less than 0.7 were also removed. ρ_{HV} values greater than 0.6. (Balakrishnan and Zrni'c, 1990) represent regions of high signal to noise ratios and valid hydrometeor signatures. The threshold was raised to 0.7 to better eliminate foothill ground clutter. From Balakrishnan and Zrni'c's paper, by raising the threshold to 0.7, there is the potential of eliminating valid cases of 5 cm (2 in.) or greater size hail and/or cases hail with large protuberance. Neither of the case study days using the CHILL had any hail reported greater than one inch in diameter. Therefore, the higher threshold value of 0.7 is considered valid.

4.1.3 Infinite Impulse Response Smoothing and K_{DP} calculation (CHILL)

CSU's Electrical Engineering Department's computer program, MPLT, was used to compute the specific differential phase field from the CHILL data. The MPLT program's original range limit of 80 km was expanded to compute the specific differential phase out to 120 km, since the gage networks reached to 120 km from the radar. This program uses the differential phase and correlation coefficients to compute the range derived differential phase, or specific differential phase. Before the program does this computation, the program passes the radar data through an Infinite Impulse Response filter as described in Hubbert et al. (1993), which smoothes the data from the 150 m gate spacing to a resolution of 250 m. The MPLT program produces smoothed fields of specific differential phase. After running the CHILL data through MPLT, the data had to be passed through RDSS to remove below threshold data as specified above, due to the smoothing process introduction of below threshold values.

4.1.4 Conversion to Cartesian Grids

National Center for Atmospheric Research's (NCAR) program REORDER was used to produce Cartesian coordinate constant altitude horizontal cross section. A Cressman interpolation technique (Cressman, 1959) was used to interpolate the polar coordinate (range, azimuth and elevation angles) to a three dimensional Cartesian grid (Mohr and Miller, 1983; Mohr et al., 1981). REORDER allows two methods to determine the radius of influence, fixed and variable. Using the fixed method, one specifies the desired Δx, Δy, and Δz used to define the radii of influence about each grid point. The variable method

requires an azimuth and an elevation angle to be specified. The azimuth and elevation angles, along with the range, are used to compute the resulting Δx, Δy, and Δz used to define the radii of influence for each grid point. The variable method allows the resulting radii of influence to expand in range, just as the radar sample volume expands due to beam spreading. The variable method was selected to convert the radar data to Cartesian coordinates using 0.75 degrees for the azimuth and elevation angles for the CHILL radar data and for the KFTG, 1.0 degree was used for the azimuth and elevation angles. After reviewing the results of a variety of fixed and variable values, the azimuth and elevation angle values selected most closely compared with the initial data across the region of interest as displayed by RDSS. A grid resolution (Δx, Δy) was chosen to be 0.5 km at a 0.5 km constant altitude height above the selected radar. The program CED2CDF was used to convert the REORDER produced CEDRIC files (Mohr and Miller, 1983), to a more universal netCDF file format (Rew and Davis, 1990)

4.1.5 Computation of Rain Rates

For each grid point and every volume of radar data, a rain rate was computed and a valid time period established. The valid time period for each rain rate was the midpoint between radar's time stamp for every grid point. These rain rates were then averaged into fifteen and five-minute time blocks for each rain rate used. From the KFTG data, the default NEXRAD Z-R relationship (equation 2.8) was computed imposing three reflectivity cut off values, 53, 55, and 57 dBZ. From the CHILL data, the $R(K_{DP})$ relationship (equation 2.11) was computed. The fifteen-minute radar-derived precipitation was then accumulated for the specific case study day's period of study for total areal

coverage plots. Special consideration was given to the grids containing missing data values introduced by the thresholding process as discussed above. If there was not at least one valid scan during the fifteen-minute interval, that fifteen-minute interval was assigned a missing value. For the 20 June, the CHILL scan volume's azimuth range only covered a select portion of the region of study. This created gaps in the data during some point of the four-hour period of study. Therefore, any fifteen-minute interval considered missing was ignored in the accumulated precipitation value. On the other two case study days, 21 June 1994 and 10 August 1994, since the period of study were shorter, one and two hours respectively, if one fifteen-minute interval accumulation grid point value was missing, the entire period of study's accumulation for that grid point was assigned as missing.

For each case study day, for each rain rate calculated, the gridded time period storm totals were plotted and overlaid with rain gage accumulations for the same time periods. The minimum contour selected was 0.25 cm (0.10 in.) of precipitation. For gage to radar-derived precipitation comparison, the closest four grid point values around the gage location where inversely weight averaged according to the distance from the gage location. The product of this weight average was the radar-derived precipitation to compare to the gage value.

For the time series plots, only the closest grid point's data to the gage were used for comparison to the gage data. The three WSR-88D cut off rain rates and the $R(K_{DP})$ (CHILL data only) were used in the time series comparison. In the time series plots, periods of missing data are identified by a dotted line between time intervals.

CHAPTER V

ANALYSIS

5.1 20 JUNE 1994

5.1.1. Gage versus Radar Derived Precipitation

5.1.1.1 R(KDP) -- CHILL

The areal coverage of R(KDP) is depicted in figure 5.1 with gage precipitation overlaid in bold (gage site is located at lower left of label) for the four-hour period of study. R(KDP) shows many distinct regions of local precipitation maxima. Three such regions of local maxima occurred near rain gages. These gage sites were the Fort Collins mesonet site (FOR) at x, y coordinate (-42, 16) with 7.77 cm accumulated precipitation, the NCWCD Loveland site (LOVE) at x, y coordinate (-40, -4) with 6.67 cm accumulated precipitation, and the UDFCD station 1110 at x, y coordinate (-46, -41) with 4.78 cm accumulated precipitation. The respective R(KDP) precipitation values were 8.45, 7.71, and 2.63 cm.

Figure 5.2 shows the gage versus R(KDP) derived precipitation scatter diagram on a log-log plot. The solid line shows 1:1 gage to R(KDP) ratio, and the dotted lines show the 2:1 and 1:2 gage to R(KDP) ratios. The diagram shows a general R(KDP) overestimate in gage precipitation less than 1.5 cm and a slight underestimate greater than 1.5 with the FOR and LOVE sites being the exception. Figure 5.3 and table A.1 shows

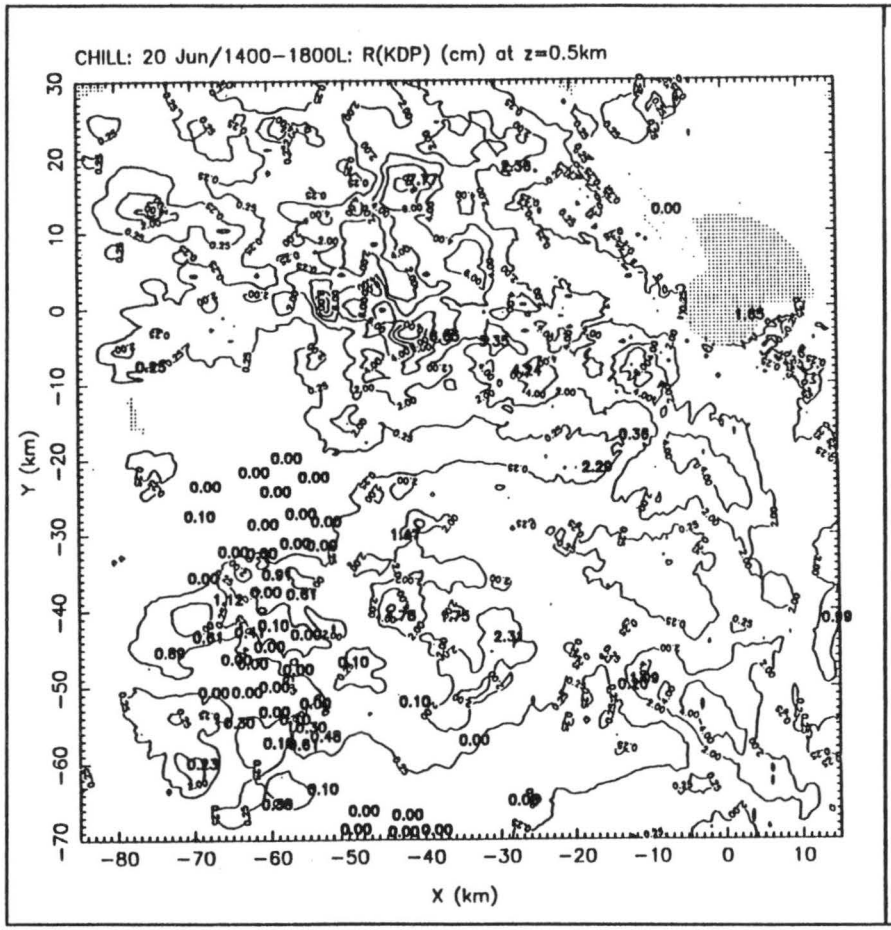

Figure 5.1 Areal Coverage of R(KDP) from 14:00 to 18:00 MDT on 20 June 1994. Contours labeled are 0.25, 2, 4, 6, 8, 10, and 12 cm. Gage precipitation for same period is shown in bold. Gage location is at lower left of label.

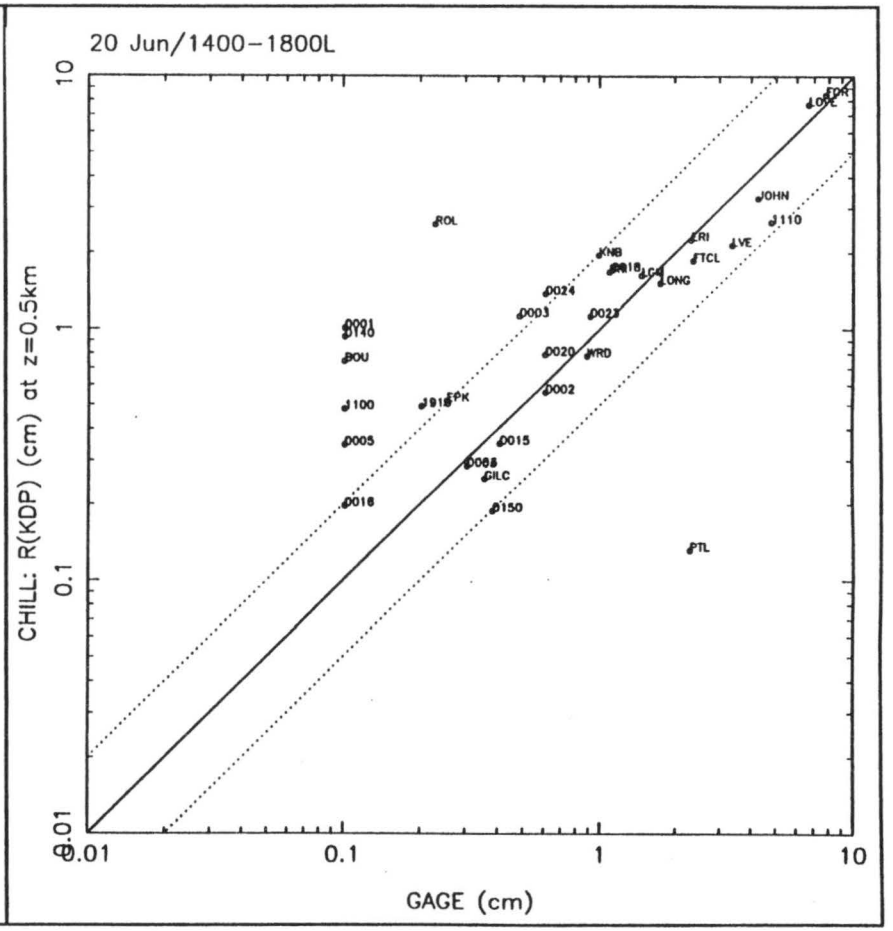

Figure 5.2 Scatter diagram of gage versus R(KDP) precipitation from 14:00 to 18:00 MDT on 20 June 1994. All units are in cm. Solid line represents a 1:1 correspondence, dotted lines represents 2:1 and 1:2 correspondence.

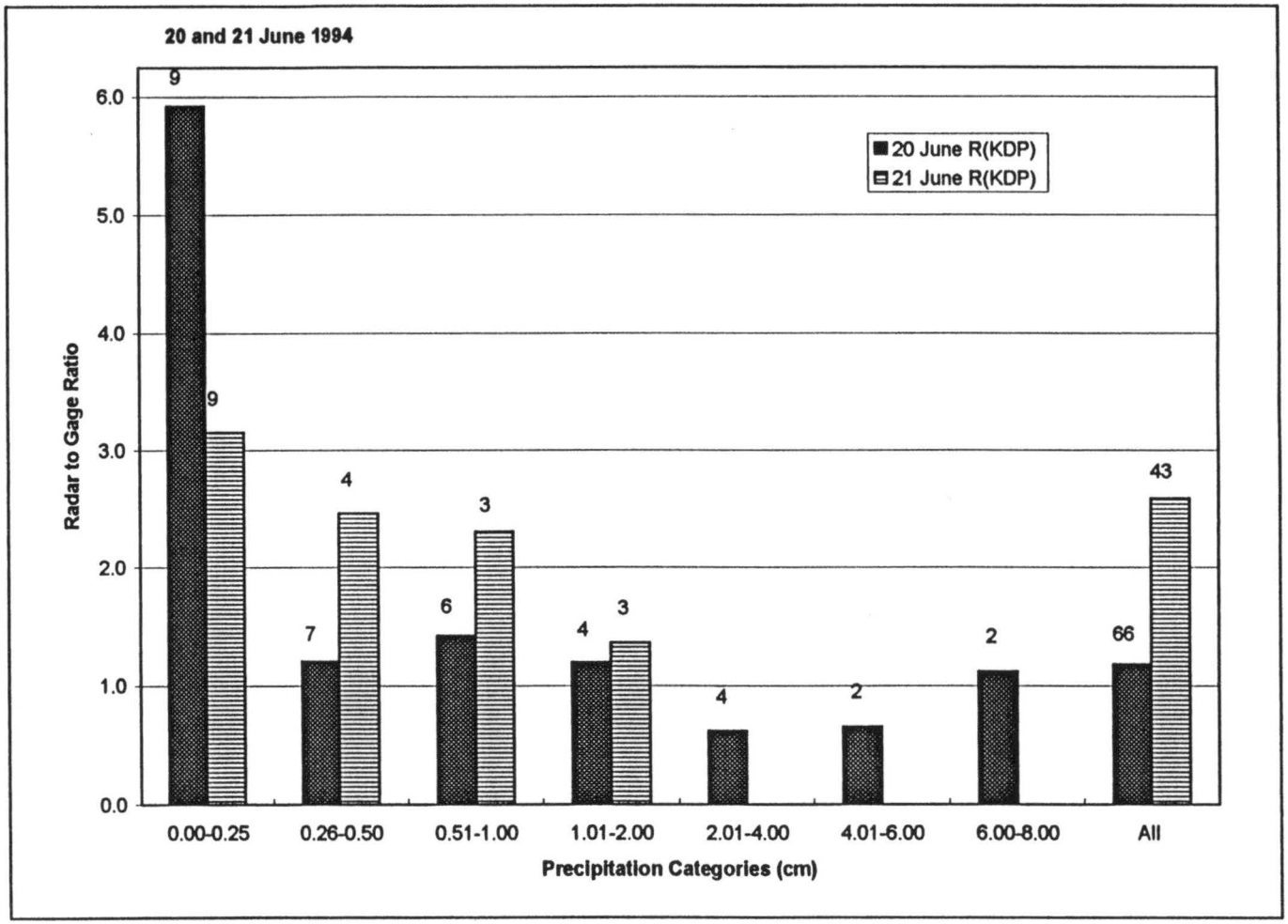

Figure 5.3 Average R(KDP) to gage precipitation ratios for ranges of gage values and all gages for 20 and 21 June 1994. Numbers at top of columns represents number of values in category.

average R(KDP) to gage ratios for all gages and ranges of gage values. These charts show and quantify the R(KDP) overestimate in comparison to gage precipitation less than 1.5 cm and underestimate in moderate precipitation between 2 and 4 cm. R(KDP) shows a good approximation for heavy precipitation, a low 12 percent overestimate. This result is not surprising. Sachidananda and Zrni'c (1986), Chandrasekar et al. (1990) and Rhyzhov and Zrni'c (1995), all declare K_{DP}'s usefulness in heavy precipitation and its inapplicability in low rain rate conditions. For all gages, the R(KDP) averages to an 18 percent overestimate of the gage precipitation.

5.1.2 Time Series Analysis

5.1.2.1 Station FOR

Figure 5.4 shows the five-minute precipitation time series for the FOR rain gage and R(KDP) derived precipitation for the four-hour period. There is an unexplained 10 to 15 minute time offset between the gage and radar time series. The time problem has not been resolved and potentially is related to a clock problem or the data processing method. Aside from this offset, the gage and R(KDP) precipitation compares well in time. The R(KDP) shows a slight overestimate to the gage in the first peak about 14:20 MDT and a slight underestimate of the two secondary peaks at 15:00 and 15:20 MDT. Recall, this day had 30 minutes of 1 cm hail reported less than 0.5 km from this gage beginning just after 14:00 MDT. This result demonstrates K_{DP}'s ability to accurately measure precipitation in mixed phase precipitation.

Figure 5.5 shows the accumulated precipitation in time for the same precipitation time series and four-hour period. Besides the 10-15 minute offset, the accumulated

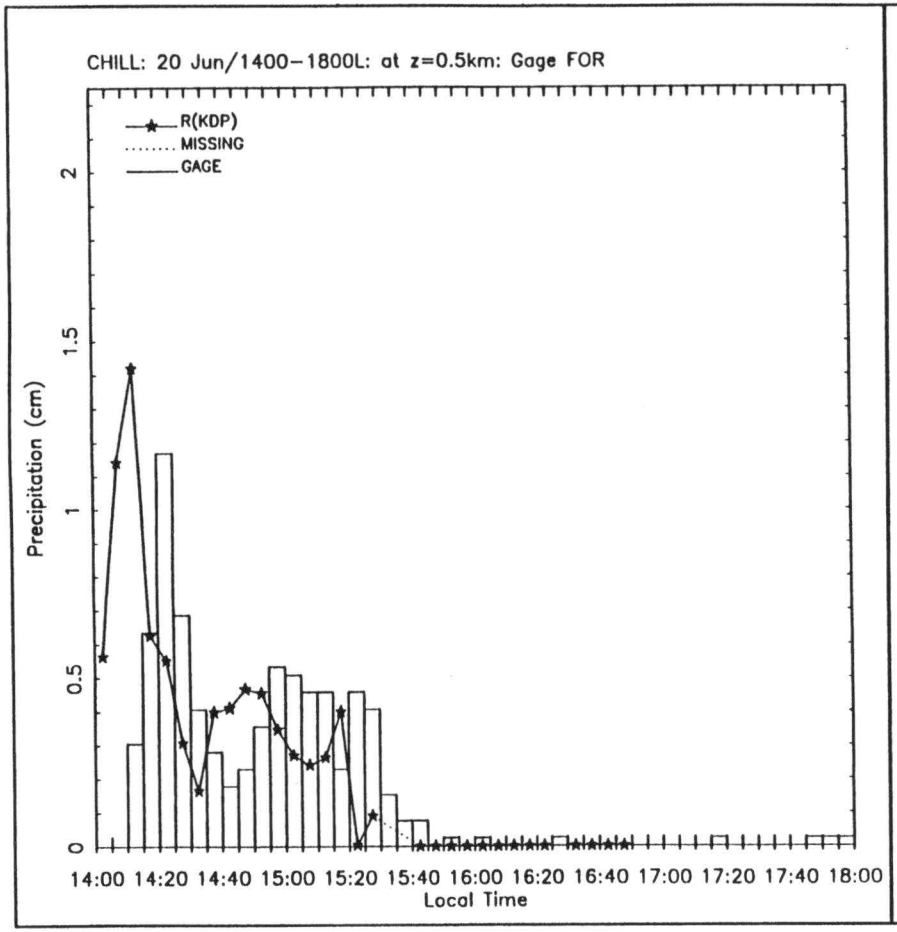

Figure 5.4 Five minute precipitation time series for gage and R(KDP) from 14:00 to 18:00 MDT on 20 June 1994 for station FOR.

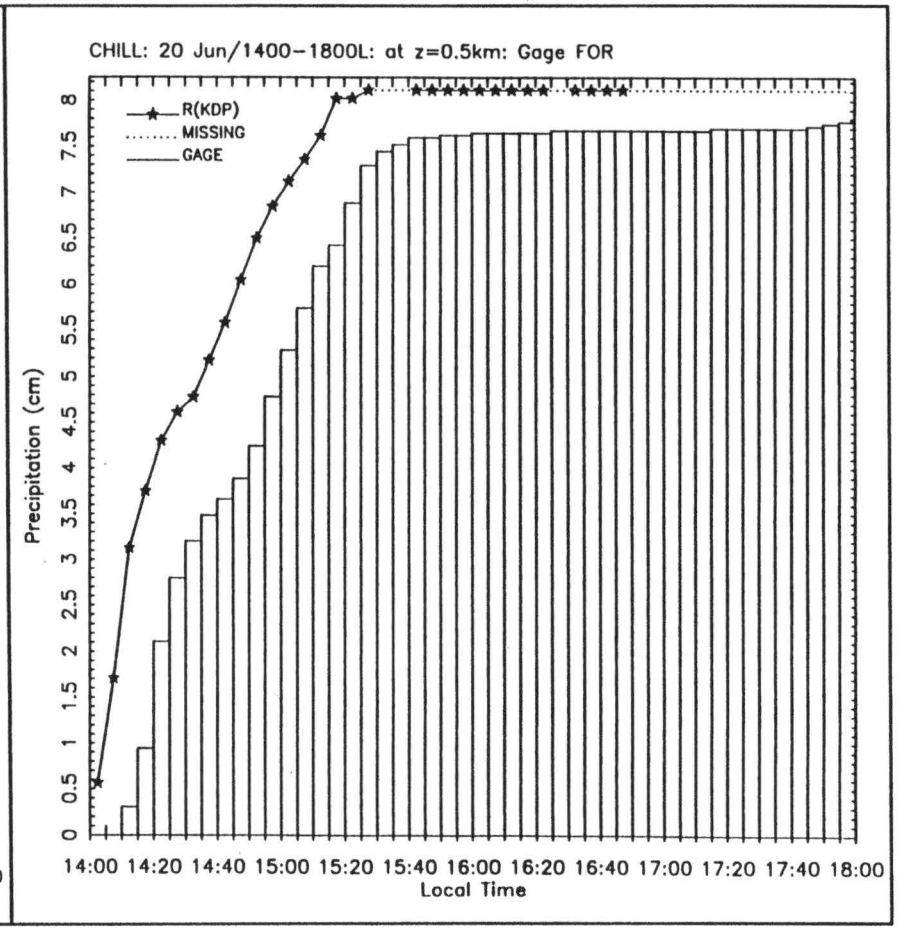

Figure 5.5 Five minute precipitation accumulations time series for gage and R(KDP) from 14:00 to 18:00 MDT on 20 June 1994 for station FOR.

precipitation shows how the R(KDP)'s initial overestimate is carried through the time series and never recovers, for an overall R(KDP) overestimate for this site.

5.1.2.2 Station LOVE

Figure 5.6 shows the 15-minute time series for the LOVE rain gage and R(KDP) derived precipitation for the four-hour period. Again the 10-15 minute time offset is present. Aside from the offset, the time series depicts the precipitation event well. The R(KDP) again overestimates the gage's first precipitation peak at 15:00 MDT, this time by almost 1 cm of precipitation. The R(KDP) does show the weak secondary maximum, but slightly underestimates the amount.

The accumulated precipitation for the gage and R(KDP) for the same time period is shown in figure 5.7. Similar to FOR accumulated precipitation, the R(KDP) overestimated the initial peak of gage precipitation and never recovered, resulting in a time period overestimation for LOVE.

5.1.2.3 Station 1110

Figure 5.8 shows the precipitation time series for gage 1110 and R(KDP) for the four-hour period. Unlike FOR and LOVE, R(KDP) did not compare well with the gage precipitation. The 10-15 minute time offset is not as apparent as in the previous two sites. The gage data shows one large precipitation peak with a maximum 5-minute total of 1.98 cm event centered about 16:40 MDT, with a secondary peak of two 0.21 5-minute totals around 17:05 MDT. There is a lapse in gage precipitation until the period beginning 17:30 MDT for a 5-minute total of 0.10 cm. R(KDP) shows the majority of precipitation falling in two peaks. If a 10-minute offset is applied, R(KDP) grossly

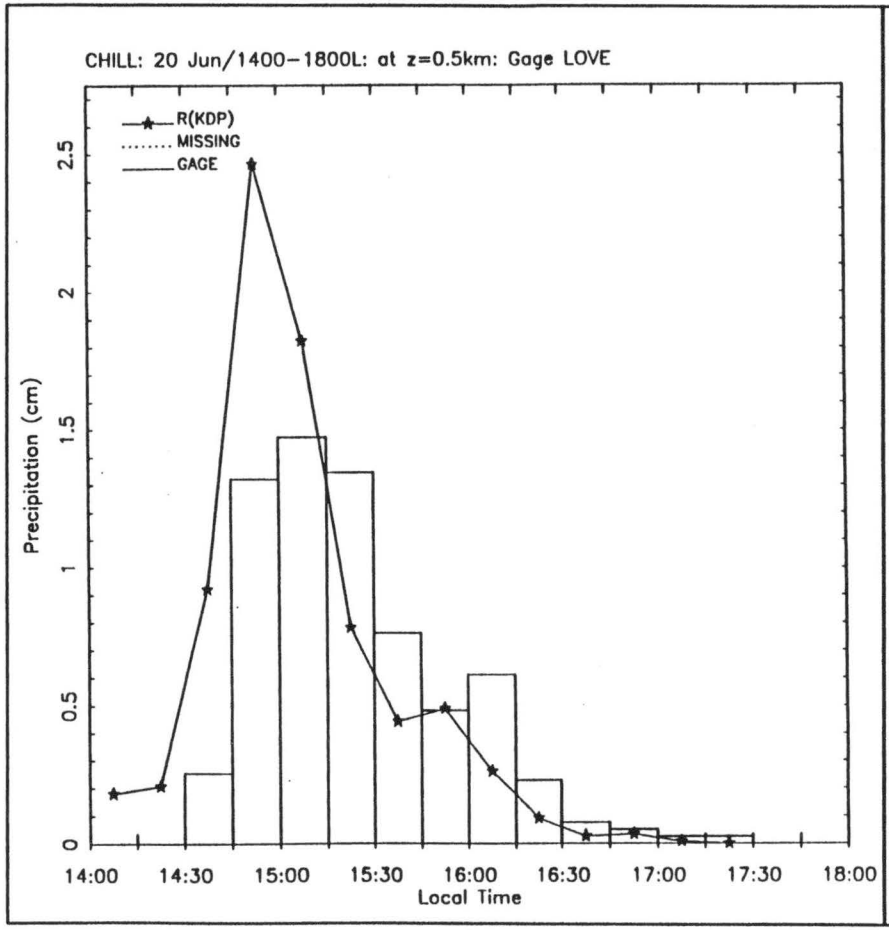

Figure 5.6 Fifteen minute precipitation time series for gage and R(KDP) from 14:00 to 18:00 MDT on 20 June 1994 for station LOVE.

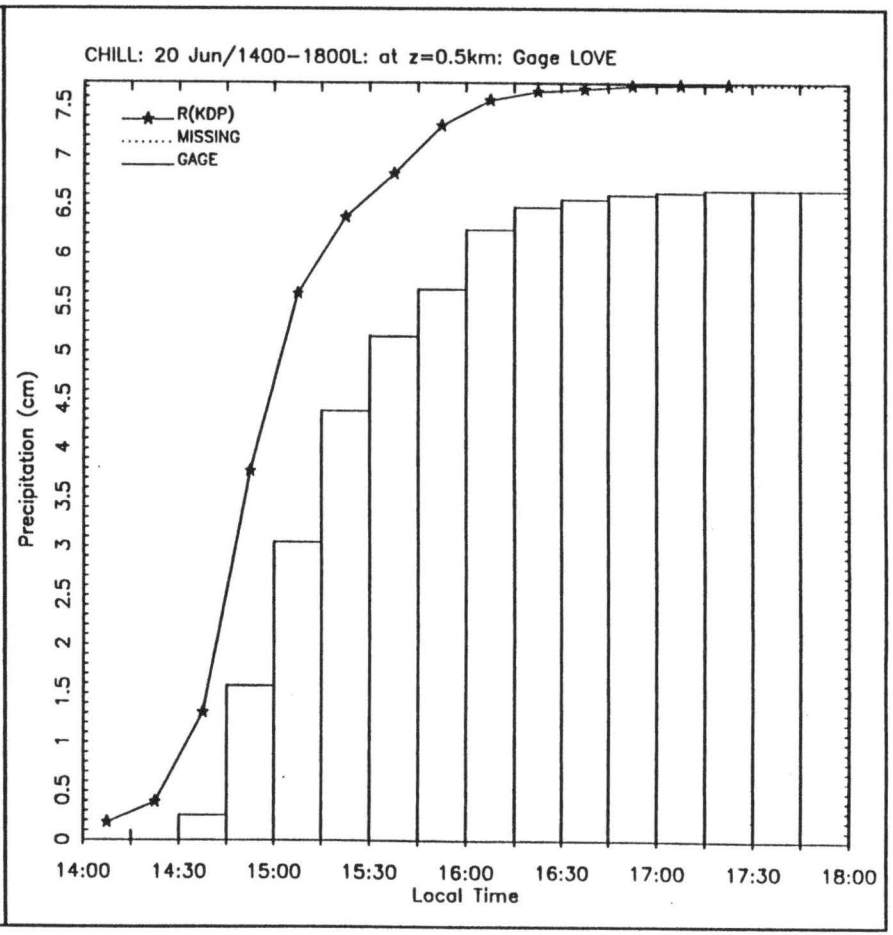

Figure 5.7 Fifteen minute precipitation accumulations time series for gage and R(KDP) from 14:00 to 18:00 MDT on 20 June 1994 for station LOVE.

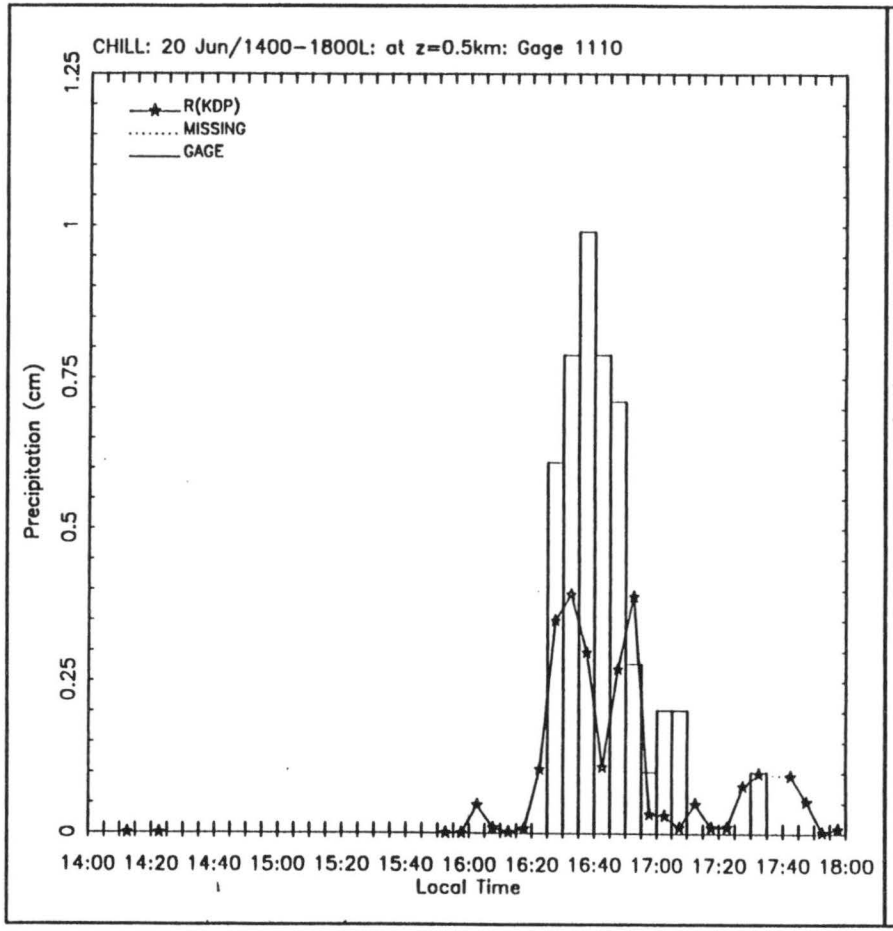

Figure 5.8 Five minute precipitation time series for gage and R(KDP) from 14:00 to 18:00 MDT on 20 June 1994 for station 1110.

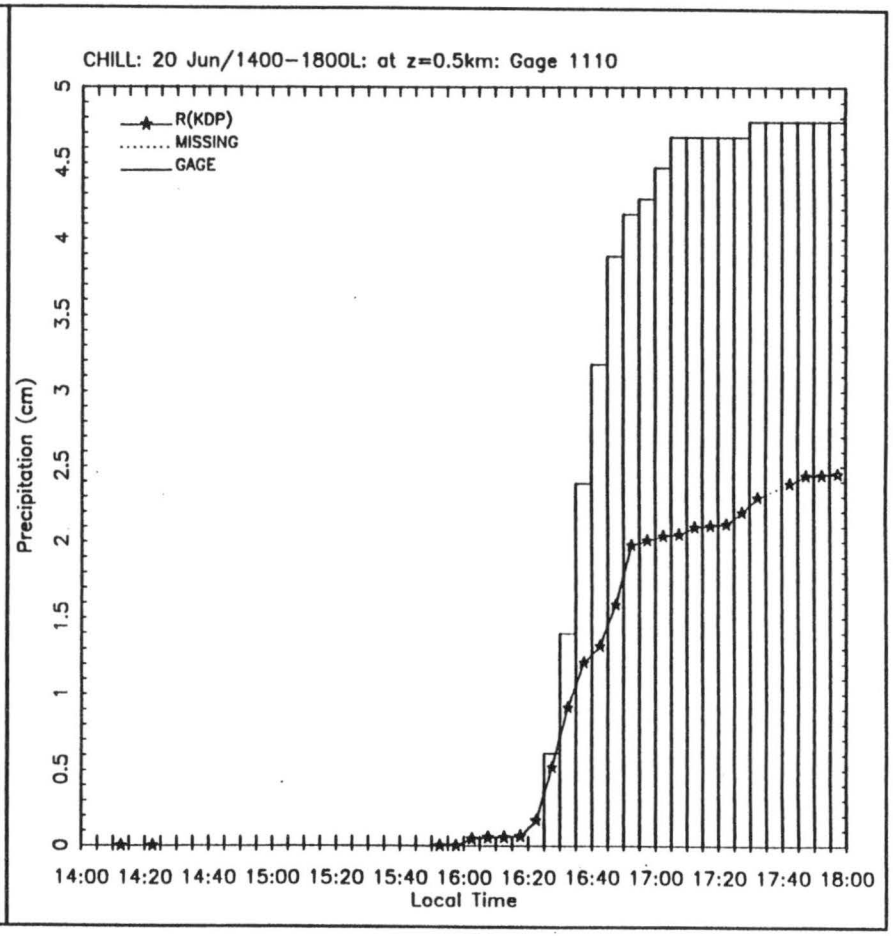

Figure 5.9 Five minute precipitation accumulations time series for gage and R(KDP) from 14:00 to 18:00 MDT on 20 June 1994 for station 1110.

underestimated the gage's primary 16:40 MDT precipitation peak and slightly overestimated the gage's secondary peak at 17:05 MDT. The R(KDP) derived precipitation also shows a tertiary maximum precipitation peak around 17:35 MDT.

The accumulated precipitation time series for this period (figure 5.9) shows how R(KDP) underestimated the precipitation by nearly a factor of two. The cause for this underestimate in R(KDP) was due to R(KDP)'s large underestimate during the heaviest period of precipitation.

5.2 21 JUNE 1994

5.2.1 Gage vs. Radar Derived Precipitation

5.2.1.1 R(KDP) - CHILL

The areal coverage of R(KDP) derived precipitation with gage precipitation overlaid for the one-hour time period is shown in figure 5.10. The areal coverage of R(KDP) precipitation shows one major core of the heaviest precipitation in the vicinity of x, y coordinate (-71, -49) with a closed contour of 5 cm. The gage closest to this core of significant precipitation was UDFCD station 2010 at x, y coordinate (-70, -51) which reported 1.98 cm of precipitation. Another local R(KDP) maximum of 2 cm occurred near UDFCD station 0018 at x, y coordinate (-69, -40) with 1.22 cm of precipitation reported. Between these two local R(KDP) maximums was UDFCD station 0024. 0024 is located at x, y coordinates (-71, -44) and observed 1.22 cm of precipitation. Table 5.1 shows the R(KDP) derived precipitation values for these three stations.

Figure 5.11 shows the scatter diagram of gage versus R(KDP) derived precipitation for the same one-hour period. The figure shows R(KDP) generally overestimated gage

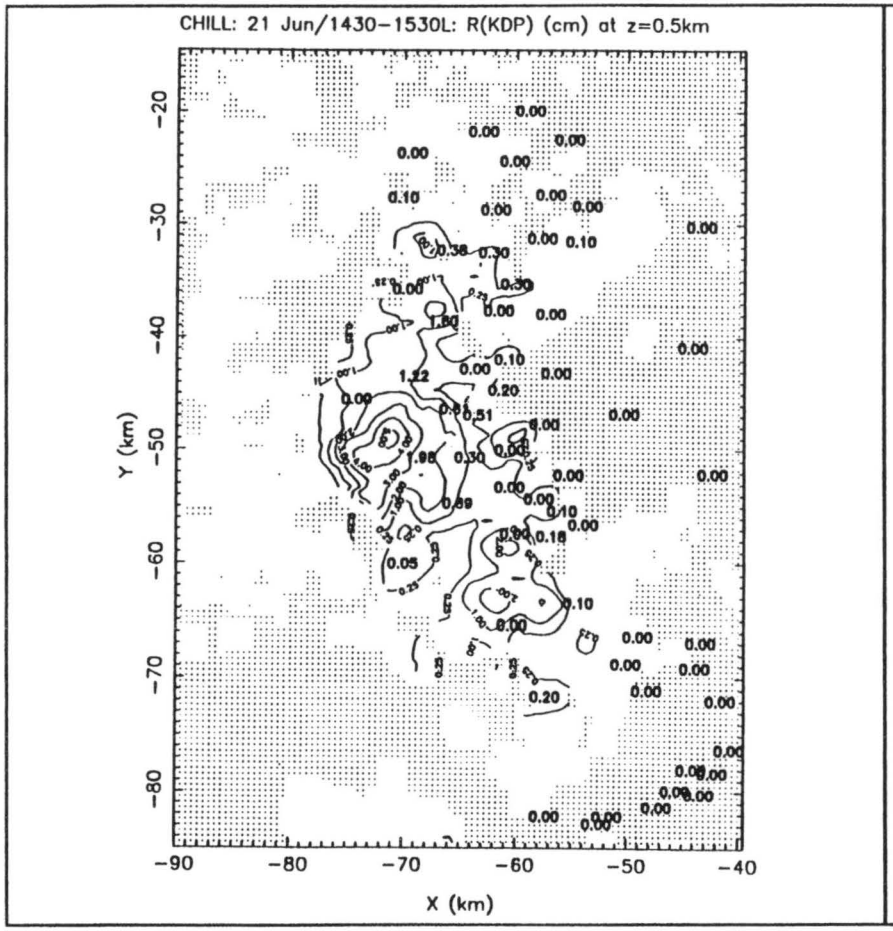

Figure 5.10 Areal Coverage of R(KDP) from 14:30 to 15:30 MDT on 21 June 1994. Contours labeled are 0.25, 1, 2, 3, 4, 5, 6, 7, and 8 cm. Gage precipitation for same period is shown in bold. Gage location is at lower left of label.

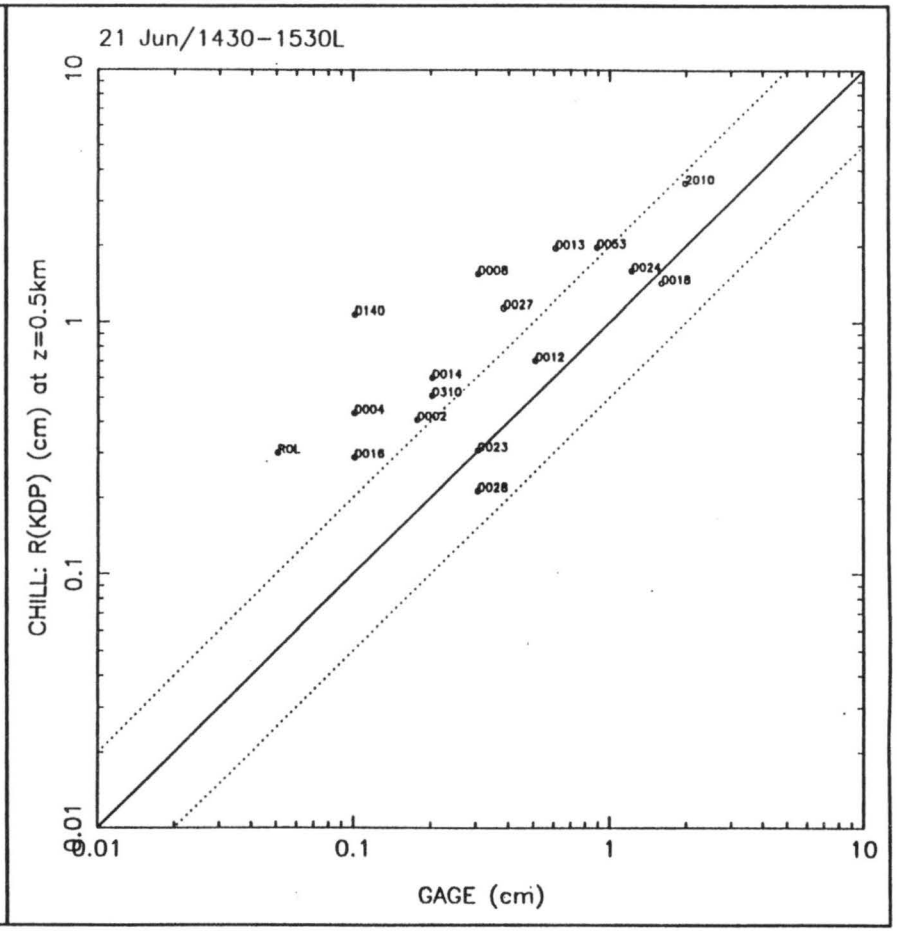

Figure 5.11 Scatter diagram of gage versus R(KDP) precipitation from 14:30 to 15:30 MDT on 21 June 1994. All units are in cm. Solid line represents a 1:1 correspondence, dotted lines represents 2:1 and 1:2 correspondence.

Table 5.1 Gage Versus Radar Derived Precipitation for Three Stations on 21 June 1994.

Station:	2010	0018	0024
GAGE (cm)	1.98	1.6	1.22
R(KDP) -- CHILL (cm)	3.54	1.42	1.59
R(NX57) -- KFTG (cm)	5.61	3.29	2.87
R(NX55) -- KFTG (cm)	5.23	3.29	2.87
R(NX53) -- KFTG (cm)	4.60	3.13	2.87
R(OSF) -- KFTG (cm)	3.30	1.37	2.57

precipitation. Figure 5.3 and table A.2 show the average R(KDP) to gage precipitation ratios for all gages and ranges of gage precipitation values. The high average R(KDP) to gage ratio in the lower range of gage precipitation values is primarily due to the questionable validity of the low values of K_{DP} values used and the resulting high bias. Since the precipitation for this day's period of study was generally of short duration and low intensity, the one-hour total has a higher percentage of low K_{DP} values used. The R(KDP) to gage ratio shows improvement with increasing amount of total precipitation.

5.2.1.2 R(NX57) - KFTG

The areal coverage of KFTG's R(NX57) with corresponding gage precipitation totals overlaid, is shown in figure 5.12. R(NX57) identifies three core regions of maximum precipitation. The highest core, hereafter referred to as region 1, is located in the vicinity of x, y coordinate (-72, -51) with a 6-cm closed contour. A second region of maximum precipitation (region 2) is defined as the area in the vicinity of x, y coordinate (-70, -38). This region of 3 cm of precipitation extends in an arc to the southwest to join region 1.

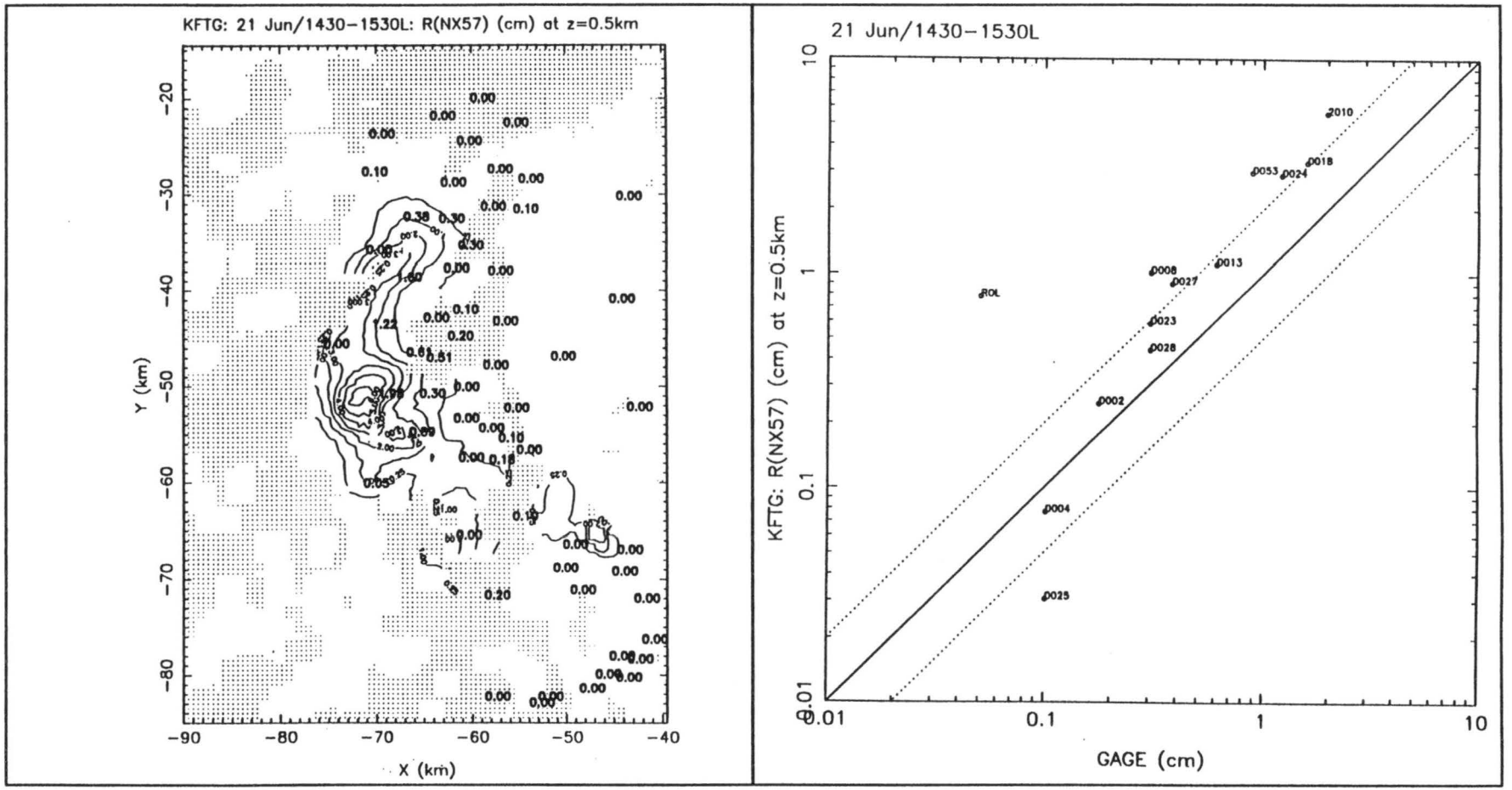

Figure 5.12 Areal Coverage of R(NX57) from 14:30 to 15:30 MDT on 21 June 1994. Contours labeled are 0.25, 1, 2, 3, 4, 5, 6, 7, and 8 cm. Gage precipitation for same period is shown in bold. Gage location is at lower left of label.

Figure 5.13 Scatter diagram of gage versus R(NX57) precipitation from 14:30 to 15:30 MDT on 21 June 1994. All units are in cm. Solid line represents a 1:1 correspondence, dotted lines represents 2:1 and 1:2 correspondence.

There is a third region (region 3) of maximum precipitation located in the vicinity of x, y coordinate (-46, -66). Unfortunately, there were no gages in this region for comparison. Table 5.1 gives R(NX57) derived precipitation values for stations 2010, 0018, and 0024.

The scatter diagram of gage versus R(NX57) for the same one-hour time period is shown in figure 5.13. This scatter diagram shows R(NX57) consistently overestimated the gage precipitation. Figure 5.14 and table A.3 gives the average R(NX57) to gage precipitation ratios for all gages and ranges of gage precipitation values. The average R(NX57) to gage ratio for all gages is 3.12 or R(NX57) overestimates the gage by an average 212 percent. The highest average overestimate (2.70) occurs in the 1 to 2 cm category.

5.2.1.3 R(NX55) -- KFTG

Figure 5.15 shows the areal coverage for R(NX55) derived precipitation overlaid with gage precipitation values in bold. In region 1, R(NX55) shows the area defined by the 6-cm contour has been reduced to just a point from the R(NX57)'s areal coverage. Reflectivity in region 2 never exceeded 55 dBZ resulting in no areal coverage differences between R(NX55) and R(NX57) derived precipitation. R(NX55) in Region 3, shows the R(NX57)'s 2 cm precipitation contour has been reduced to a much smaller area. R(NX55) precipitation values over the three gages, 2010, 0018, and 0024, are shown in table 5.1.

The scatter diagram for gage versus R(NX55) derived precipitation (figure 5.16) continues to show that R(NX55) grossly overestimated the gage precipitation. The only change from R(NX57)'s scatter diagram was station 2010's precipitation was reduced

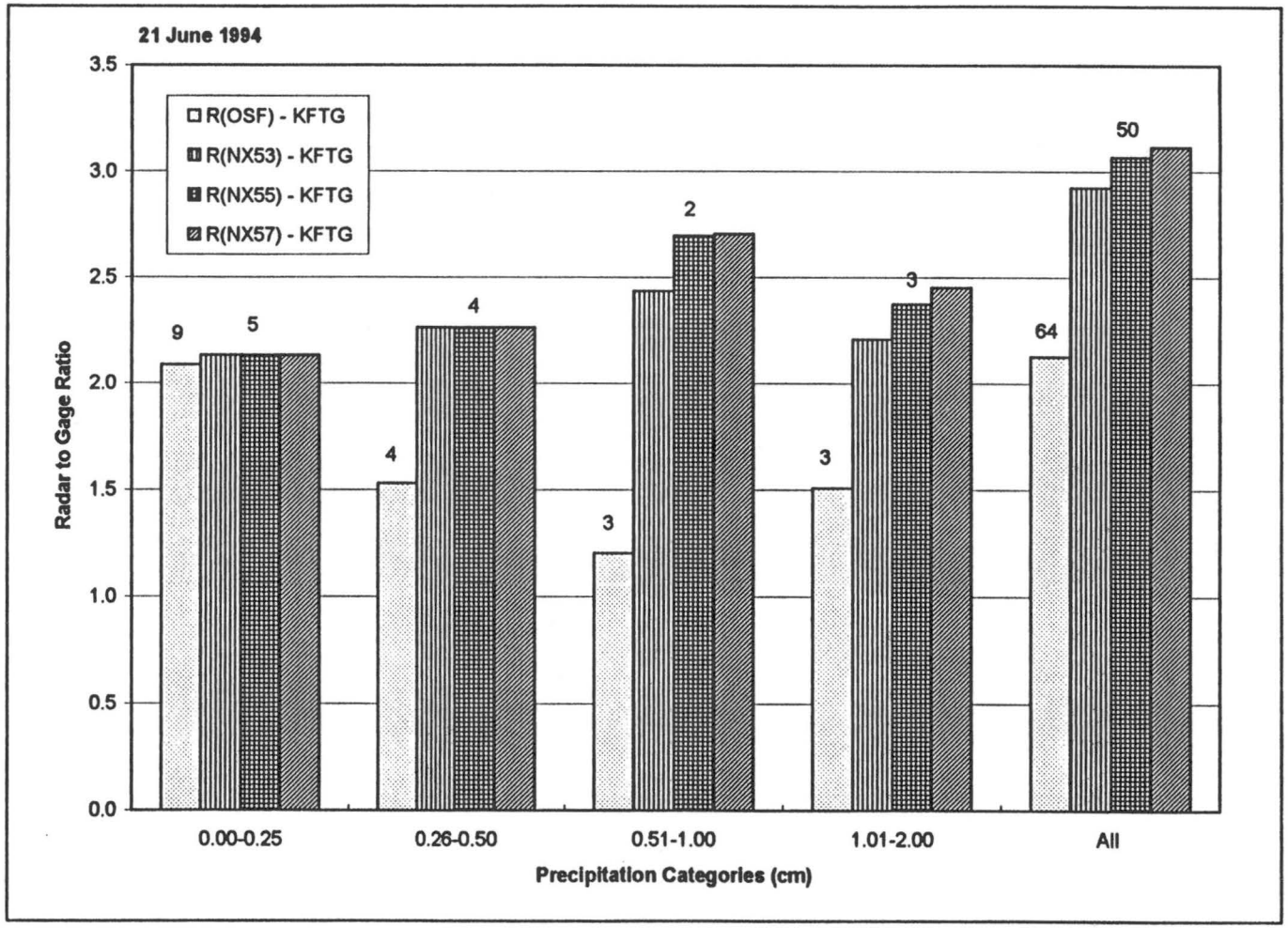

Figure 5.14 Average radar-derived to gage precipitation ratios for ranges of gage values and all gages for 21 June 1994. Numbers at top of columns represents number of values in category.

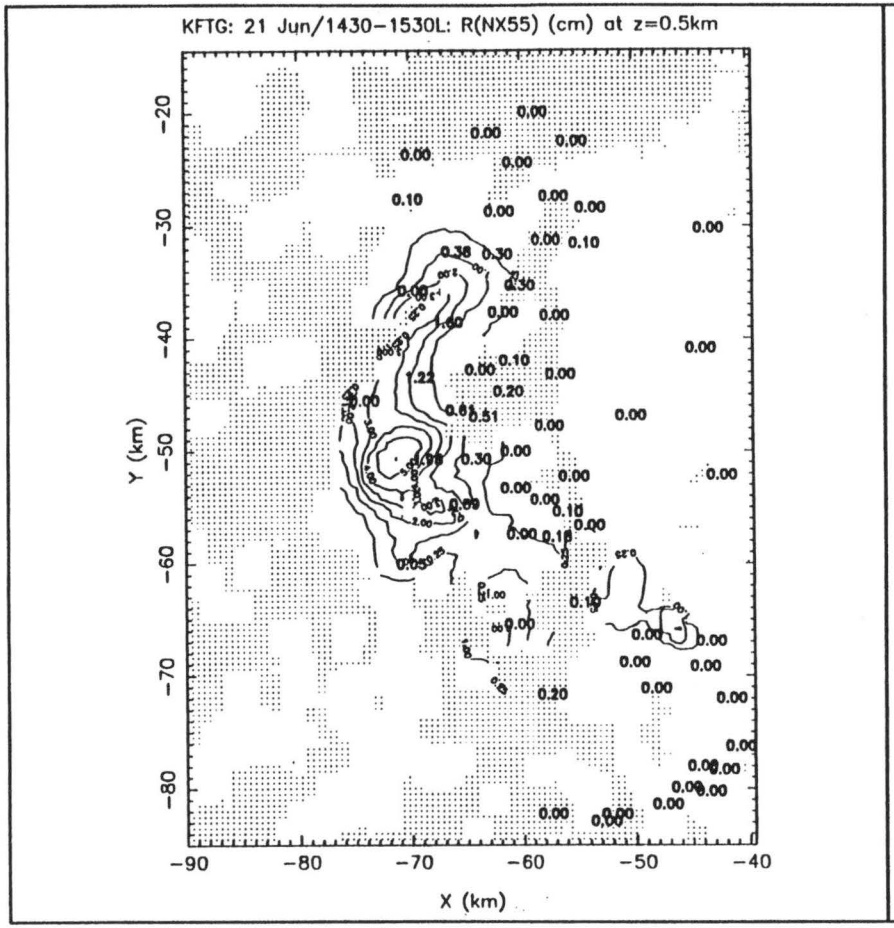

Figure 5.15 Areal Coverage of R(NX55) from 14:30 to 15:30 MDT on 21 June 1994. Contours labeled are 0.25, 1, 2, 3, 4, 5, 6, 7, and 8 cm. Gage precipitation for same period is shown in bold. Gage location is at lower left of label.

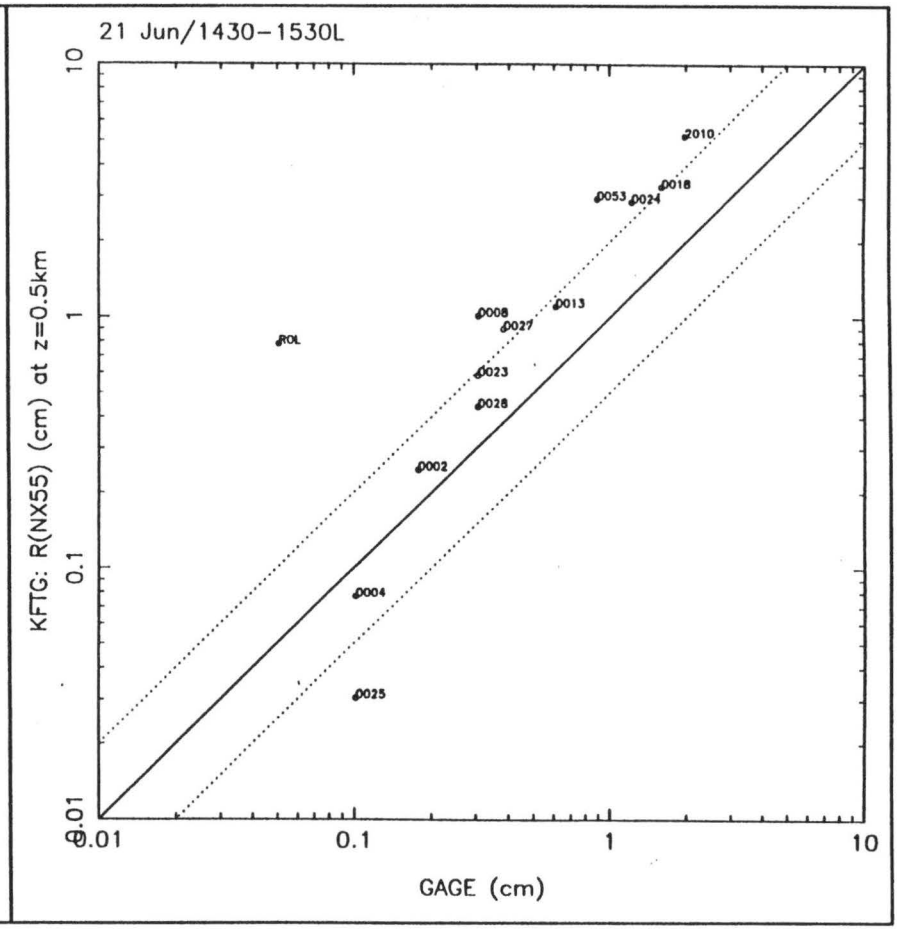

Figure 5.16 Scatter diagram of gage versus R(NX55) precipitation from 14:30 to 15:30 MDT on 21 June 1994. All units are in cm. Solid line represents a 1:1 correspondence, dotted lines represents 2:1 and 1:2 correspondence.

0.38 cm, due to the 2 dBZ reduction in the reflectivity cut off. Figure 5.14 and table A.4 gives the average R(NX55) to gage precipitation ratios for all gages and ranges of gage precipitation values. The average R(NX55) to gage ratio for all gages is 3.07 which shows a five percent drop from R(NX57) overestimate. The average R(NX55) to gage ratio for gages with precipitation shows an overestimate by a factor of 2.40. The 2 dBZ reduction from 57 dBZ has effected the ratios by reducing the 1 to 2 cm category by eight percent.

5.2.1.4 R(NX53) -- KFTG

Figure 5.17 shows the areal coverage of R(NX53) derived precipitation with gage precipitation overlaid for the one-hour period of study. Region 1 shows the most change from R(NX55)'s areal precipitation coverage, as the areas within the 5 and 4 cm contours have been greatly reduced. In region 2, the 3-cm precipitation contour has become a closed contour. In region 3, only a closed 1-cm contour remains. The R(NX53) precipitation values for stations 2010, 0018, and 0024 are listed in table 5.1.

The scatter diagram for gage versus R(NX53) scatter diagram (figure 5.18) shows three stations, 2010, 0018, and 0053, have been reduced by 0.63, 0.16, and 0.39 cm respectively, from the 2 dBZ reduction in reflectivity cut off. Figure 5.14 and table A.5 shows average R(NX53) to gage ratio for all gages and ranges of gage values. These charts quantitatively show how R(NX53) overestimates gage precipitation by a factor of 2.92. A general improvement in the ratios occurs with each decrement of the reflectivity cut off. The 2 dBZ reduction from the 55 to 53 dBZ shows its greatest influence in reducing the ratio in the 1 - 2 cm category.

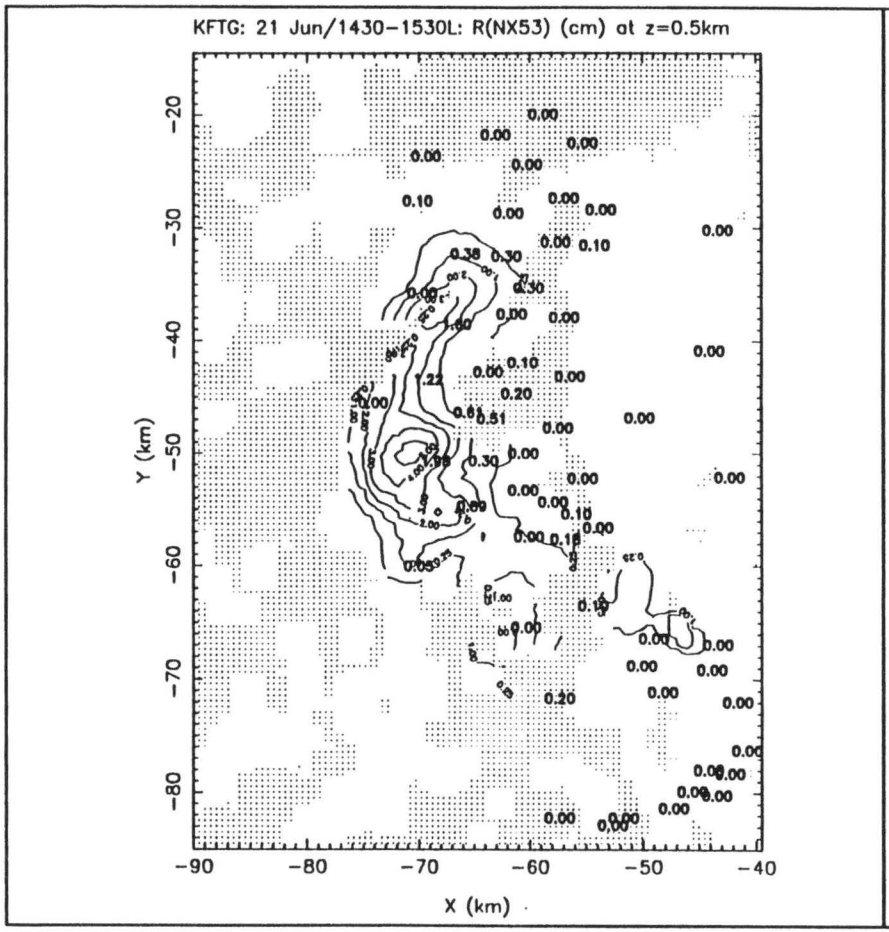

Figure 5.17 Areal Coverage of R(NX53) from 14:30 to 15:30 MDT on 21 June 1994. Contours labeled are 0.25, 1, 2, 3, 4, 5, 6, 7, and 8 cm. Gage precipitation for same period is shown in bold. Gage location is at lower left of label.

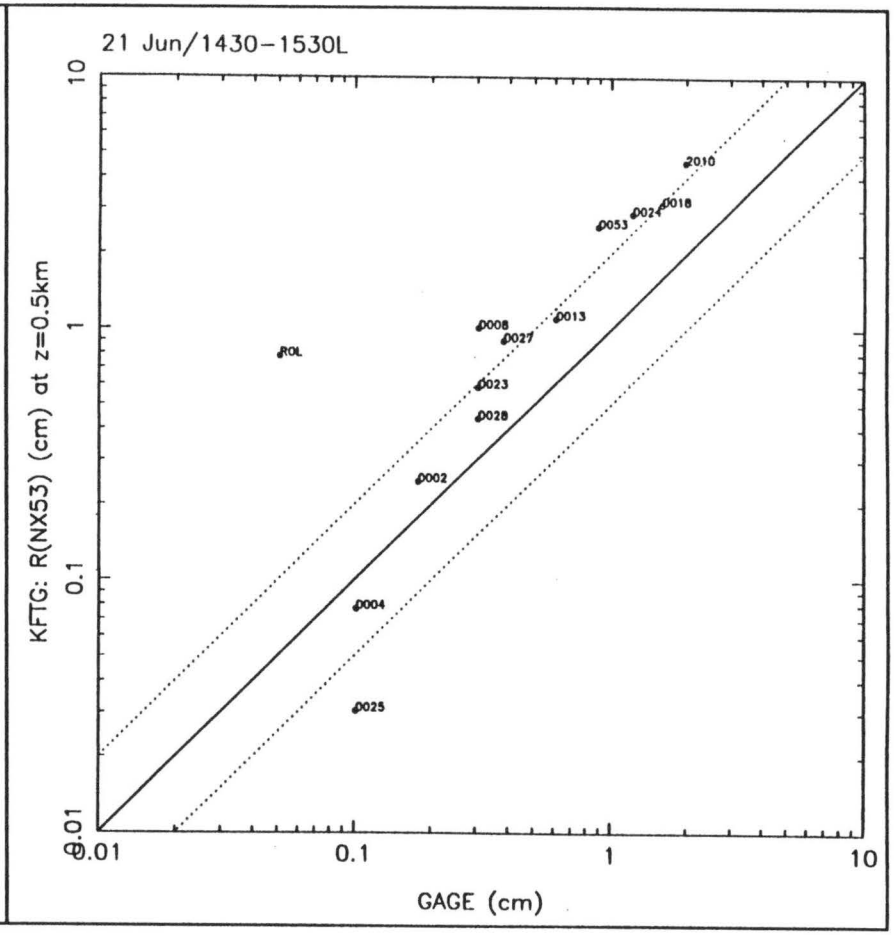

Figure 5.18 Scatter diagram of gage versus R(NX53) precipitation from 14:30 to 15:30 MDT on 21 June 1994. All units are in cm. Solid line represents a 1:1 correspondence, dotted lines represents 2:1 and 1:2 correspondence.

5.2.1.5 R(OSF) -- KFTG

Figure 5.19 shows the areal coverage of the precipitation from the WSR-88D algorithm as provided by OSF, with the corresponding gage precipitation totals in bold for the same one-hour period. The R(OSF) precipitation defines region 1's maximum precipitation contour as 4 cm as compared to the R(NX53) 5-cm maximum precipitation contour. R(OSF) also displaces the center of the maximum precipitation approximately 2.5 km to the southwest to x, y coordinate (-72, -51). Region 2's R(OSF) and R(NX53) areal coverage compares quite well with each other. R(OSF) does not show any enhanced local maximum in region 3. Finally, the R(OSF) areal coverage shows a region of 2 cm maximum precipitation in the vicinity of x, y coordinate (-63, -66). This region is an area of missing or invalid data for the R(NX53) precipitation, but there is a barely discernible 2-cm contour in the R(NX53) data in this region. The UDFCD gage 0150 is located at x, y coordinate (-62, -66), but detected no precipitation. Table 5.1 shows the R(OSF) precipitation values for stations 2010, 0018, and 0024.

The scatter diagram for gage versus R(OSF) derived precipitation (figure 5.20) continues to show that R(OSF) overestimated the gage precipitation, but not as bad as R(NX53). Figure 5.14 and table A.6 gives the average R(OSF) to gage precipitation ratios for all gages and ranges of gage precipitation values. The average for all gages shows that R(OSF) overestimated the gage precipitation by a factor of 2.13. For the gages with precipitation observed, the ratio improves to a 52 percent overestimation of the gage amounts. The ratios show a general improvement with increasing precipitation totals until the category greater than 2 cm.

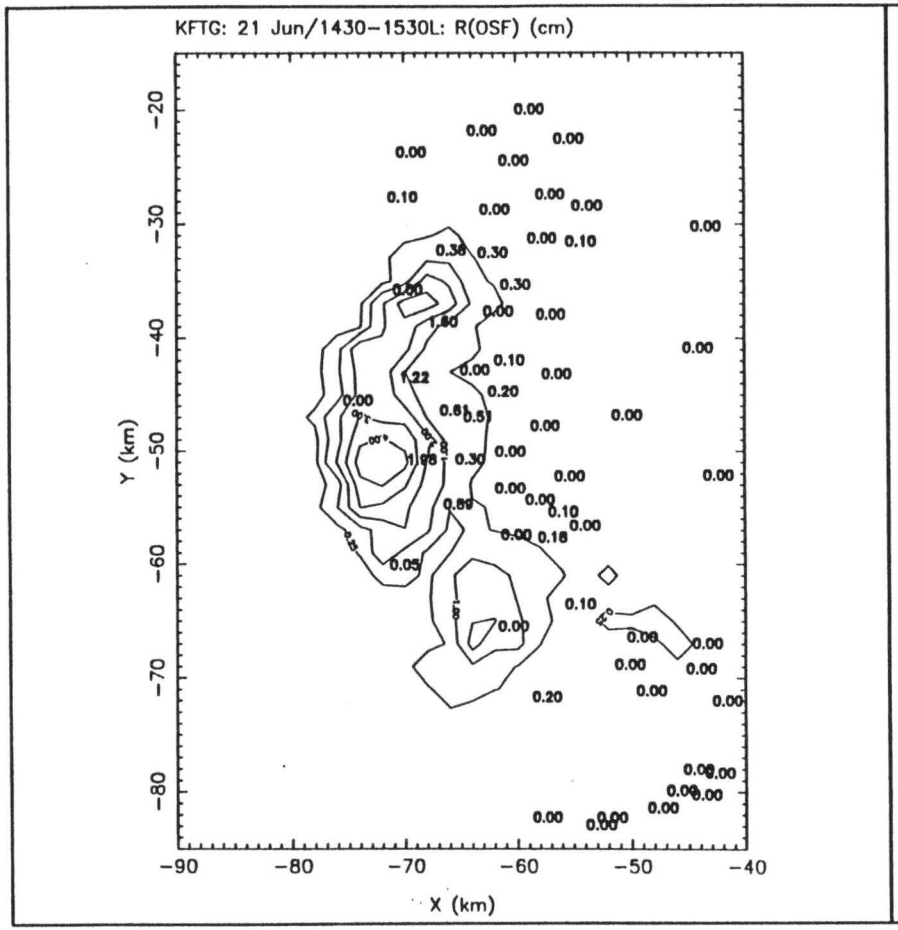

Figure 5.19 Areal Coverage of R(OSF) from 14:30 to 15:30 MDT on 21 June 1994. Contours labeled are 0.25, 1, 2, 3, 4, 5, 6, 7, 8 cm. Gage precipitation for same period is shown in bold. Gage location is at lower left of label.

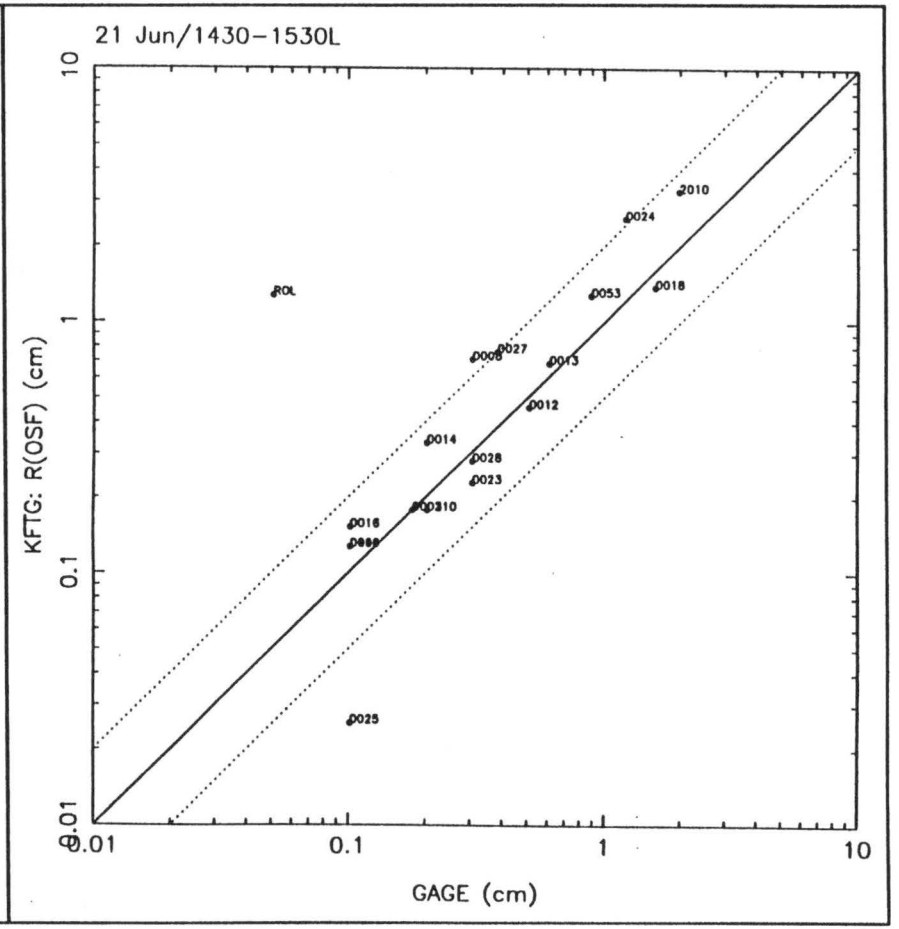

Figure 5.20 Scatter diagram of gage versus R(OSF) precipitation from 14:30 to 15:30 MDT on 21 June 1994. All units are in cm. Solid line represents a 1:1 correspondence, dotted lines represents 2:1 and 1:2 correspondence.

Figure 5.21 compares R(NX53) with R(OSF) derived precipitation. Essentially, this figure shows the differences of this study's approximation of the WSR-88D algorithm -- R(NX53), with the actual WSR-88D algorithm. The comparison shows a decent relationship between R(OSF) and R(NX53) with a R(NX53) bias to overestimate R(OSF) which has been shown in figure 5.14 and tables A.5 and A.6.

5.2.2 Time Series Analysis

5.2.2.1 Station 2010

Figure 5.22 shows the 5-minute precipitation time series for the 2010 rain gage and CHILL's R(KDP), and KFTG's R(NX57), R(NX55) and R(NX53) derived precipitation for the one-hour period. The gage time series shows light intermittent precipitation until 15:05 MDT. After which, moderate rain, 6 cm per hour, lasts for 15 minutes with light rain continuing to the end of the period. R(KDP) precipitation time series picked up the light intermittent precipitation as a minor local maximum at 14:15 MDT. R(KDP) continues to increase the precipitation until reaching a peak during the 15:05 period with almost twice the gage amount for this time period. R(KDP) then gradually decreases the precipitation through to the end of the one-hour period. R(KDP) generally captures the gage precipitation event better than R(NXxx) (xx refers to all three reflectivity cut off values). The R(NXxx) precipitation time series shows one broad region of increasing precipitation from 14:30 MDT, until the 15:00 time period where the R(NXxx) decreases precipitation through to the end of the one-hour period of study. The 5-minute time periods beginning 15:00 and 15:05 had averaged reflectivity greater than 55 dBZ and the time period beginning 15:10 MDT had an averaged reflectivity greater than 53 dBZ. The

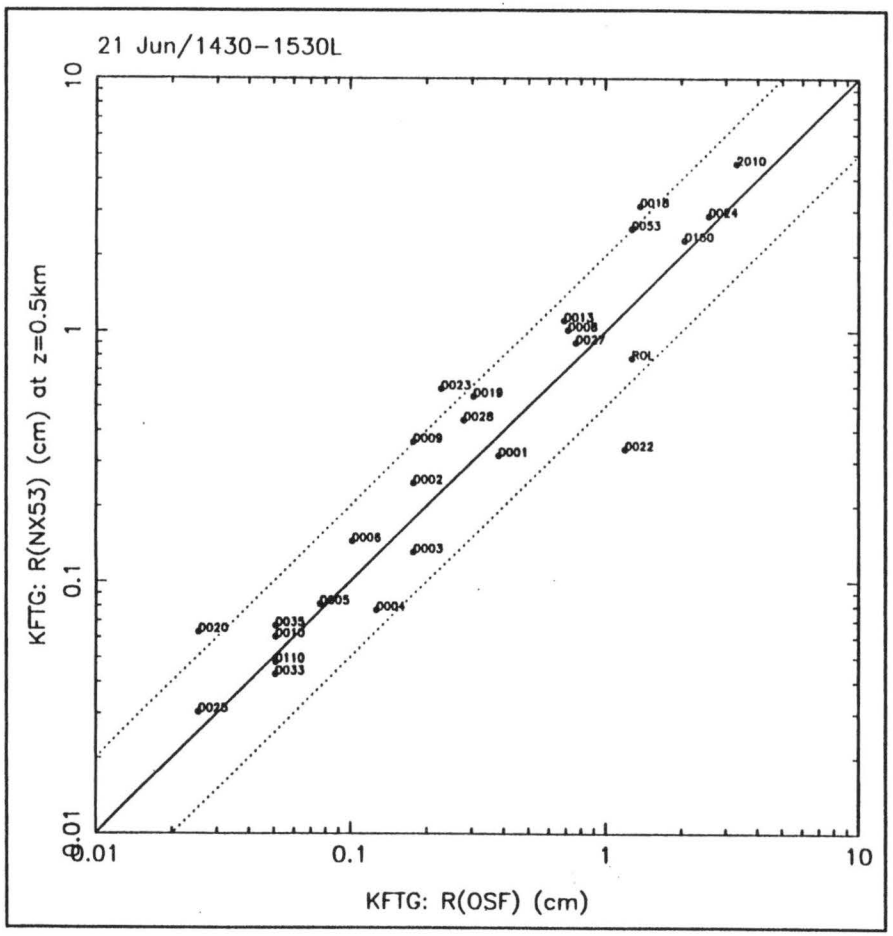

Figure 5.21 Scatter diagram of R(OSF) versus R(NX53) precipitation from 14:30 to 15:30 MDT on 21 June 1994. All units are in cm. Solid line represents a 1:1 correspondence, dotted lines represents 2:1 and 1:2 correspondence.

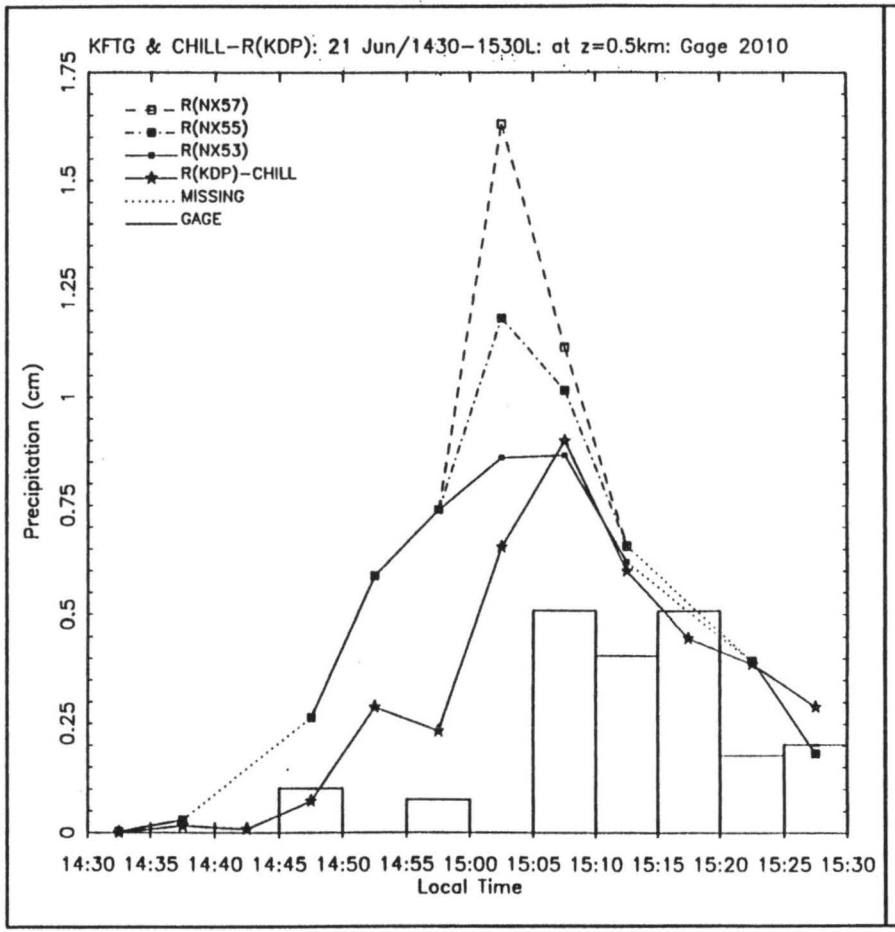

Figure 5.22 Five minute precipitation time series for gage, R(KDP), and R(NXxx) from 14:30 to 15:30 MDT on 21 June 1994 for station 2010.

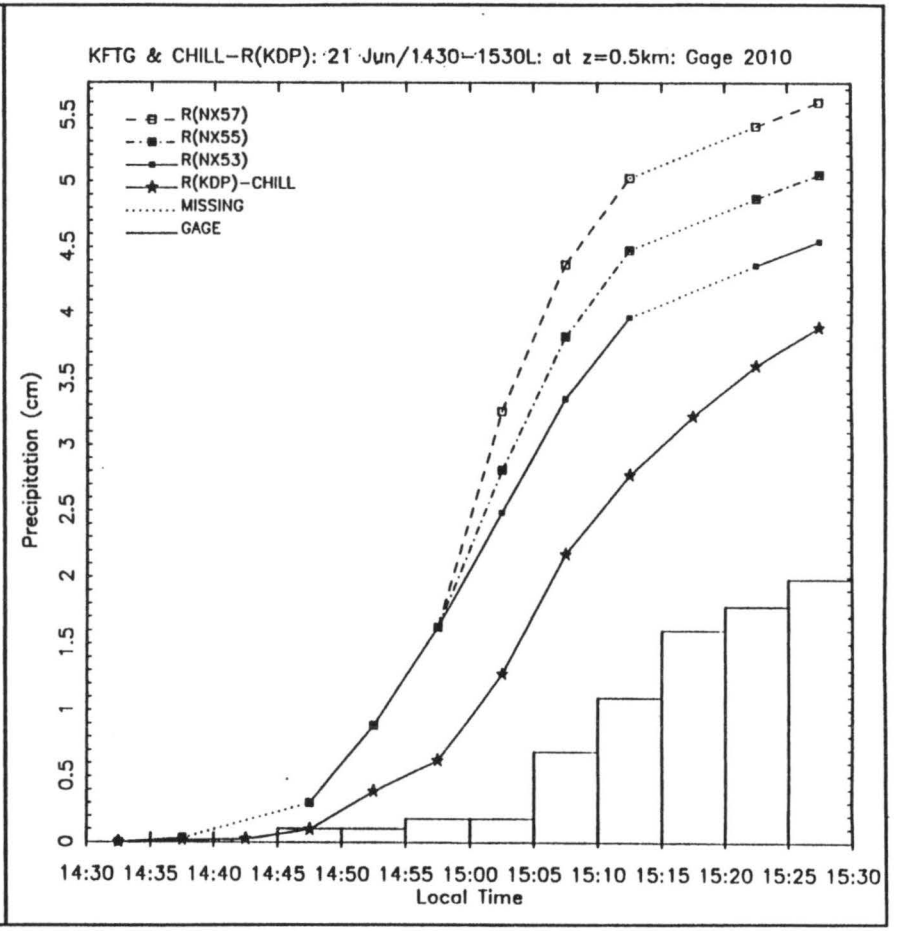

Figure 5.23 Five minute precipitation accumulations time series for gage, R(KDP), and R(NXxx) from 14:30 to 15:30 MDT on 21 June 1994 for station 2010.

R(NX53) reaches its maximum rate between 15:00 and 15:10 MDT with ~0.9 cm per 5-minute period. R(NX55) and R(NX57) reach their peaks in the 15:00 time period with values of 1.18 and 1.63 cm per 5-minute period, respectively. R(NX53) shows how the 53 dBZ cut off kept the radar-derived peak precipitation in better approximation to the gage.

Figure 5.23 shows the accumulated precipitation in time for the same precipitation time series and one-hour time period. Both R(KDP) and R(NXxx) begin appreciable precipitation too early and too much in comparison to the gage. All four rain rate algorithms overestimated the gage precipitation. For total precipitation, both R(KDP) and R(NXxx) overestimated precipitation with R(KDP) providing the least overestimation.

5.2.2.2 Station 0018

Figure 5.24 shows the 5-minute time series for the 0018 rain gage and with the time series for the radar-derived precipitation during the one-hour period. The gage data shows an initial onset of precipitation around 14:40 MDT, maintaining moderate precipitation for 10 minutes and ending at 15:05 MDT. The R(KDP) captures the beginning of the precipitation, but greatly underestimates the gage's peak. R(KDP) also has a peak in the 14:55 time period during the gage's time period of decreasing precipitation. The R(NXxx) captures this station's pattern of precipitation the best, but R(NXxx) values overestimated the gage's peak precipitation. The reflectivity barely got above 52 dBZ, prohibiting a reflectivity cut off comparison.

The accumulated precipitation for the gage and four radar-derived accumulated precipitation for the same time period are shown in figure 5.25. The R(KDP)

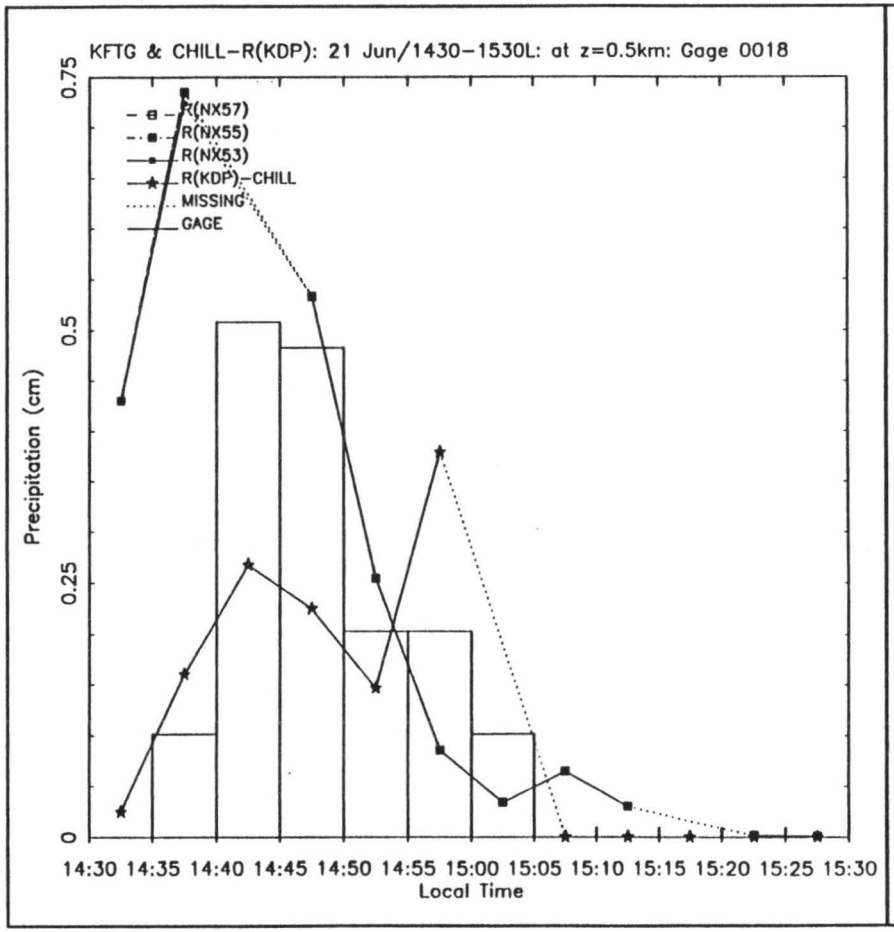

Figure 5.24 Five minute precipitation time series for gage, R(KDP), and R(NXxx) from 14:30 to 15:30 MDT on 21 June 1994 for station 0018.

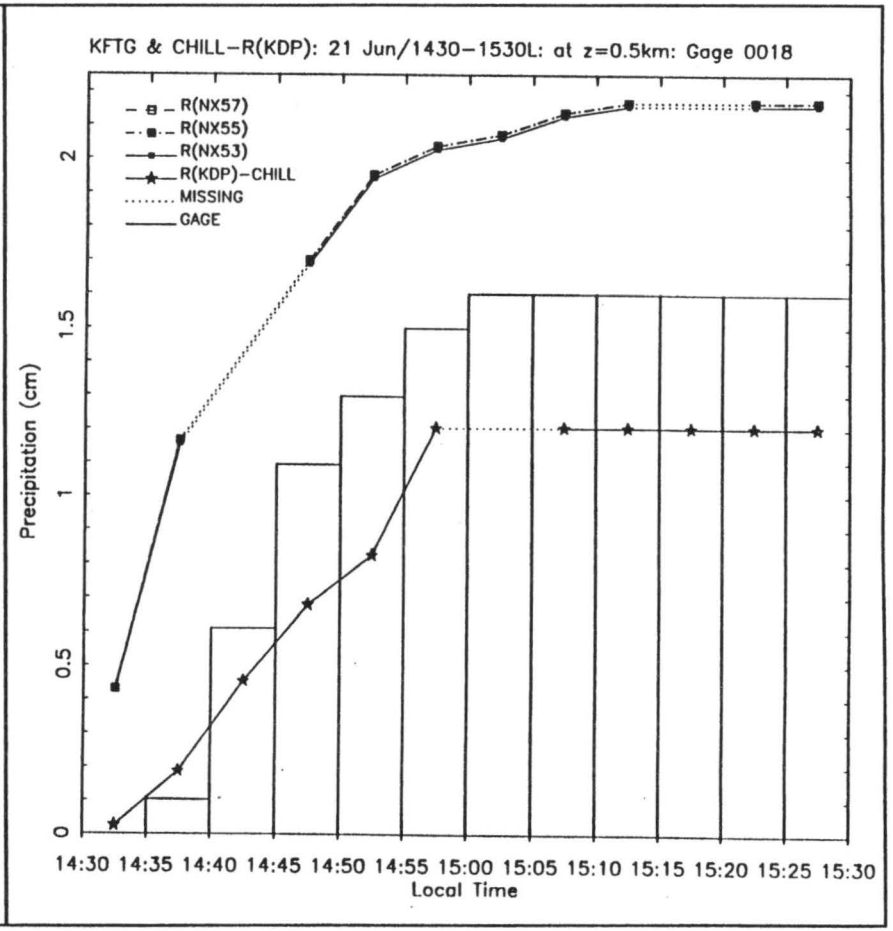

Figure 5.25 Five minute precipitation accumulations time series for gage, R(KDP), and R(NXxx) from 14:30 to 15:30 MDT on 21 June 1994 for station 0018.

persistent underestimate is improved by the 14:55 period precipitation maximum. The R(NXxx) clearly shows the initial overestimate is reduced through the period by a slight underestimate. Both R(KDP) and R(NXxx) show periods of missing data, where no precipitation is added to the accumulation. Based on this, the R(KDP) proves to be the better total precipitation estimator. However, given the initial overestimate in R(NXxx), the R(NXxx) captured the precipitation event's structure much better.

5.2.2.3 Station 0024

Figure 5.26 shows the precipitation time series for gage 0024 and the four radar-derived precipitation for the one-hour period. The gage data shows a precipitation peak early in the one-hour time period at 14:35 MDT with 0.30 cm of precipitation, followed by a gradual decrease in precipitation, with precipitation ending by 15:05 MDT. Both R(KDP) and R(NXxx) captured the precipitation event's structure accurately and both overestimate the gage amounts at all but two 5-minute time periods. R(NXxx) overestimated the gage amounts greater than R(KDP).

The accumulated precipitation time series for this period (figure 5.27) clearly shows R(KDP) being better than R(NXxx) for this station. R(NXxx) persistent overestimate continued to expand the accumulations in time from the gage totals.

5.3 10 AUGUST 1994

5.3.1 Gage versus Radar Derived Precipitation

5.3.1.1 R(NX57) - KFTG

The areal coverage of R(NX57) derived precipitation with gage precipitation overlaid for the two-hour time period is shown in figure 5.28. This plot of R(NX57)

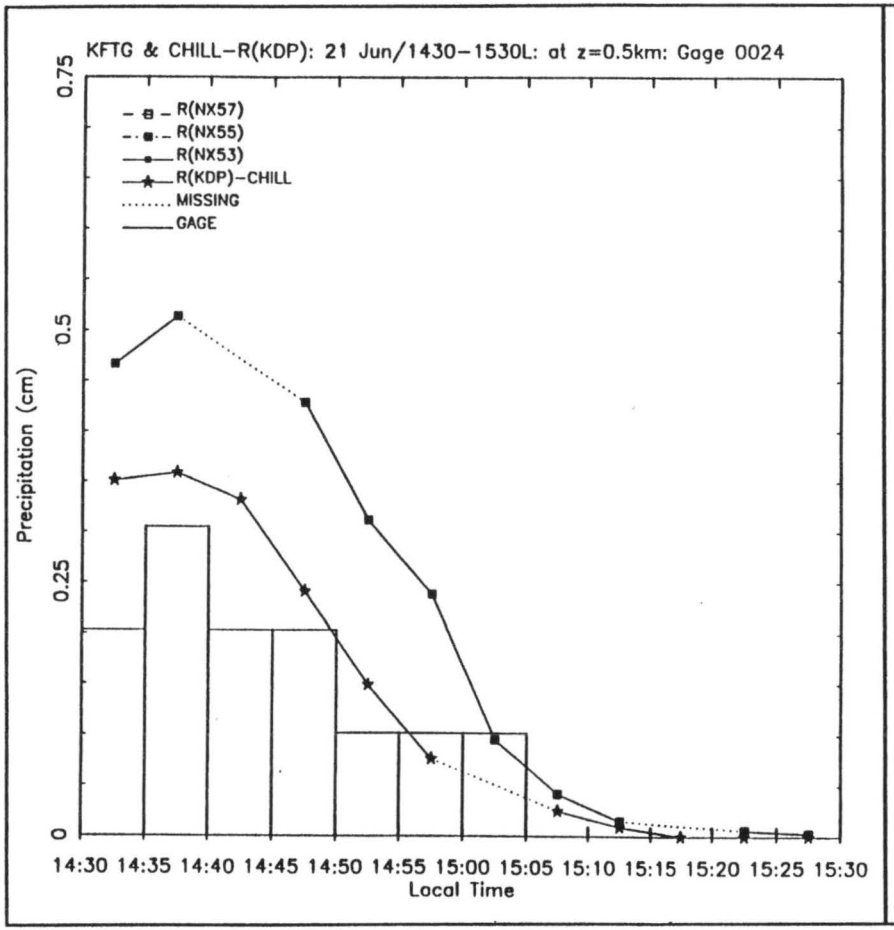

Figure 5.26 Five minute precipitation time series for gage, R(KDP), and R(NXxx) from 14:30 to 15:30 MDT on 21 June 1994 for station 0024.

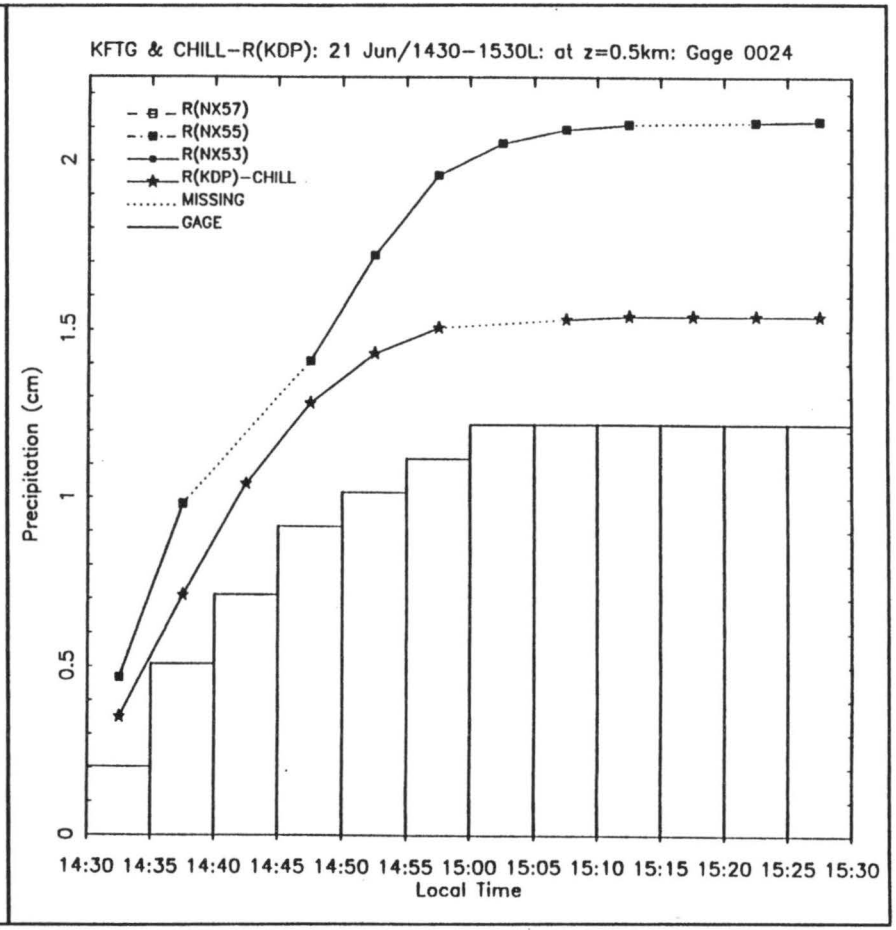

Figure 5.27 Five minute precipitation accumulations time series for gage, R(KDP), and R(NXxx) from 14:30 to 15:30 MDT on 21 June 1994 for station 0024.

areal coverage shows four regions of heavy precipitation of interest. The first region, region 1, is located in the vicinity of x, y coordinate (-57 ,72) and is 14 km to the west of Loveland, CO (LOVE). Region 1 has a maximum local precipitation contour of 12 cm. The second region, region 2, is located 4 km to the east of Arvada, CO (ARV) in the vicinity of x, y coordinate (-55, 2), with a maximum precipitation contour of 10 cm. The last region, region 3, is located 7 km to the west-southwest of Lakewood, CO (LAK) in the vicinity x, y coordinate (-55, -10). This region is identified by the maximum precipitation contour of 12 cm. There are two gage sites around region 4. The first gage, Lakewood mesonet site (LAK) located at x, y coordinate (-52, -10), had a maximum period total precipitation of 4.95 cm. The second gage, UDFCD station 2370 located at x, y coordinate (-56, -12), had a 4.78 cm maximum precipitation accumulation. The next highest precipitation gage site, UDFCD station 0084, was located 10 km to the southwest of Boulder, CO (BOU) at x, y coordinate (-54, -7) and had a maximum period precipitation total of 3.30 cm. Table 5.2 shows the R(NX57) derived precipitation values for these three stations.

The scatter diagram of the gage versus R(NX57) is shown in figure 5.29. The scatter diagram shows R(NX57) derived precipitation to generally overestimate the gage precipitation. The scatter also shows a high degree of variance in the data. Figure 5.30 and table A.7 shows average R(NX57) to gage ratio for categories of gage total precipitation and all gages. The R(NX57) shows improvement of the ratios with increasing precipitation totals with the slight exception of the heaviest, 4 to 6 cm category.

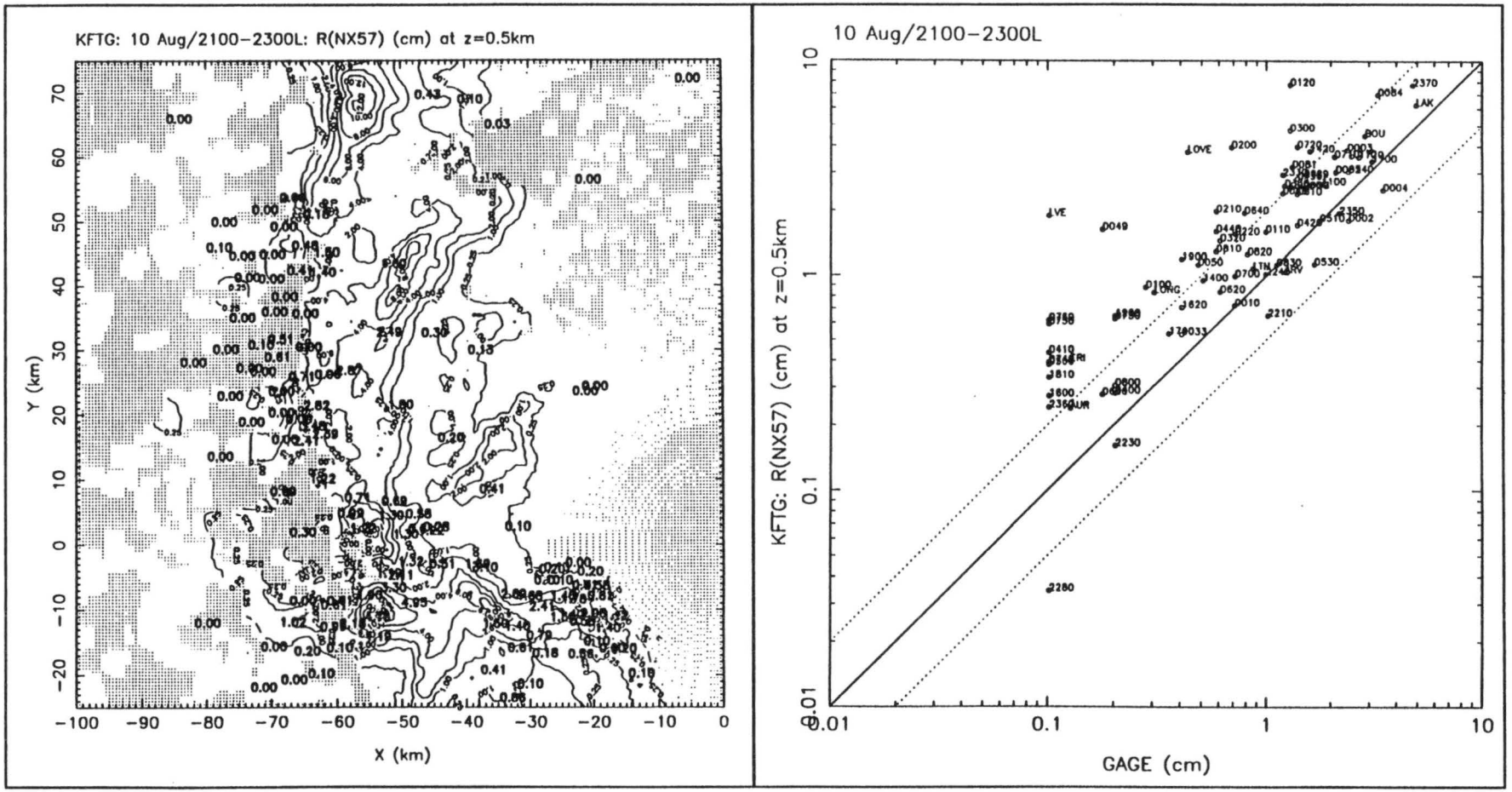

Figure 5.28 Areal Coverage of R(NX57) from 21:00 to 23:00 MDT on 10 August 1994. Contours labeled are 0.25, 1, 2, 4, 6, 8, 10, and 12 cm. Gage precipitation for same period is shown in bold. Gage location is at lower left of label.

Figure 5.29 Scatter diagram of gage versus R(NX57) precipitation from 21:00 to 23:00 MDT on 10 August 1994. All units are in cm. Solid line represents a 1:1 correspondence, dotted lines represents 2:1 and 1:2 correspondence.

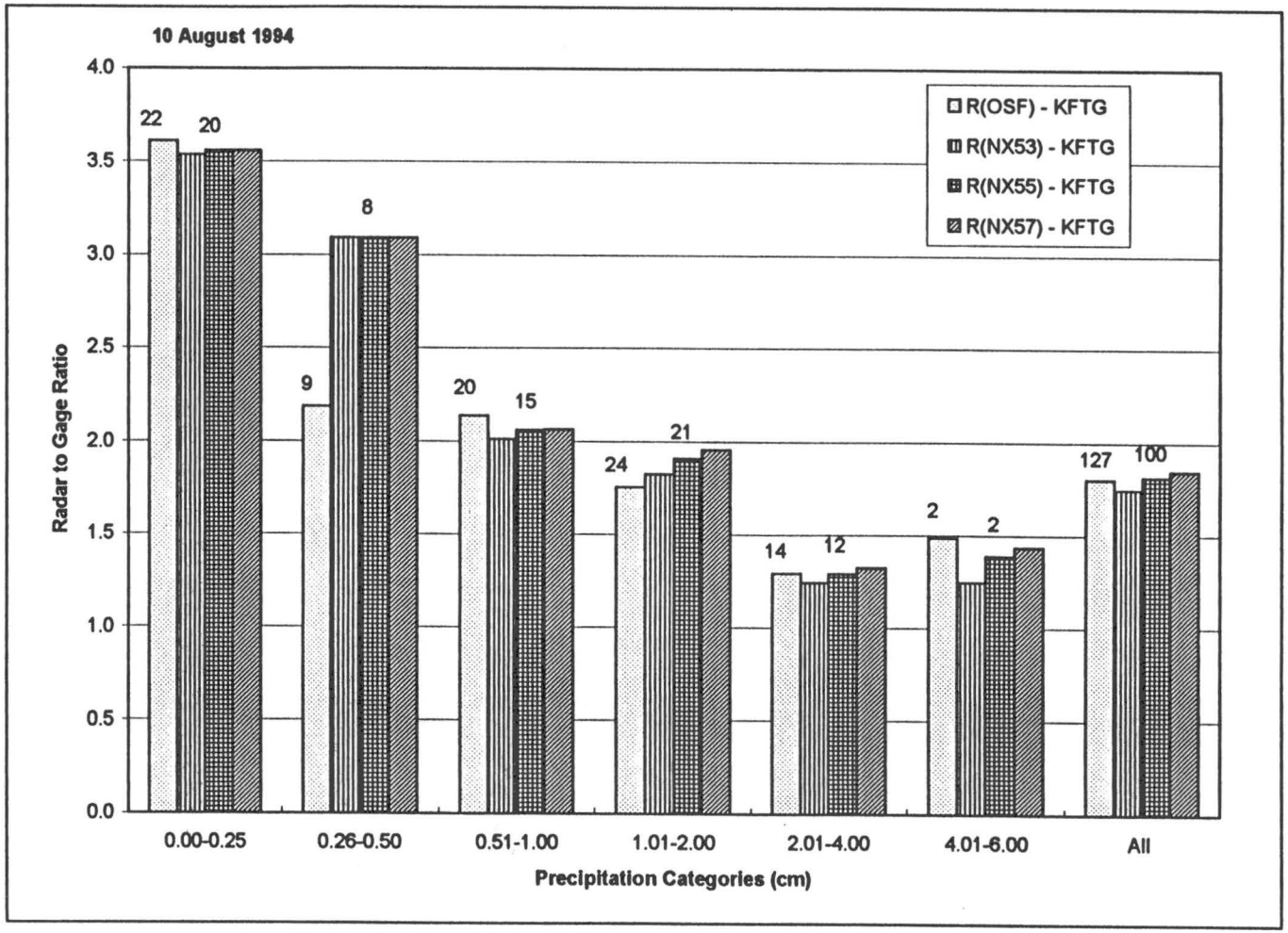

Figure 5.30 Average radar-derived to gage precipitation ratios for ranges of gage values and all gages for 10 August 1994. Numbers at top of columns represents number of values in category.

Table 5.2 Gage Versus Radar Derived Precipitation for Three Stations on 10 August 1994.

Station:	LAK	2370	0084
GAGE (cm)	4.95	4.78	3.30
R(NX57) -- KFTG (cm)	6.24	7.72	6.97
R(NX55) -- KFTG (cm)	5.96	7.54	6.10
R(NX53) -- KFTG (cm)	5.39	6.71	5.31
R(OSF) -- KFTG (cm)	5.31	9.14	4.50

For all gages the average R(NX57) to gage ratio is 1.85 and for the gages with precipitation, the ratio is 1.75.

5.3.1.2 R(NX55) -- KFTG

The areal coverage of R(NX55) derived precipitation, along with gage precipitation in bold is shown in figure 5.31. In comparison to R(NX57), region 1's, maximum precipitation contour has been reduced to 10 cm. In region 2, R(NX57)'s maximum precipitation contour has been reduced from 10 to 8 cm. Similarly, region 3's maximum precipitation contour was reduced from 12 to 10 cm.

Figure 5.32 shows the scatter diagram for gage versus R(NX55) derived precipitation. R(NX55) persists to overestimate the gage precipitation. Seven stations had R(NX55) precipitation totals less than R(NX57). R(NX55) precipitation values for the three gages, LAK, 2370, and 0084 are located in table 5.2.

Figure 5.30 and table A.8 shows average R(NX55) to gage ratios for categories of gage total precipitation and all gages. The average R(NX55) to gage ratio for all gages is 1.81 and shows a 4 percent drop from the R(NX57) overestimate. R(NX55)

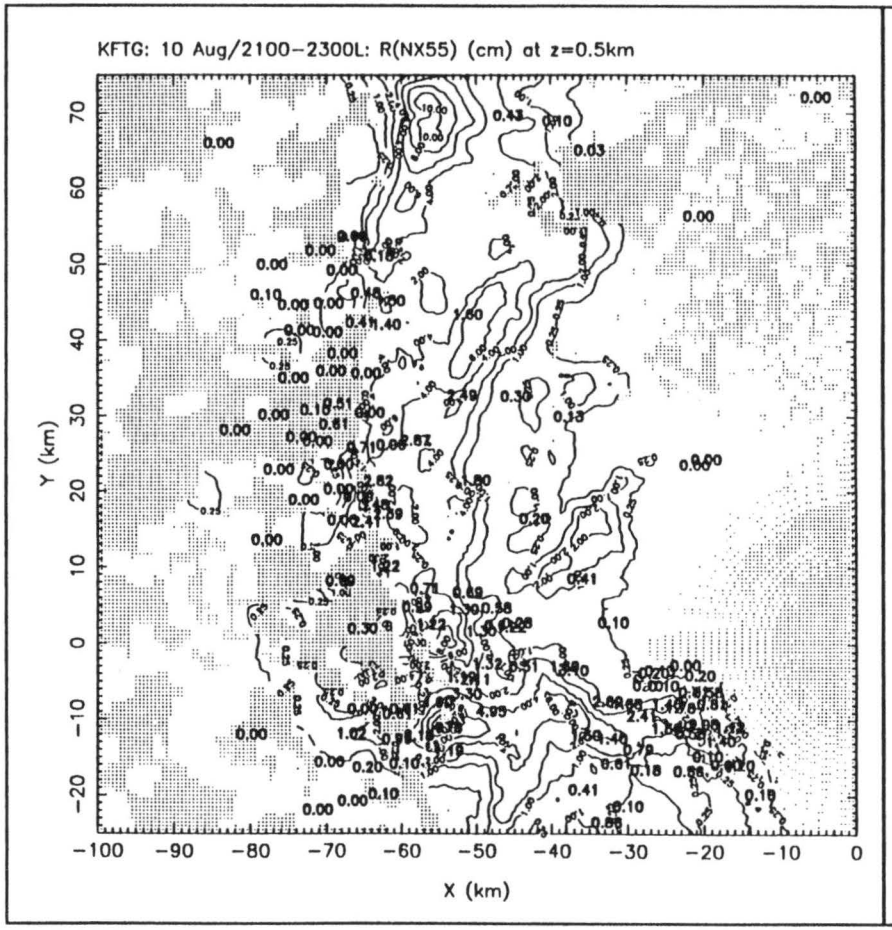

Figure 5.31 Areal Coverage of R(NX55) from 21:00 to 23:00 MDT on 10 August 1994. Contours labeled are 0.25, 1, 2, 4, 6, 8, 10, and 12 cm. Gage precipitation for same period is shown in bold. Gage location is at lower left of label.

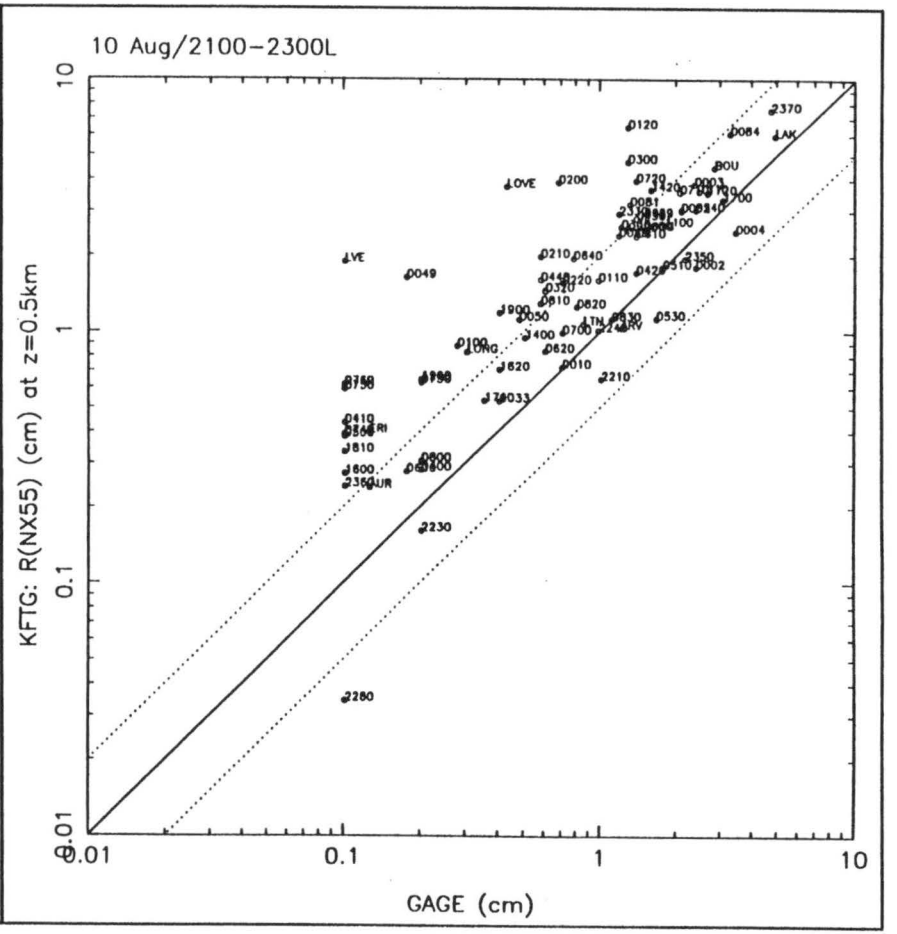

Figure 5.32 Scatter diagram of gage versus R(NX55) precipitation from 21:00 to 23:00 MDT on 10 August 1994. All units are in cm. Solid line represents a 1:1 correspondence, dotted lines represents 2:1 and 1:2 correspondence.

overestimates the gage by an average 81 percent. The average R(NX55) to gage ratio for gages with precipitation shows a 1.74 overestimation factor.

5.3.1.3 R(NX53) -- KFTG

Figure 5.33 shows the areal coverage of precipitation for R(NX53) derived precipitation with gage precipitation values overlaid. The R(NX53) continues to show decreased amounts and areal coverage of maximum precipitation from R(NX55). Region 1 shows a significantly less areal extent of the 10-cm contour. Region 2, no longer has 8-cm contour and only shows a 6-cm maximum precipitation contour. Region 3, has also experienced a decrease in its center's maximum precipitation contour from 10 to 8 cm.

The scatter diagram for gage versus R(NX53) derived precipitation (figure 5.34). Fifteen stations have lower precipitation values than R(NX55), but the overestimate bias is still strongly present. Figure 5.10 and table A.9 shows average R(NX53) to gage ratio for categories of gage total precipitation and all gages. The average R(NX53) to gage ratios show improving performance at higher rain fall for all categories. For precipitation totals greater than 2 cm, the R(NX53) shows a 34 percent overestimate of the gage. The average R(NX53) to gage ratio for all gages is 1.75 and for gages with precipitation, the ratio is reduced to 1.67. Table 5.2 contains R(NX53) for the sites used in the time series figures.

5.3.1.4 R(OSF) -- KFTG

Figure 5.35 shows the areal coverage of precipitation from R(OSF) with gage precipitation overlaid in bold. In region 1, R(OSF) is shown with an 8-cm maximum precipitation contour versus the R(NX53)'s 10-cm contour. The R(OSF) also has a 4 km

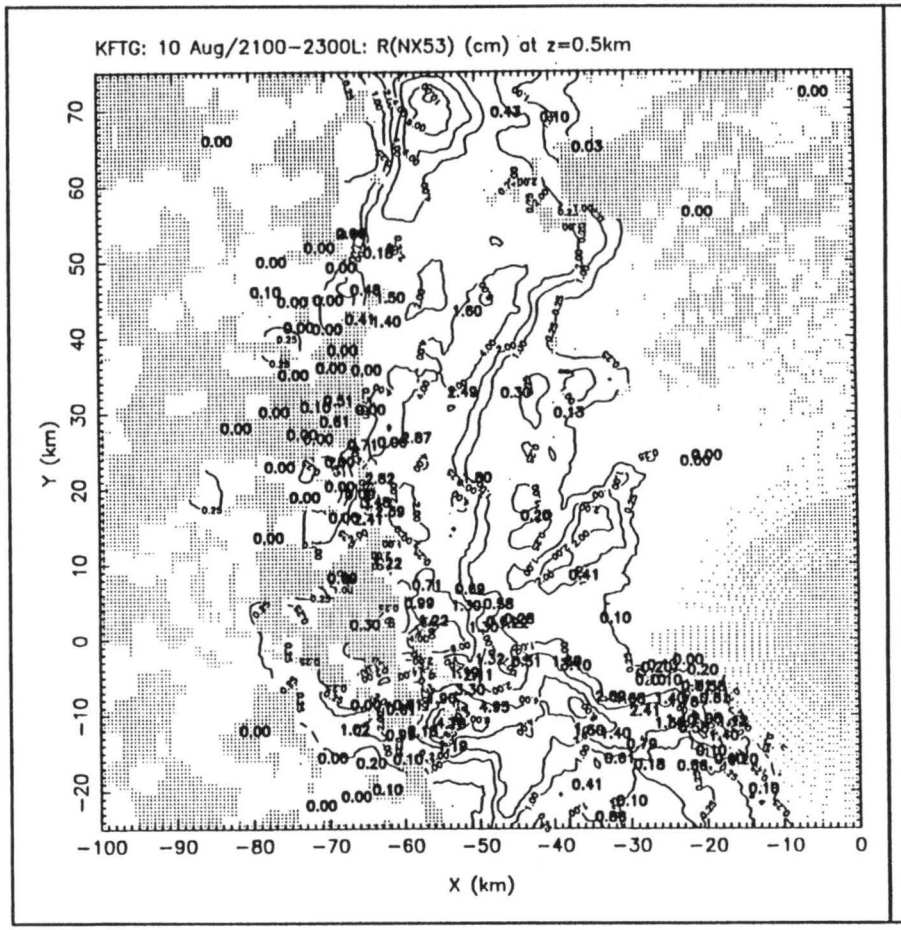

Figure 5.33 Areal Coverage of R(NX53) from 21:00 to 23:00 MDT on 10 August 1994. Contours labeled are 0.25, 1, 2, 4, 6, 8, 10, and 12 cm. Gage precipitation for same period is shown in bold. Gage location is at lower left of label.

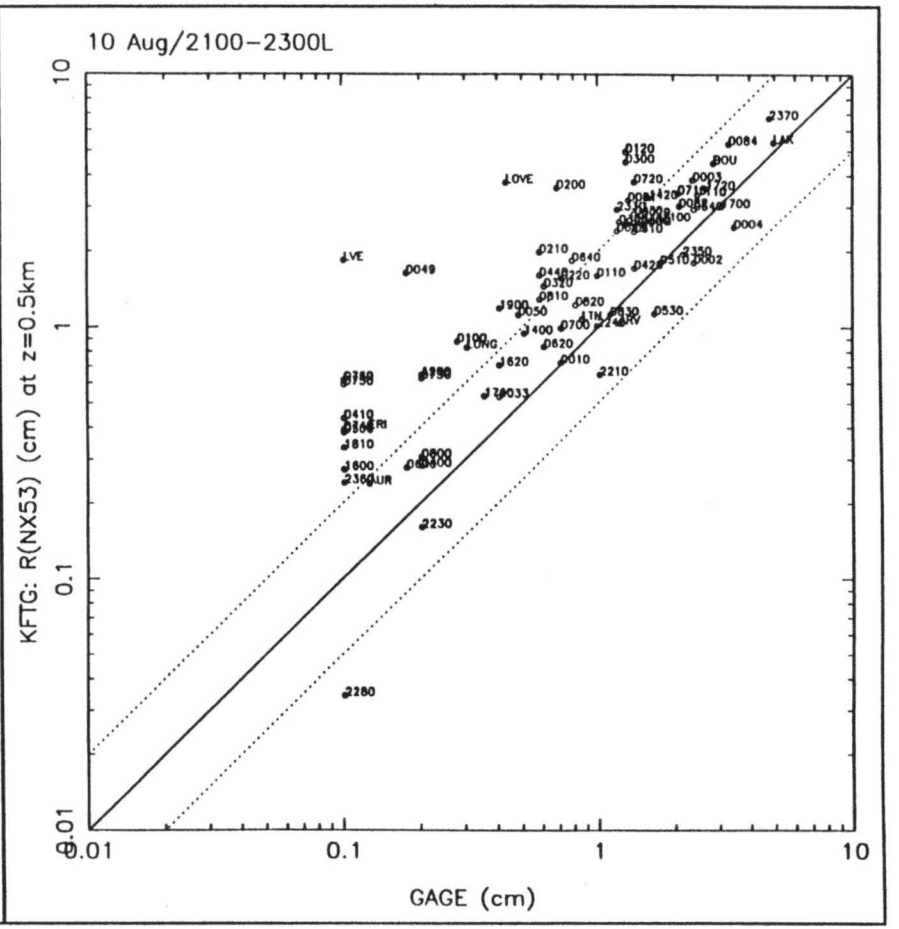

Figure 5.34 Scatter diagram of gage versus R(NX53) precipitation from 21:00 to 23:00 MDT on 10 August 1994. All units are in cm. Solid line represents a 1:1 correspondence, dotted lines represents 2:1 and 1:2 correspondence.

westward displacement of region 1's center of maximum precipitation. Region 2's R(OSF) maximum precipitation contour is 4 cm compared to R(NX53)'s 6-cm contour. This region has also experienced a 5 km northwestward displacement of its maximum precipitation center. Region 3's R(OSF) shows the same value of the maximum precipitation contour as R(NX53)'s. Again R(OSF)'s region of maximum precipitation is displaced 4 km to the west of R(NX53)'s. Just the centers of maximum precipitation show this displacement. The rest of R(OSF)'s areal coverage compare wells with R(NX53)'s areal coverage. Table 5.2 contains the values of R(OSF) for the sites used in the time series figures.

The scatter diagram comparing gage and R(OSF) derived precipitation (figure 5.36) shows a persistent overestimate, but with a tighter scatter than R(NX53)'s. Figure 5.30 and table A.10 shows the average R(OSF) to gage ratios for all gages and categories of different gage totals. The R(OSF) shows the same trend of lower overestimate at higher rainfall totals. The average R(OSF) to gage ratio for all gages is 1.80 and the ratio for gages with precipitation is 1.68. Figure 5.37 shows the scatter diagram comparison of R(OSF) and R(NX53). This diagram shows a large variance amongst the two algorithms with no perceptible bias.

5.3.2. Time Series Analysis

5.3.2.1 Station LAK

Figure 5.38 shows the 5-minute precipitation time series for station LAK and the R(NXxx) derived precipitation for the two-hour period. The gage data shows two precipitation events. The first begins at 21:00 MDT and lasts until the 21:35 time period

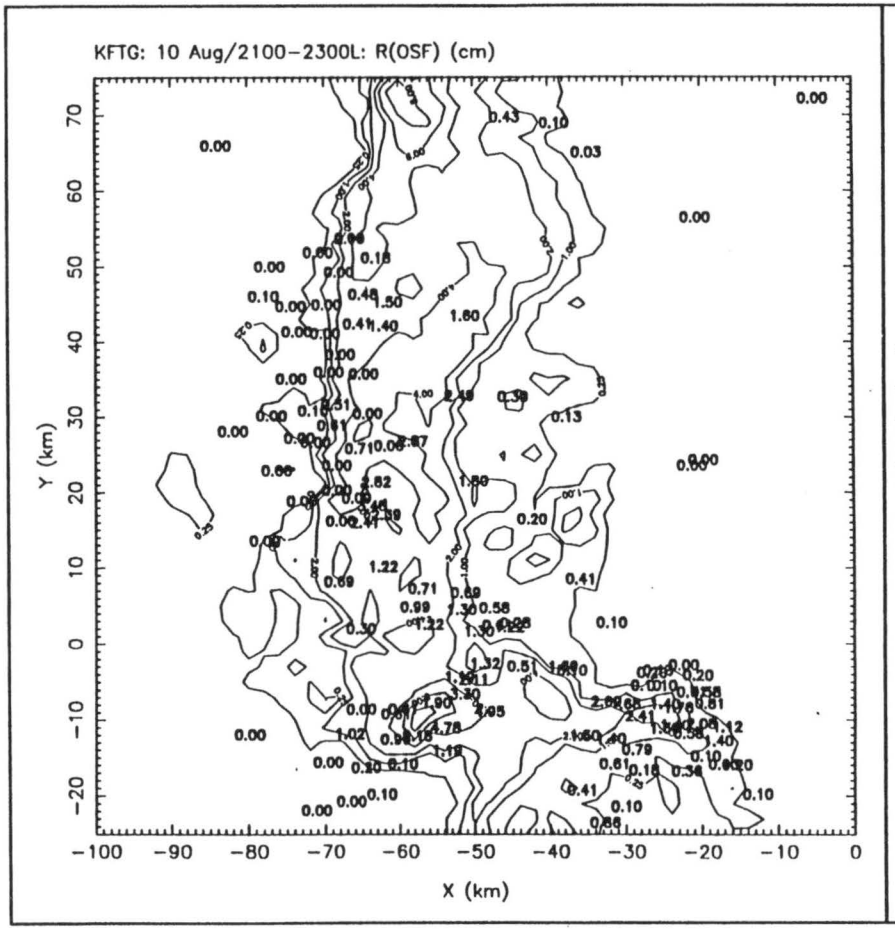

Figure 5.35 Areal Coverage of R(OSF) from 21:00 to 23:00 MDT on 10 August 1994. Contours labeled are 0.25, 1, 2, 4, 6, 8, 10, and 12 cm. Gage precipitation for same period is shown in bold. Gage location is at lower left of label.

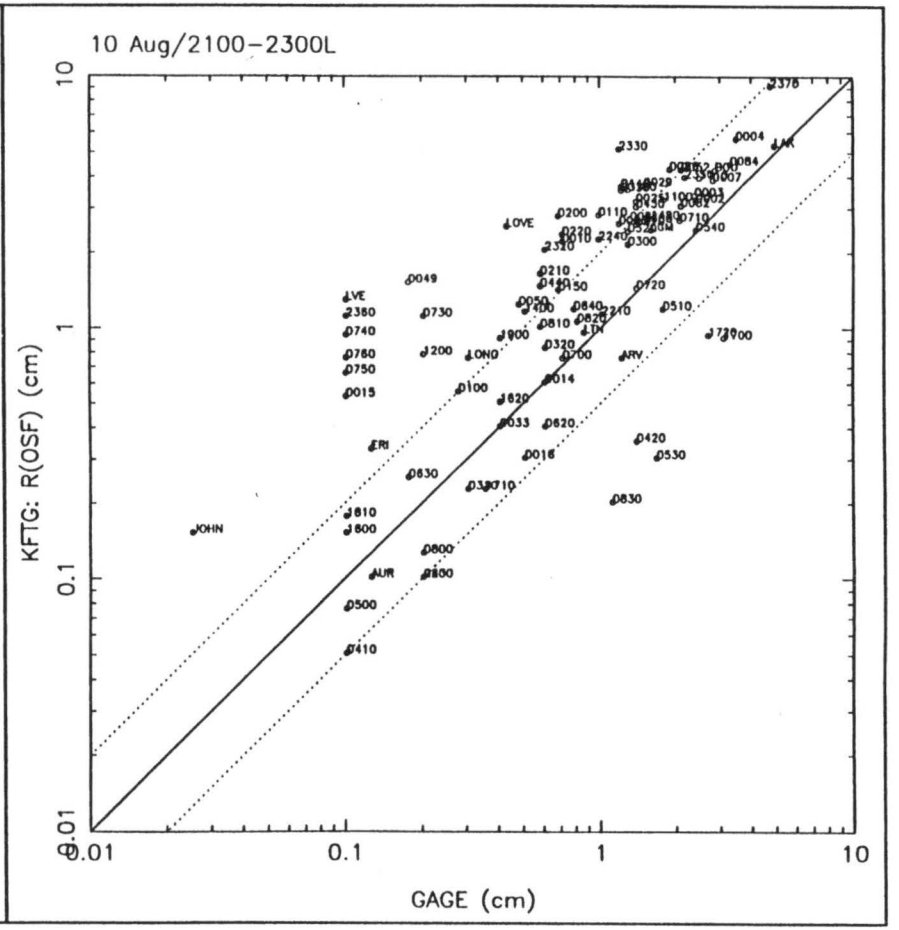

Figure 5.36 Scatter diagram of gage versus R(OSF) precipitation from 21:00 to 23:00 MDT on 10 August 1994. All units are in cm. Solid line represents a 1:1 correspondence, dotted lines represents 2:1 and 1:2 correspondence.

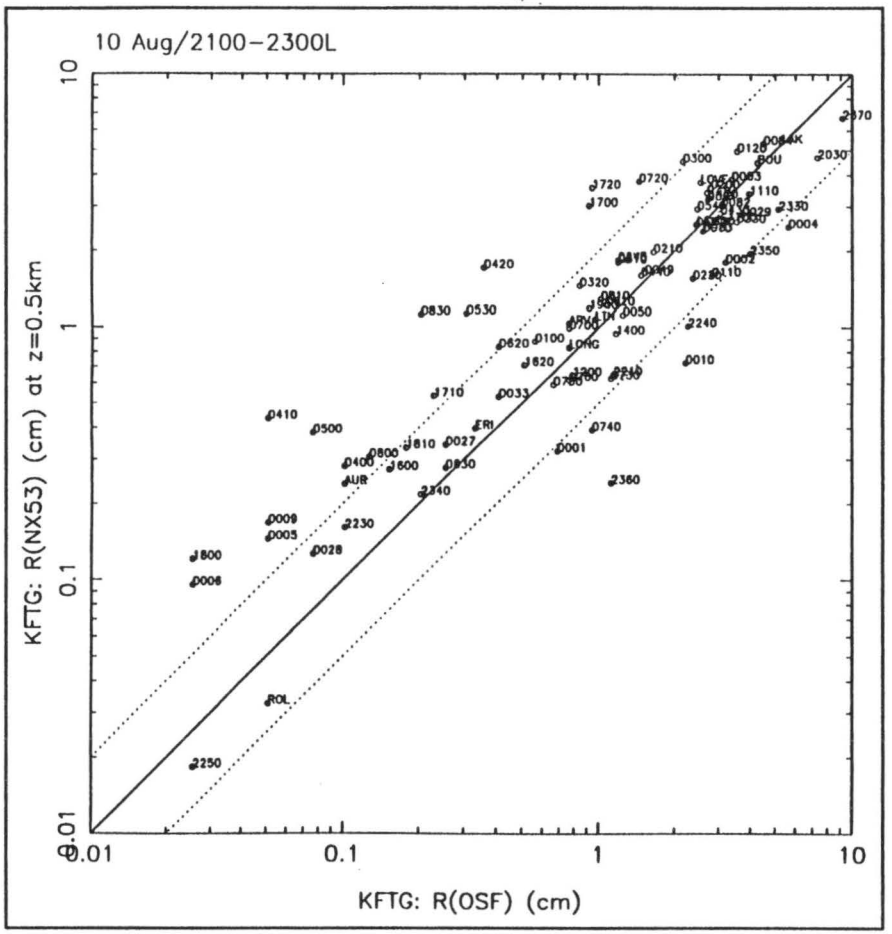

Figure 5.37 Scatter diagram of R(OSF) versus R(NX53) precipitation from 21:00 to 23:00 MDT on 10 August 1994. All units are in cm. Solid line represents a 1:1 correspondence, dotted lines represents 2:1 and 1:2 correspondence.

with peak precipitation near 0.45 cm during 21:20 time period. The second and more intense precipitation occurred from 21:35 until 22:10 MDT. The peak precipitation was during the 21:45 time period with 1 cm recorded in this 5-minute period. R(NXxx) did not capture the structure of gage's first precipitation event. R(NXxx) was high at the start of the two-hour period and decreased until the 21:25 time period. R(NXxx) did capture the structure of the gage's second precipitation event quite well. Reflectivity was higher than 55 dBZ for the 15-minute period from 21:45 until 22:00 MDT. The largest deviation amongst the reflectivity cut off was during the 21:50 time period. Here, the 53 dBZ performed the best, appropriately capping the precipitation for this period.

The accumulated precipitation time series for this period (figure 5.39) shows how well R(NX53) total precipitation compared with gage total. Even though R(NXxx) did not capture the structure of the gage's first precipitation event, R(NXxx) accumulated a comparable amount of precipitation to the gage for the first event. R(NX53) best captured the gage's second precipitation event, to perform best overall for this gage.

5.3.2.2 Station 2370

Figure 5.40 compares the station's 2370 five-minute precipitation time series with the R(NXxx) precipitation time series. The gage precipitation begins at 21:05 MDT and reaches a peak of 0.81 cm during the 21:20 time period. After this peak, the gage goes through 40 minutes of fluctuating precipitation intensities before ending at 22:05 MDT. R(NXxx) captures the onset and peak of precipitation well. R(NXxx) then represents the periods of gage fluctuations as a secondary precipitation maximum before ending the precipitation around 22:10 MDT. The reflectivity averaged between 53 and 55 dBZ for a

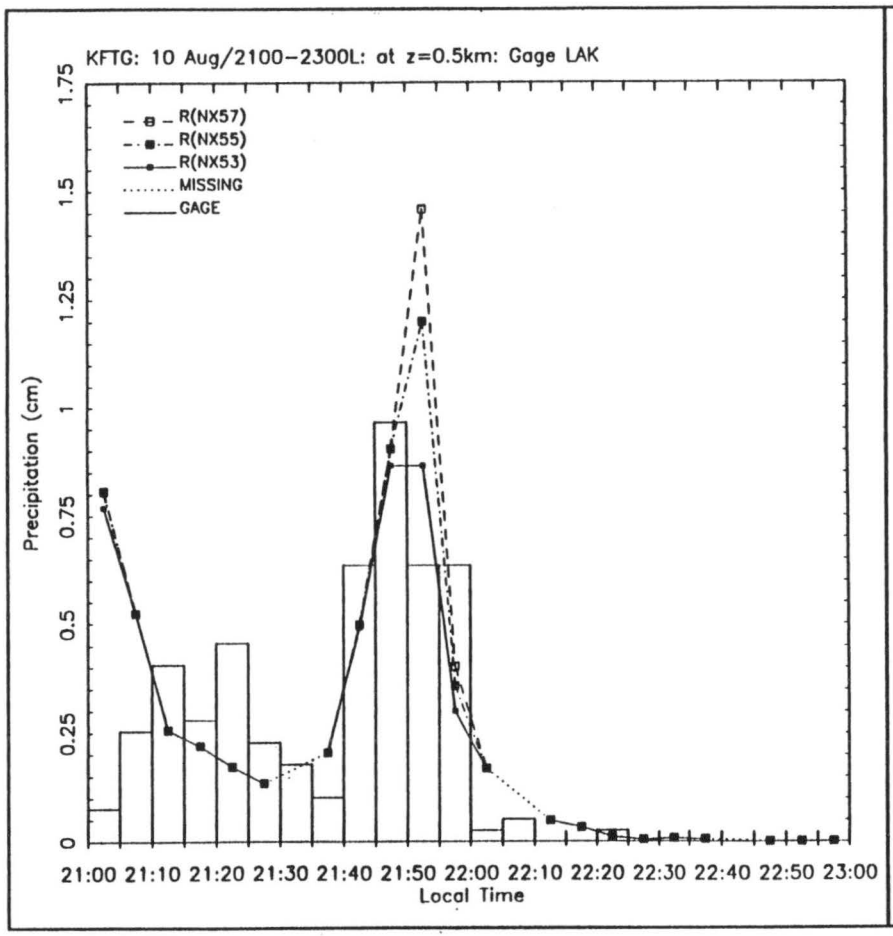

Figure 5.38 Five minute precipitation time series for gage and R(NXxx) from 21:00 to 23:00 MDT on 10 August 1994 for station LAK.

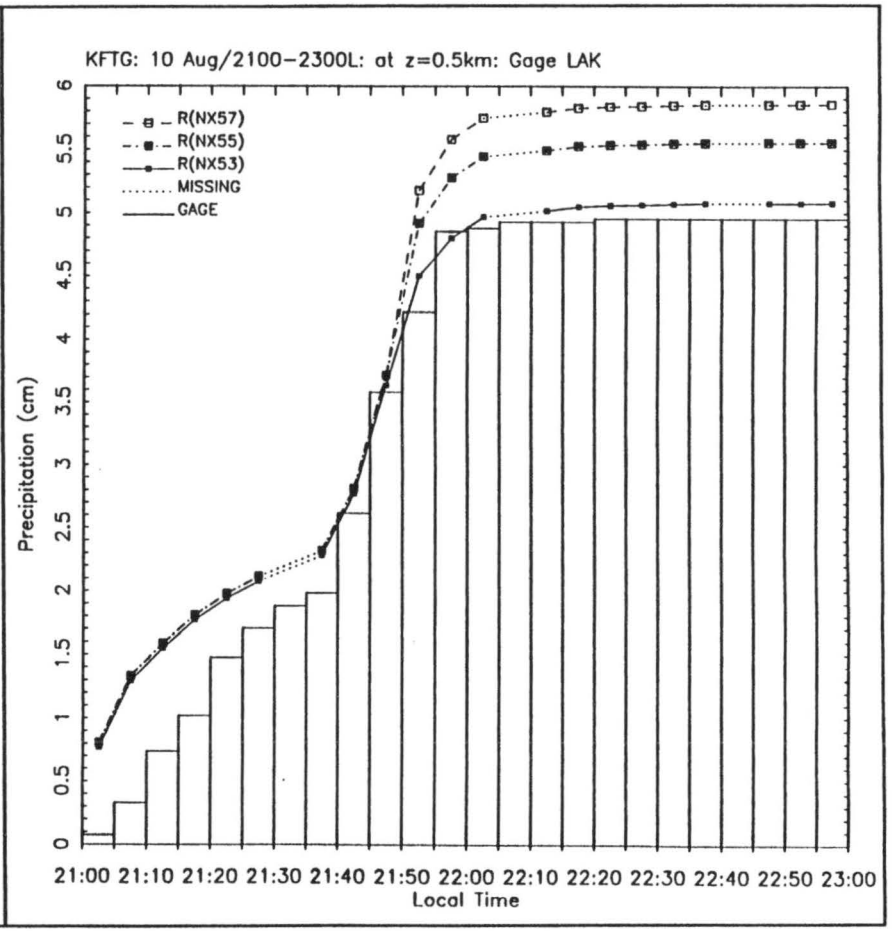

Figure 5.39 Five minute precipitation accumulations time series for gage and R(NXxx) from 21:00 to 23:00 MDT on 10 August 1994 for station LAK.

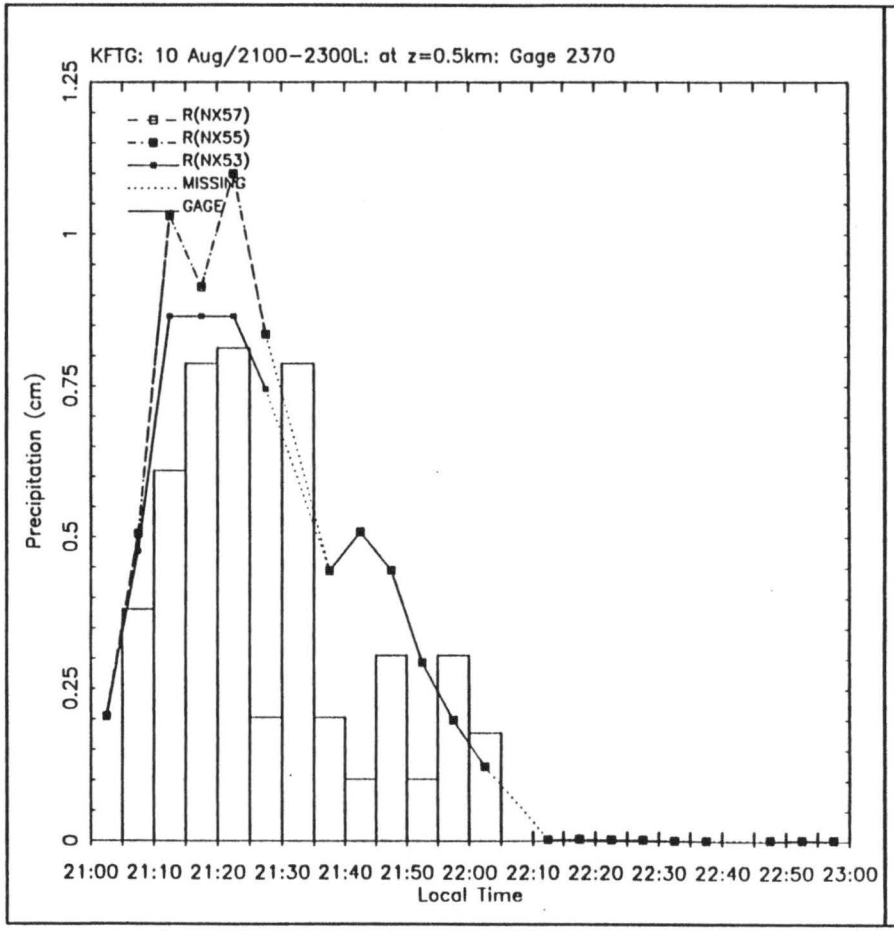

Figure 5.40 Five minute precipitation time series for gage and R(NXxx) from 21:00 to 23:00 MDT on 10 August 1994 for station 2370.

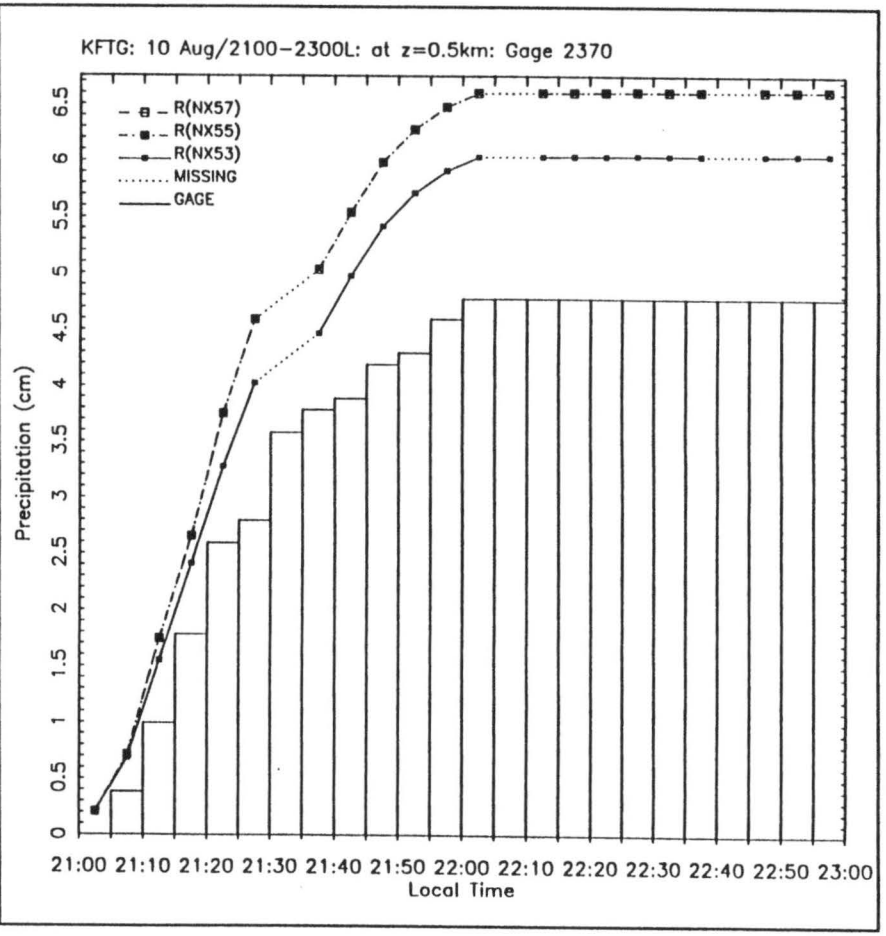

Figure 5.41 Five minute precipitation accumulations time series for gage and R(NXxx) from 21:00 to 23:00 MDT on 10 August 1994 for station 2370.

20-minute period beginning 21:10 MDT. The R(NX53) capped the precipitation during this 20-minute period much better than R(NX55).

Figure 5.41 shows the accumulated precipitation for station 2370 and R(NXxx) for the same two-hour time period. This accumulated precipitation time series shows R(NXxx) persistently overestimated throughout the entire time period. The five-minute period beginning 21:30 MDT shows a missing value (no accumulation) for R(NXxx) which helps keep the final accumulated total low. With a valid R(NXxx) precipitation amount during this missung period the overestimate of gage precipitation would have been worse. The R(NX53) proved to be the better reflectivity cut off, in terms of the total precipitation accumulation.

5.3.2.3 Station 0084

Figure 5.42 shows the five-minute time series for station 0084's rain gage and R(NXxx) derived precipitation for the two-hour period. The gage time series shows an initial minor peak in precipitation at 21:35, before reaching the precipitation events main peak of 0.71 cm for two consecutive five-minute periods beginning 21:45 MDT. The gage precipitation decreases thereafter and ends at 22:25 MDT. The R(NXxx) captures the gage's precipitation event quite well. The reflectivity exceeds 55 dBZ for a 20-minute time period beginning 21:20 MDT. The R(NX53) again proves to cap the precipitation closest to the gage values.

The accumulated precipitation for the gage and R(NXxx) for the same time period is shown in figure 5.43. The accumulated precipitation time series shows R(NXxx) consistently overestimated the gage measurement throughout the gage's precipitation

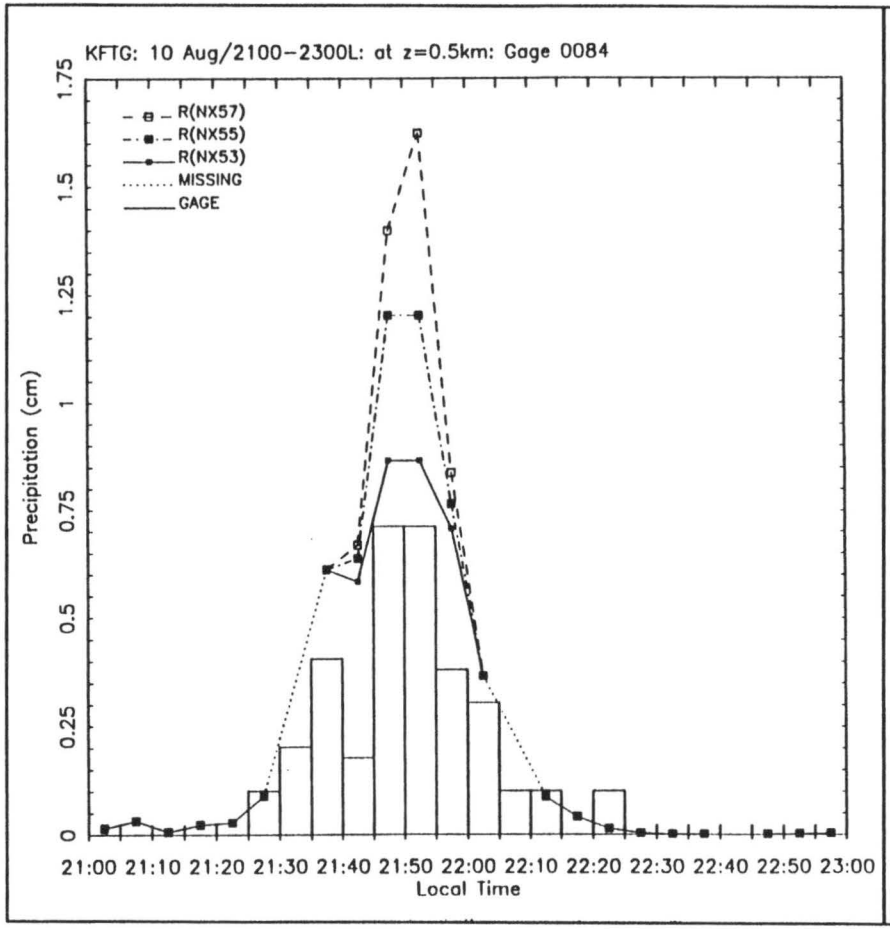

Figure 5.42 Five minute precipitation time series for gage and R(NXxx) from 21:00 to 23:00 MDT on 10 August 1994 for station 0084.

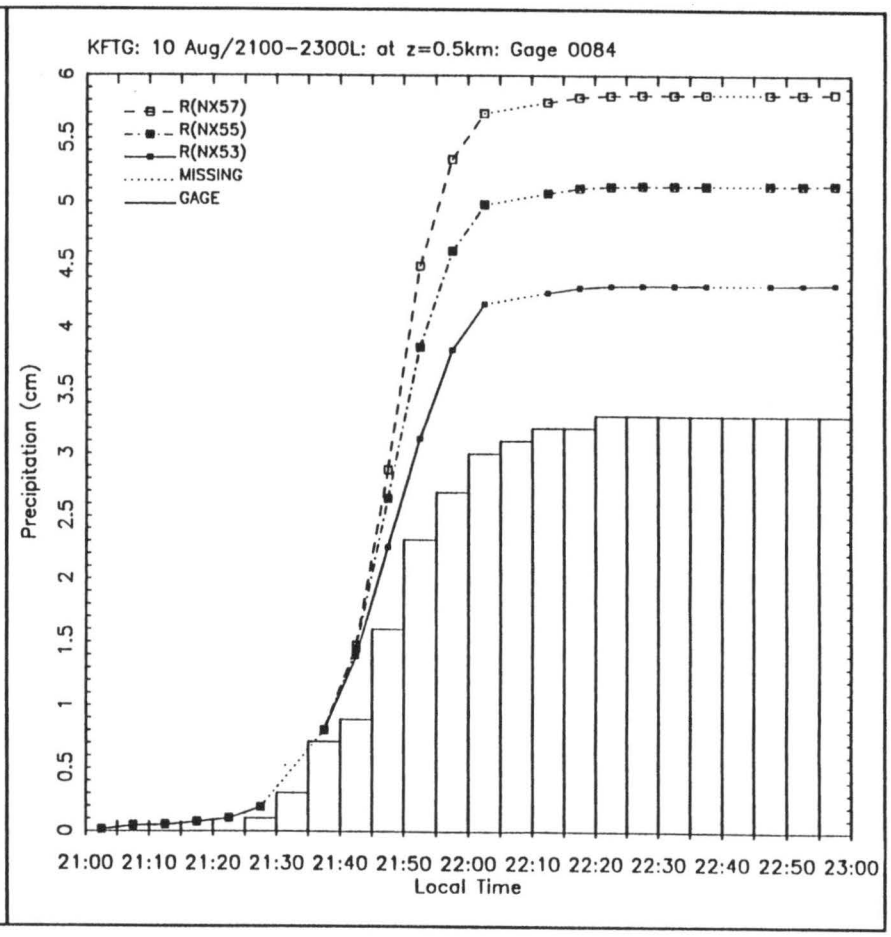

Figure 5.43 Five minute precipitation accumulations time series for gage and R(NXxx) from 21:00 to 23:00 MDT on 10 August 1994 for station 0084.

event, resulting in a R(NXxx) excess of the gage. The R(NX53) overestimated the gage the least, making R(NX53) the preferred reflectivity cut off for this gage.

CHAPTER VI

CONCLUSIONS

This study finds the multiparameter variable, specific differential phase derived precipitation (R(KDP)) compared well with gage precipitation for rainfall accumulations greater than 1 cm. On 20 June 1994 for 12 gages with four-hour accumulated precipitation greater than 1 cm, the R(KDP) to gage precipitation ratio was 0.89. On 21 June 1994 for 3 gages with one-hour accumulated precipitation greater than 1 cm, the R(KDP) to gage ratio was 1.37. For precipitation accumulations less than 1 cm, R(KDP) greatly overestimated gage precipitation which is consistent with previous findings. On 20 June at one gage site (FOR) with a known 30-minute period of mixed phase precipitation, R(KDP) showed an eight percent overestimate of gage precipitation. This result demonstrates R(KDP)'s ability to accurately measure rainfall in mixed phase precipitation.

The time distribution of precipitation rates for the radar and gage are in reasonable agreement. In most cases, the radar-derived precipitation captures the temporal pattern of the gage's precipitation event well. However, the amplitude of the precipitation amounts differed appreciably.

Of the three reflectivity cut offs used to minimize excessive rain rates, the 53 dBZ reflectivity cut off performed the best in comparison to the gage's peak precipitation. This

result agrees with Denver WSR-88D's use of 53 dBZ as their reflectivity cut off for summer convective precipitation in northeastern Colorado.

The precipitation derived by the actual WSR-88D precipitation algorithm provided by the WSR-88D Operational Support Facility, R(OSF), consistently overestimated the gage precipitation for two days of convective storms in Colorado. On 21 June 1994 for 64 gages with one-hour accumulated precipitation, the R(OSF) to gage precipitation ratio was 2.13. On 10 August 1994 for 127 gages with two-hour accumulated precipitation, the R(OSF) to gage ratio was 1.80. Over both days, the R(OSF) provided a somewhat smaller overestimate of gage precipitation than this study's elementary use of same level II data and Z-R relationship. This result indicates the details of data processing are extremely important.

CHAPTER VII

REFERENCES

Atlas, D., 1990: *Radar in Meteorology*, Amer. Meteor. Soc., Boston, MA, 806 pp.

Aydin, K., V. N. Bringi, and L. Liu, 1994: Rain rate estimation in presence of hail using S-band specific differential phase and other radar parameters. *J. Appl. Meteor.*, **34**, 404-410.

Balakrishnan, N., and D. S. Zrni'c, 1990: Use of polarization to characterize precipitation and discriminate large hail, *J. Atmos. Sci.*, **47**, 1525-1540.

Barnes, S. L., 1980: Report on a meeting to establish a common Doppler radar data exchange format. *Bull. Amer. Meteor. Soc.*, **61**, 1401-1404.

Battan, L. J., 1973; *Radar Observations of the Atmosphere*, University of Chicago Press 342 pp.

Brandes, E. A., 1975: Optimizating rainfall estimates with the aid of radar. *J. Appl. Meteor.*, **14**, 1339-1345.

Bringi, V. N., D. Brunkow, V. Chandrasekar, S. Rutledge, P. Kennedy, and A. Mudukutore, 1993: Polarimetric measurements in Colorado convective storms using the CSU-CHILL radar. Preprints, *26th Int'l Conf. on Radar Meteorology*, Norman, Amer. Meteor. Soc., 519-521.

Brock, F., 1990: *Lecture Notes on Meteorological Measurement Systems*, Ver 1.2.

Chandrasekar, V., V. N. Bringi, V. N. Balakrishnan, and D. S. Zrni'c, 1990: Error structure of multiparameter radar and surface measurements of rainfall. Part III: Specific differential phase. *J. Atmos. Oceanic Technol.*, **7**, 621-629.

Cressman, G. P., 1959: An operational objective analysis system. *Mon. Wea. Rev.*, **87**, 367-374.

Crum, T. D., R. L. Alberty, and D. L. Burgess, 1993: Recording, archiving, and using WSR-88D data. *Bull. Amer. Meteor. Soc.*, **74**, 645-653.

--------, and --------, 1993: The WSR-88D and the WSR-88D operational Support facility. *Bull. Amer. Meteor. Soc.*, **74**, 1669-1687.

Doviak R. J. and D. S. Zrni'c, 1993: *Doppler Radar and Weather Observations.* Academic Press, 562 pp.

Green, A. W., 1975: An approximation for the shape of large raindrops. *J. Appl. Meteor.*, **14**, 1578-1583.

Golestani. Y., V. Chandraseker and V. N. Bringi, 1989: Intercomparison of multiparameter radar measurements. Preprints, *24th Conf. on Radar Meteorology*, Tallahassee, Amer. Meteor. Soc., 309-314.

Hubbert, J., V. Chandrasekar, V. N. Bringi, and P. Meischner, 1993: Processing and interpolation of coherent dual-polarized radar measurements. *J. Atmos. Oceanic Technol.*, **10**, 155-164.

Humphries, R. G., 1974: Depolarization effects at 3 GHz due to precipitation. Stormy Weather Scientific Report MW-82, McGill University, Montreal, Quebec, 84 pp.

Illingworth, A. J., and I. J. Caylor, 1989: Polarization radar estimates of raindrop spectra and rainfall rates. *J. Atmos. Oceanic Technol.*, **6**, 939-949.

Jameson, A. R., 1985: Microphysical interpretation of multi-parameter radar measurements in rain. Part III: Interpretation and measurement of propagation differential phase shift between orthogonal linear polarizations. *J. Atmos. Sci.*, **42**, 607-614.

Jameson, A. R., 1993: The meteorological parameterization of specific attenuation and polarization differential phase shift in rain. *J. Appl. Meteor.*, **32**, 1741-1750.

Joss, J., K. Schram, J. C. Thaus, and A. Waldvogel, 1970: On the quantitative determination of precipitation by radar. Eidgenössischen Kommission Zum Studium der Hagelabwehr, Nr. 63, Locarno-Monti, Switzerland, pp 38.

Kelsch, M., 1988: An evaluation of the NEXRAD hydrology sequence for different types of convective storms in northeastern Colorado. Preprints, *24th Conf. on Radar Meteorology*, Tallahassee, Amer. Meteor. Soc., 207-210.

Kennedy, P. C., and S. A. Rutledge, 1995: Dual-Doppler and multiparameter radar observations of a bow-echo hailstorm. *Mon. Wea. Rev.*, **123**, 921-943.

Knight, C.A., and N. C. Knight, 1970: The falling behavior of hailstones. *J. Atmos. Sci.*, **27**, 672-681.

Maddox, R. A., L. E. Hoxit, C. F. Chappell, and F. Caraena, 1978: Meteorological characteristics of flash flood over the Western United States. *Mon. Wea. Rev.*, **108**, 1866-1877.

Manion, J. D., and G. E. Klazura, 1993: A comparison of data from the WSR-88D storm total precipitation product and a network of gages: preliminary results. Preprints, *26th Int'l Conf. on Radar Meteorology*, Norman, Amer. Meteor. Soc., 151-153.

Marshall, J. S., and W. M. K. Palmer, 1948: The distribution of raindrops with size. *J. Meteor.*, **5**, 165-166.

Mohr, C. G., and L. J. Miller, 1983: CEDRIC - A software package for Cartesian space editing, synthesis and display of radar fields under interactive control. Preprints, *21st Conf. on Radar Meteorology*, Edmonton, Alberta, Canada, Amer. Meteor. Soc., 569-574.

--------, --------, and R. L. Vaughan, 1981: An interactive software package for the rectification of radar data to three dimensional Cartesian coordinates. Preprints, *20th Conf. on Radar Meteorology*, Boston, Amer. Meteor. Soc., 690-695.

Neff, E. L., 1977. How Much Rain Does a Rain Gage Gage? *J. Hydrology*, **35**, 213-220.

Oye, R., and R. E. Carbone, 1981: Interactive Doppler Editing Software, Preprints, *20th Conf. on Radar Meteorology*, Boston, Amer. Meteor. Soc., 683-689.

Pruppacher, H. R., and K. V. Beard, 1970: A wind tunnel investigation of the internal circulation and shape of water drops falling at terminal velocity in air. *Quart. J. Roy. Meteor. Soc.*, **96**, 247-256.

--------, and R. L. Pitter, 1971: A semi-empirical determination of the shape of cloud and rain drops. *J. Atmos. Sci.*, **28**, 86-94.

Rew, R. K., and G. P. Davis, 1990: The Unidata netCDF: Software for scientific data access. Preprints, *5th International Conf. on Information and Processing Systems for Meteorology, Oceanography and Hydrology*, Anaheim, p 33-40.

Richards, W., and C. Crozier, 1983: Precipitation measurements with a C-band radar in Southern Ontario. *Atmos.-Ocean*, **21**, 125-137.

Ryzhkov, A. V., and D. S. Zrni'c, 1995: Comparison of Dual-Polarization Radar Estimators of Rain. *J. Atmos. Oceanic Technol.*, **12**, 249-256.

Sachidananda, M., and D. S. Zrni'c, 1987: Rain rate estimated from differential polarization measurements. *J. Atmos. Oceanic Technol.*, **4**, 588-598.

Seliga, T. A., and V. N. Bringi, 1976: Potential use of radar differential reflectivity measurements at orthogonal polarizations for measuring precipitation. *J. Appl. Meteor.*, **15**, 69-76.

--------, and --------, 1978: Differential reflectivity and differential phase shift: applications in radar meteorology. *Radio Sci.*, **13**, 271-275.

Smith, C. B., Lakhtakia, M. N., Capehart, W. J., and Carlson, T. N., 1994: Initialization of Soil-Water Content in Regional-Scale Atmospheric Prediction Models. *Bull. Amer. Meteor. Soc.*, **75**, 585-592.

Spilhaus, A. F., 1948: Raindrop size, shape, and falling speed. *J. Meteor.*, **5**, 108-110.

Stout, G.E., and E. A. Mueller, 1968: Summary of relationships between rainfall rates and radar reflectivity in measurement of precipitation. *J. Appl. Meteor.*, 7, 465-474.

Wang, J. Y., and C. M. M. Felton, 1983: *Instruments for Physical Environmental Measurements, Volume 1*, Second Edition, Kendall/Hunt Publishing Company, Dubuque, Iowa

Weaver, J. F., and N. J. Doesken, 1991: High plains severe weather -- ten years after. *Wea. Forecasting*, **6**, 411-414.

Wexler, R., 1948: Rain intensities by radar, *J. Meteor.*, **5**, 171-173.

Wilson, J. W., and E. A. Brandes, 1979: Radar measurement of rainfall -- a summary. *Bull. Amer. Meteor. Soc.*, **60**, 1048-1058.

Woodley, W. L., and A. Herndon, 1970: A raingage evaluation of the Miami reflectivity-rainfall rate relation. *J. Appl. Meteor.*, **9**, 258-264.

--------, A. R. Olsen, A. Herndon, and V. Wiggert, 1975: Comparison of gage and radar methods of convective rain measurement. *J. Appl. Meteor.*, **14**, 909-928.

Zawadzki, I., 1975: On radar-raingage comparison. *J. Appl. Meteor.*, **14**, 1430-1436.

--------, 1982: The Quantitative interpretation of weather radar measurements. *Atmos.-Ocean*, **20**, 158-180.

--------, 1984: Factors affecting the precision of radar measurements of rain. Preprints, *22nd Conference on Radar Meteorology*, Zurich, Switzerland, Amer. Meteor. Soc., 251-256.

APPENDIX A

RADAR-DERIVED PRECIPITATION TO GAGE PRECIPITATION RATIOS

Table A.1 Average R(KDP) to Gage Ratios for All Gages and Range of Gage Values for 20 June 1994.

Range of Gage Precipitation (cm)	Number of Gages in Range	Average of Gage Precipitation in Range (cm)	Average of R(KDP) Precipitation in Range (cm)	Ratio of Average of R(KDP) / Average of Gage
0	19	0	0	
0	13	0	0.37	
0.000-0.25	9	0.13	0.75	5.92
0.251-0.50	7	0.36	0.43	1.20
0.501-1.00	6	0.77	1.10	1.42
1.001-2.00	4	1.36	1.63	1.20
2.001-4.00	4	2.58	1.59	0.62
4.001-6.00	2	4.51	2.96	0.66
6.001-8.00	2	7.21	8.08	1.12
Range of Gage Precipitation (cm)	Number of Gages in Range	Sum of Gage Precipitation in Range (cm)	Sum of R(KDP) Precipitation in Range (cm)	Ratio of Sum of R(KDP) / Sum of Gage
All Gages > 0	34	47.45	51.32	1.08
All Gages	66	47.45	56.15	1.18

Table A.2 Average R(KDP) to Gage Ratios for All Gages and Ranges of Gage Values for 21 June 1994.

Range of Gage Precipitation (cm)	Number of Gages in Range	Average of Gage Precipitation in Range (cm)	Average of R(KDP) Precipitation in Range (cm)	Ratio of Average of R(KDP) / Average of Gage
0	10	0	0	
0	14	0	0.43	
0.000-0.25	9	0.13	0.40	3.15
0.251-0.50	4	0.32	0.80	2.46
0.501-1.00	3	0.67	1.54	2.30
1.001-2.00	3	1.60	2.19	1.37
Range of Gage Precipitation (cm)	Number of Gages in Range	Sum of Gage Precipitation in Range (cm)	Sum of R(KDP) Precipitation in Range (cm)	Ratio of Sum of R(KDP) / Sum of Gage
All Gages > 0	19	9.25	17.97	1.94
All Gages	43	9.25	23.95	2.59

Table A.3 Average R(NX57) to Gage Ratios for All Gages and Ranges of Gage Values for 21 June 1994.

Range of Gage Precipitation (cm)	Number of Gages in Range	Average of Gage Precipitation in Range (cm)	Average of R(NX57) Precipitation in Range (cm)	Ratio of Average of R(NX57) / Average of Gage
0	0	0	0	
0	36	0	0.15	
0.000-0.25	5	0.11	0.23	2.13
0.251-0.50	4	0.32	0.73	2.27
0.501-1.00	2	0.75	2.03	2.70
1.001-2.00	3	1.60	3.93	2.45
Range of Gage Precipitation (cm)	Number of Gages in Range	Sum of Gage Precipitation in Range (cm)	Sum of R(NX57) Precipitation in Range (cm)	Ratio of Sum of R(NX57) / Sum of Gage
All Gages > 0	14	8.13	19.90	2.45
All Gages	50	8.13	25.33	3.12

Table A.4 Average R(NX55) to Gage Ratios for All Gages and Ranges of Gage Values for 21 June 1994.

Range of Gage Precipitation (cm)	Number of Gages in Range	Average of Gage Precipitation in Range (cm)	Average of R(NX55) Precipitation in Range (cm)	Ratio of Average of R(NX55) / Average of Gage
0	0	0	0	
0	36	0	0.15	
0.000-0.25	5	0.11	0.23	2.13
0.251-0.50	4	0.32	0.73	2.27
0.501-1.00	2	0.75	2.02	2.70
1.001-2.00	3	1.60	3.80	2.37
Range of Gage Precipitation (cm)	Number of Gages in Range	Sum of Gage Precipitation in Range (cm)	Sum of R(NX55) Precipitation in Range (cm)	Ratio of Sum of R(NX55) / Sum of Gage
All Gages > 0	14	8.13	19.51	2.40
All Gages	50	8.13	24.94	3.07

Table A.5 Average R(NX53) to Gage Ratios for All Gages and Ranges of Gage Values for 21 June 1994.

Range of Gage Precipitation (cm)	Number of Gages in Range	Average of Gage Precipitation in Range (cm)	Average of R(NX53) Precipitation in Range (cm)	Ratio of Average of R(NX53) / Average of Gage
0	0	0	0	
0	36	0	0.15	
0.000-0.25	5	0.11	0.23	2.13
0.251-0.50	4	0.32	0.73	2.27
0.501-1.00	2	0.75	1.83	2.44
1.001-2.00	3	1.60	3.53	2.21
Range of Gage Precipitation (cm)	Number of Gages in Range	Sum of Gage Precipitation in Range (cm)	Sum of R(NX53) Precipitation in Range (cm)	Ratio of Sum of R(NX53) / Sum of Gage
All Gages > 0	14	8.13	18.33	2.25
All Gages	50	8.13	23.76	2.92

Table A.6 Average R(OSF) to Gage Ratios for All Gages and Ranges of Gage Values for 21 June 1994.

Range of Gage Precipitation (cm)	Number of Gages in Range	Average of Gage Precipitation in Range (cm)	Average of R(OSF) Precipitation in Range (cm)	Ratio of Average of R(OSF) / Average of Gage
0	28	0	0	
0	17	0	0.33	
0.000-0.25	9	0.13	0.27	2.09
0.251-0.50	4	0.32	0.50	1.53
0.501-1.00	3	0.67	0.80	1.20
1.001-2.00	3	1.60	2.41	1.51
Range of Gage Precipitation (cm)	Number of Gages in Range	Sum of Gage Precipitation in Range (cm)	Sum of R(OSF) Precipitation in Range (cm)	Ratio of Sum of R(OSF) / Sum of Gage
All Gages > 0	19	9.25	14.02	1.52
All Gages	64	9.25	19.69	2.13

Table A.7 Average R(NX57) to Gage Ratios for All Gages and Ranges of Gage Values for 10 August 1994.

Range of Gage Precipitation (cm)	Number of Gages in Range	Average of Gage Precipitation in Range (cm)	Average of R(NX57) Precipitation in Range (cm)	Ratio of Average of R(NX57) / Average of Gage
0	0	0	0	
0	22	0	0.29	
0.000-0.25	20	0.14	0.49	3.56
0.251-0.50	8	0.38	1.19	3.09
0.501-1.00	15	0.72	1.48	2.06
1.001-2.00	21	1.39	2.72	1.96
2.001-4.00	12	2.63	3.47	1.32
4.001-6.00	2	4.86	6.98	1.44
Range of Gage Precipitation (cm)	Number of Gages in Range	Sum of Gage Precipitation in Range (cm)	Sum of R(NX57) Precipitation in Range (cm)	Ratio of Sum of R(NX57) / Sum of Gage
All Gages > 0	78	87.02	154.23	1.77
All Gages	100	87.02	160.68	1.85

Table A.8 Average R(NX55) to Gage Ratios for All Gages and Ranges of Gage Values for 10 August 1994.

Range of Gage Precipitation (cm)	Number of Gages in Range	Average of Gage Precipitation in Range (cm)	Average of R(NX55) Precipitation in Range (cm)	Ratio of Average of R(NX55) / Average of Gage
0	0	0	0	
0	22	0	0.29	
0.000-0.25	20	0.14	0.49	3.56
0.251-0.50	8	0.38	1.19	3.09
0.501-1.00	15	0.72	1.47	2.06
1.001-2.00	21	1.39	2.65	1.91
2.001-4.00	12	2.63	3.40	1.29
4.001-6.00	2	4.86	6.75	1.39
Range of Gage Precipitation (cm)	Number of Gages in Range	Sum of Gage Precipitation in Range (cm)	Sum of R(NX55) Precipitation in Range (cm)	Ratio of Sum of R(NX55) / Sum of Gage
All Gages > 0	78	87.02	151.36	1.74
All Gages	100	87.02	157.82	1.81

Table A.9 Average R(NX53) to Gage Ratios for All Gages and Ranges of Gage Values for 10 August 1994.

Range of Gage Precipitation (cm)	Number of Gages in Range	Average of Gage Precipitation in Range (cm)	Average of R(NX53) Precipitation in Range (cm)	Ratio of Average of R(NX53) / Average of Gage
0	0	0	0	
0	22	0	0.29	
0.000-0.25	20	0.14	0.49	3.54
0.251-0.50	8	0.38	1.19	3.09
0.501-1.00	15	0.72	1.44	2.01
1.001-2.00	21	1.39	2.54	1.83
2.001-4.00	12	2.63	3.26	1.24
4.001-6.00	2	4.86	6.05	1.24
Range of Gage Precipitation (cm)	Number of Gages in Range	Sum of Gage Precipitation in Range (cm)	Sum of R(NX53) Precipitation in Range (cm)	Ratio of Sum of R(NX53) / Sum of Gage
All Gages > 0	78	87.02	145.43	1.67
All Gages	100	87.02	151.89	1.75

Table A.10 Average R(OSF) to Gage Ratios for All Gages and Ranges of Gage Values for 10 August 1994.

Range of Gage Precipitation (cm)	Number of Gages in Range	Average of Gage Precipitation in Range (cm)	Average of R(OSF) Precipitation in Range (cm)	Ratio of Average of R(OSF) / Average of Gage
0	19	0	0	
0	17	0	0.71	
0.000-0.25	22	0.13	0.47	3.61
0.251-0.50	9	0.38	0.82	2.19
0.501-1.00	20	0.69	1.47	2.14
1.001-2.00	24	1.41	2.47	1.76
2.001-4.00	14	2.60	3.37	1.29
4.001-6.00	2	4.86	7.23	1.49
Range of Gage Precipitation (cm)	Number of Gages in Range	Sum of Gage Precipitation in Range (cm)	Sum of R(OSF) Precipitation in Range (cm)	Ratio of Sum of R(OSF) / Sum of Gage
All Gages > 0	91	99.92	168.02	1.68
All Gages	127	99.92	180.04	1.80